DOE/ET/27111-4

CONTINUITY AND INTERNAL PROPERTIES OF GULF COAST SANDSTONES AND THEIR IMPLICATIONS FOR GEOPRESSURED ENERGY DEVELOPMENT

by

R. A. Morton, T. E. Ewing, and N. Tyler

Assisted by

B. E. Bullock

Annual Report for the period

November 1, 1980 - October 31, 1981

Prepared for
U.S. Department of Energy
Division of Geothermal Energy

under Contract No. DE-AC08-79ET27111

Bureau of Economic Geology
The University of Texas at Austin
Austin, Texas 78712

W. L. Fisher, Director

June 1982

TABLE OF CONTENTS

	Page
ABSTRACT	1
INTRODUCTION	2
Quantification of Inhomogeneities	3
STRUCTURAL AND STRATIGRAPHIC LIMITS OF SANDSTONE RESERVOIRS	5
Sand-Body and Reservoir Hierarchy	5
Possible External Contributions	7
CHARACTERISTICS AND DIMENSIONS OF GULF COAST SANDSTONES	9
Limitations of Data	9
Late Quaternary Sediments	10
Fluvial Sandstones	14
Mississippi River	14
Rio Grande	14
Brazos River	15
Deltaic Sandstones	16
Mississippi delta	17
Rio Grande delta	18
Brazos delta	18
Barrier and Strandplain Sandstones	20
Padre Island	22
Galveston Island	23
Grande Isle	23
South Padre Island	24
Ingleside Strandplain	24
Shelf-Slope Sandstones	25

Page

Tertiary Sediments 25

Fluvial Sandstones 26

Deltaic Sandstones 27

Barrier and Strandplain Sandstones 28

Shelf-Slope Sandstones 28

Sediments of Other Ages 29

FAULT COMPARTMENT AREAS 30

COMPARISON OF PRODUCTION AND GEOLOGIC ESTIMATES OF AQUIFER VOLUME . . . 35

Calculation of Aquifer Volume from Production Data 38

South Cook Field 40

Stratigraphy of Producing Sands 40

Structure of the South Cook Area 41

Reservoir Volume - B Sand 41

Reservoir Volume - C Sand 44

Summary 45

Yorktown and South Yorktown Fields 45

Stratigraphy of the Migura Sand 45

Structure of the Yorktown Area 48

Reservoir Volume - Yorktown Field 49

Reservoir Volume - South Yorktown Field 51

Summary 52

Christmas Field 52

Stratigraphy of the Migura Sand 52

Structure of the Christmas Area 54

Reservoir Volume - Christmas Field 56

Page

Pettus SE Field 57

Stratigraphy of the First Massive Sand 57

Structure of the Pettus Area 60

Reservoir Volume - First Massive Sand 60

Braslau South Field 61

Stratigraphy of the First Tom Lyne Sand 61

Structure of the Braslau South Area 62

Reservoir Volume - Braslau South Field 65

South Peach Point Field 66

Stratigraphy of the Frio A Sand 66

Structure of the Peach Point Area 69

Reservoir Volume - South Peach Point Field 71

Mobil-David "L" Field 71

Stratigraphy of the Anderson Sand 72

Structure of the Mobil-David Area 72

Reservoir Volume - Anderson Sand 75

Comparisons and Conclusions 76

GEOLOGIC SETTING AND RESERVOIR CHARACTERISTICS, WELLS OF OPPORTUNITY . . 79

Riddle #2 Saldana 79

Stratigraphy of the First Hinnant Sand 83

Reservoir Character and Volume 86

Ross (Coastal States) #1 Pauline Kraft 87

Structure of the Mobil-David Area 87

Reservoir Volume of the Anderson Sand 89

Lear #1 Koelemay 89

Stratigraphy of the Leger Sand 90

Page

Structure 93

Reservoir Volume and Continuity 93

Conclusion, Well of Opportunity Study 94

INTERNAL PROPERTIES OF SANDSTONES 95

Porosity and Permeability of Modern Sands 95

Detailed Investigation of Vertical Changes in Porosity and Permeability 96

Variations in Grain Size and Sedimentary Structure 104

Bioturbation and Texture 105

Induration 109

Porosity and Permeability as a Function of Depositional Environment . 109

Facies Control on Reservoir Continuity 110

Vertical Patterns 117

Pore Properties and Stratification 119

Frequency and Arrangement of Flow Barriers 119

IMPLICATIONS FOR GEOPRESSURED ENERGY DEVELOPMENT 122

ACKNOWLEDGMENTS 124

REFERENCES 125

APPENDIX: Microfossil Recovery and Paleoenvironmental Interpretation for #1 and #2 Pleasant Bayou Cores 138

FIGURES

1. Stratigraphic dip cross section of Late Quaternary Rio Grande deltas near South Padre Island 6

2. Subaerial distribution of subenvironments and subsurface distribution of sediment types in the new Brazos delta 19

3. Histograms of fault compartment areas 32

Page

4. Calculation procedures for estimating aquifer volume 36

5. Location of geopressured trends, geothermal test wells, and areas studied for this report, Texas Gulf Coast 37

6. Net-sand map, B sand, South Cook field 42

7. Net-sand map, C sand, South Cook field 43

8. Structure and net-sand map, Yorktown area 46

9. Stratigraphic section of lower Wilcox Group sands, Yorktown area . . 47

10. Structure sections, Yorktown area 50

11. Structure and net-sand map, Christmas area 53

12. Stratigraphic section of lower Wilcox Group sands, Christmas area . 55

13. Structure and net-sand map, Pettus area 58

14. Stratigraphic section of upper Wilcox Group sands, Pettus area . . 59

15. Structure and net-sand map, Braslau area 63

16. Stratigraphic section of upper Wilcox Group sands, Braslau area . . 64

17. Structure and net-sand map, Peach Point area 67

18. Stratigraphic section of T3-T4 sands of the Frio Formation, Peach Point area 68

19. Structure section, Peach Point area 70

20. Structure and net-sand map, Mobil-David area 73

21. Stratigraphic section of lower Frio sands, Mobil-David area . . . 74

22. Comparison of production and geologic estimates of aquifer volume . 77

23. Structure and net-sand map, Riddle #2 Saldana area 81

24. Porosity and permeability variations in three reservoirs tested by the well of opportunity program 82

25. Stratigraphic strike section of First Hinnant sand, Riddle Saldana #2 and northeast Thompsonville areas 84

26. Stratigraphic dip section through Riddle #2 Saldana of uppermost Wilcox sands 85

27. Structural section through Coastal States #1 P. Kraft well, Mobil-David area 88

Page

28. Structure and net-sand map, Lear #1 Koelemay area 91

29. Stratigraphic section of Yegua sands, Lear #1 Koelemay area . . . 92

30. Location of the Pleasant Bayou geopressured geothermal test well and structural fabric on top of the T5 marker 97

31. Explanation of symbols for figures 32-35 98

32. Detailed core description, core characteristics, and interpretation of the upper part of the Frio T3 correlation unit 99

33. Detailed core description, core characteristics, and interpretation of the geopressured geothermal production interval (Andrau or C sand) 100

34. Detailed core description, core characteristics, and interpretation of a part of the Frio D correlation interval (sub T5) 101

35. Detailed core description, core characteristics, and interpretation of a part of the Frio sub T5, F correlation interval 102

36. A. Large-scale cross-lamination in permeable (729 md) porous (19 percent) sandstone, interpreted as bed-load distributary-channel deposits. B. Intermediate- to small-scale crossbedded sandstone of the production interval. C. Ripple-laminated sandstone overlain by horizontally bedded sandstone with thin mud drapes 106

37. A. Interlaminated very fine grained sandstone and siltstone interpreted as shallow-marine storm-related sequences. B. Highly bioturbated sandstone 107

38. Net-sand map of the production interval (Andrau sand) and location of the fence diagram presented in figure 39 111

39. Fence diagram illustrating the continuity of depositional units of the production interval 112

40. Lobate net-sand pattern of the T3 correlation interval and location of cross sections illustrated in figure 41 114

41. Cross sections through the T3 depositional interval 115

42. Generalized patterns for vertical changes in pore properties within a sand body 118

TABLES

		Page
1.	Dimensions of late Quaternary Gulf Coast sand bodies	11
2.	Dimensions of Tertiary Gulf Coast sand bodies	12
3.	Dimensions of non-Gulf Coast sand bodies	13
4.	Areas of fault compartments in Wilcox geopressured fairways	31
5.	Areas of fault compartments in Frio geopressured fairways	34
6.	Volume estimates for geopressured gas reservoirs, Texas Gulf Coast	39
7.	Reservoir area and volume for Texas wells of opportunity	80

ABSTRACT

Continuity of sandstone reservoirs is controlled by various factors including structural trend, sand-body geometry, and the distribution of framework grains, matrix, and interstices within the sand body. Except for the limits imposed by faults, these factors are largely inherited from the depositional environment and modified during sandstone compaction and cementation. Regional and local continuity of sandstone reservoirs depends on a depositional and structural hierarchy of four levels: (1) genetically related sandstones commonly associated with a single depositional system, (2) areally extensive fault blocks, (3) individual sandstones within a fault block, and (4) isolated reservoirs within a fault-bounded sandstone.

Compilation of published and unpublished data for Tertiary and late Quaternary Gulf Coast sandstones of fluvial, deltaic, barrier-strandplain, and submarine fan origins suggests that volumes of sand systems (first hierarchical level) range from 10^{11} to 10^{13} ft^3, whereas volumes of individual sand bodies range from 10^9 to 10^{11} ft^3. The continuity and productive limits of the ancient sandstones are substantially reduced by faults and internal heterogeneity that further subdivide the sand body into individual compartments. For the Wilcox and Frio trends of Texas, fault blocks (second hierarchical level) vary greatly in size, most being between 0.3 and 52 mi^2 in area; however, the distribution is strongly skewed toward small areas. Volumes of individual reservoirs (fourth hierarchical level) determined from engineering production data are 50 percent less to 200 percent more than estimates obtained from geologic mapping. In general, mapped volumes underestimate actual volumes where faults are nonsealing and overestimate actual volumes where laterally continuous shale breaks cause reductions in porosity and permeability.

Gross variations in pore properties (porosity and permeability) can be predicted on the basis of internal stratification and sandstone facies where original sedimentological properties are not masked by diagenetic alterations. Six basic patterns are recognized that generally describe the vertical variations in pore properties within a sand body at a well site. Whole-core analyses show (1) upward increases, (2) upward decreases, (3) central increases, (4) central decreases, and (5) uniformly low, and (6) irregular changes in porosity and permeability with depth. Within these trends, porosity and permeability are generally highest in large-scale crossbedded intervals and lowest in contorted, bioturbated, and small-scale ripple cross-laminated intervals.

Sandstone facies models and regional structural fabric of the Gulf Coast Basin suggest that large and relatively continuous reservoirs should be found where barrier and strandplain sandstones parallel regional faults. These conditions should optimize the magnitude and rate of fluid production from geopressured geothermal aquifers and maximize the efficiency of primary and enhanced recovery of conventional hydrocarbons. Fluvial sandstones deposited by major streams that trend roughly normal to regional faults are probably less continuous than barrier sandstones, but together they serve as substantial targets for exploration and production of unconventional as well as conventional energy resources.

INTRODUCTION

Sandstone reservoirs are spatially confined by lateral and vertical changes in primary rock properties, such as grain size and porosity and permeability, that are largely inherited from the depositional environment. Equally important in reservoir characterization are postdepositional events including structural deformation and diagenetic alteration that cause major reductions in the

transmissibility of fluids. Studies of modern clastic environments and their ancient counterparts have led to conceptual models of the most common sandstone facies. These models have established criteria for interpreting genetic depositional systems from well cuttings, cores, and geophysical logs (Fisher and Brown, 1972; Fisher and others, 1969) and subsequently for predicting the geometry and continuity of many sandstone reservoirs (LeBlanc, 1977; Sneider and others, 1977).

In the Gulf Coast Basin, the common sandstone facies are products of deposition in fluvial, deltaic, barrier-strandplain, transgressive marine, and shelf and slope systems. These sandstone types, which commonly occur as aquifers in the geopressured zone, exhibit certain predictable properties. Accordingly, studies of reservoir continuity that combine sedimentological characteristics with reservoir engineering data for sandstone aquifers should improve those predictive capabilities. This report provides a systematic investigation, classification, and differentiation of the intrinsic properties of genetic sandstone units that typify many geopressured geothermal aquifers and hydrocarbon reservoirs of the Gulf Coast region.

Quantification of Inhomogeneities

Identifying geological factors suitable for reservoir discrimination requires two principal efforts: (1) compilation of selected geologic data for ancient sandstones and modern analogs and (2) analysis and synthesis of production data for selected reservoirs.

An example of the first type of data was reported by Pryor (1973), who analyzed nearly 1,000 sediment samples taken from three modern depositional environments. From his work, Pryor concluded that point-bar and beach sands have directional permeabilities, whereas porosity and permeability in eolian dunes have low variability and no discernible trends.

Investigations of internal properties of sandstones from cores and outcrops make possible a relative ranking of potential sandstone reservoirs suitable for primary or enhanced recovery. Qualitative results indicate which sandstone facies are likely to exhibit less variability owing to their internal stratification and other physical qualities (pore space distribution, frequency and position of shale breaks). Most studies based on outcrop samples and subsurface cores recognize reservoir heterogeneity related to internal stratification (for example, Polasek and Hutchinson, 1967), but the broader issue of improved predictive capabilities achieved by applying this knowledge to sandstone models has not been widely reported.

Attempts to quantify sand-body geometry and reservoir inhomogeneities have been largely unsuccessful owing to the inherent difficulties associated with subsurface correlations, lack of precise geological boundaries, and spatially discontinuous data. In spite of these limitations, at least two numerical expressions for reservoir continuity and internal heterogeneity have been proposed.

Fulton (1975) used a continuity index to describe spatial variations in sandstones of the ancestral Rio Grande delta. He defined horizontal continuity as the ratio of sand-body length to cross-section length and vertical continuity as the ratio of maximum thickness of continuous sand to total sand thickness.

The accuracy of numerical values reported by Fulton (1975) is questionable because the boundaries and dimensions used to calculate the index were constrained by the cross sections themselves. Nevertheless, Fulton's study demonstrates, as do many others, that (1) fluvial sands are more continuous in directions parallel to progradation than in directions perpendicular to progradation, (2) delta-front sands are widely distributed and are nearly continuous both along strike and in updip and downdip directions, and (3) prodelta sands are

thin and highly discontinuous with greatest continuity in directions parallel to progradation. Although not evaluated by Fulton, the transgressive marine sand underlying the progradational sequence (fig. 1) represents the most continuous and areally extensive sand within his study area.

Polasek and Hutchinson (1967) used a heterogeneity factor (HF) to quantify the layering or abundance of shaly material in sand sequences. Heterogeneity factors were determined empirically for several producing reservoirs, but they were not related to sandstone facies or depositional environment. Because geological factors were not included, the predictive capabilities of this method are unknown. The quantification techniques of Fulton (1975) and of Polasek and Hutchinson (1967) require artificial boundaries that severely limit the usefulness of the data. Hence, an accurate and reproducible method of quantifying sandstone inhomogeneities has not been developed.

Reservoir heterogeneities have also been statistically treated to accommodate the high variability in numerical evaluations. The normal and log-normal distributions that characterize porosity and permeability measurements grouped by depth (Law, 1944; Polasek and Hutchinson, 1967) are adequate for summarizing general reservoir properties, but they are poorer predictors than geological models that explain the variability of pore space properties within and among sandstone units.

STRUCTURAL AND STRATIGRAPHIC LIMITS OF SANDSTONE RESERVOIRS

Sand-Body and Reservoir Hierarchy

Depositional and structural conditions at various levels within a hierarchy control the volume and areal extent of sandstone reservoirs. The first level includes the entire reservoir interval, or aquifer system, that spans several

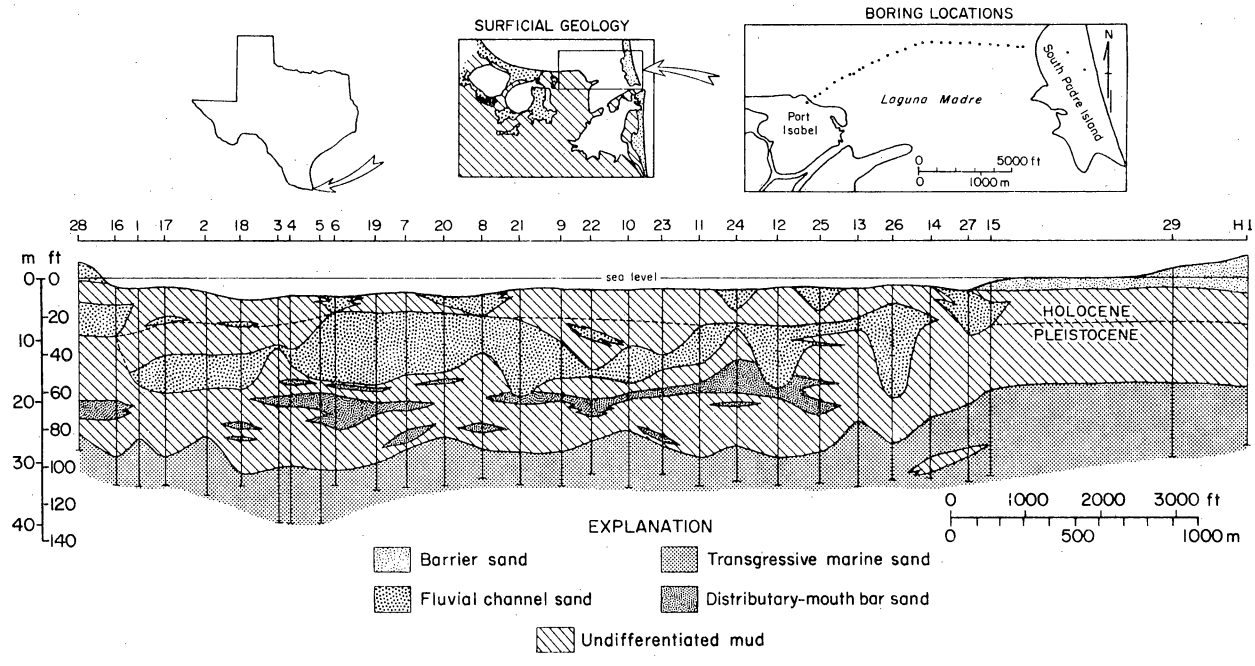

Figure 1. Stratigraphic dip cross section of late Quaternary Rio Grande deltas near South Padre Island. Interpreted from boring descriptions provided by the Texas Department of Highways and Public Transportation.

hundred to several thousand feet of interbedded sand and shale. Sandstones within the reservoir interval are commonly genetically related and associated with a single depositional system. Large fault blocks encompassing the reservoir interval comprise the second hierarchical level. Third and fourth levels respectively include individual sandstones within a fault block and isolated reservoirs within an individual fault-bounded sandstone.

Both modern and ancient sandstones can be grouped and measured according to the first and third levels of the hierarchy (genetically related sequences and individual sandstones). For this reason, the distinction between sand trends of regional or continental proportion and local sand features is important for predicting the size and arrangement of attendant sand bodies. The fourth hierarchical level represents those conditions in which interbedded shales or other permeability barriers within the sandstones reduce the effective reservoir volume, but this level does not include potential increases in reservoir capacity owing to external contributions such as shale dewatering or nonsealing faults.

Possible External Contributions

Marked decreases in permeability define the reservoir boundaries and limit the volume of sediment from which fluids can be produced. These permeability changes usually occur along the margins of a sand body and, therefore, the extent of fluid withdrawal is chiefly from a single sand within a fault block. Fluids might enter producing reservoirs across faults or from surrounding shales; however, these influxes are generally regarded as minor or ascribed to rare and unique circumstances that would not affect the cumulative production from most reservoirs. At present, the importance of nonsealing faults and the magnitude of shale dewatering are unknown; hence faults and shales cannot be eliminated as potential sources of additional fluid.

Theoretical considerations and field observations have been used to demonstrate that some faults do not prevent lateral migration of fluids, especially when correlative sand bodies are juxtaposed across a fault (Smith, 1980). Although much of the theory deals with entrapment of hydrocarbons in the hydropressured zone, the governing principles apply equally to water movement in the geopressured zone.

Structure maps for several Tertiary sandstone reservoirs in Louisiana (Smith, 1980) suggest that minor faults may not be complete barriers to flow because lithologies and capillary properties across these faults are very similar. These observations suggest that drainage areas of geopressured aquifers may not be limited by minor faults where sand thickness exceeds fault displacement.

The areal extent of water production from geopressured aquifers is uncertain. A significant reduction in reservoir pressure during production might cause an influx of water from shales surrounding the aquifer. In addition to minimizing pressure decline in the reservoir, shale recharging could substantially increase the effective reservoir volume beyond the sand-body limits. Theoretically, the vast surface area along sand margins and along interbedded shales would provide multiple pathways for fluid invasion despite the low permeabilities at these boundaries. Published field data (Wallace, 1969) and reservoir simulations (Chierici and others, 1978; Garg, 1980) indicate that only reservoirs with long life expectancies would be noticeably enhanced by shale compaction and fluid expulsion. Even under ideal circumstances, it appears doubtful that substantial volumes of shale water would flow to the well bore given the anticipated high flow rates and rapid drawdown of most geopressured reservoirs.

The vertical permeability of shale is a prime factor controlling the influx of shale-derived water (Garg, 1980). Because in situ shale permeabilities are

poorly documented and production data are scant, the reliability of dewatering predicted by model studies is uncertain. Undoubtedly, new knowledge will be gained during and following production of several design wells. A major objective of the Dow-DOE Sweezy No. 1 in the Parcperdue field is to determine the magnitude of shale dewatering in an areally limited geopressured reservoir.

CHARACTERISTICS AND DIMENSIONS OF GULF COAST SANDSTONES

The northwest margin of the Gulf of Mexico has been an area of active sedimentation for millions of years; it has also been the site of extensive exploration for and production of hydrocarbons contained in the thick clastic sequences of the Gulf Coast Basin. The geology of the Gulf Coast has been recorded in detail because the area is accessible, the depositional environments are diverse, and the geology is applicable to energy resource exploration elsewhere. Studies of modern and ancient depositional systems along the Gulf Coast have resulted in improved capabilities for predicting the external geometry and internal properties of sandstone reservoirs.

Limitations of Data

There are many advantages to reservoir studies that utilize surface exposures, electric logs, seismic sections, and subsurface cores. Because no single data base is inclusive, their integration provides a more complete picture of rock properties inherited from the original depositional environment and subsequent diagenetic modifications.

In the Gulf Coast region, modern sand-rich environments are commonly analogous to ancient sedimentary deposits. Surficial exposures of sand bodies provide excellent control on textures, directional properties, bed continuity,

spatial relationships with surrounding sediments, and the like. On the other hand, modern sand bodies tend to overestimate certain reservoir properties (volume, porosity, permeability) because compaction, cementation, and structural deformation have not reached advanced stages in modern sediments. In contrast, ancient sandstones are more realistic approximations of reservoir conditions because they represent what is actually preserved over broad areas. Common disadvantages of subsurface studies are (1) the lack of dense and deep subsurface control, (2) the necessity of indirectly measuring geological parameters, and (3) the uncertainty of log correlations in structurally complex areas. These factors greatly influence stratigraphic interpretations and paleogeographic reconstructions, which in turn affect general characterizations and volumetric estimates of particular sand bodies (tables 1 to 3). The volumetric estimates are only accurate within an order of magnitude because sand-body dimensions are averaged, and at least one dimension is usually an arbitrary truncation (dip direction for channels, strike direction for barriers) or represents the limit of available data. However, even with these discrepancies, the data show that individual sand bodies (third hierarchical level) contain from 10^9 to 10^{11} ft^3 of sand, whereas sand systems (first hierarchical level) are on the order of 10^{11} to 10^{13} ft^3 in volume (tables 1 to 3).

Late Quaternary Sediments

Most sands deposited during the late Quaternary Period remain unconsolidated and exhibit characteristics established when they were initially deposited. These geologically young sand bodies serve as a baseline for understanding physical and chemical changes that occur during burial. It should be noted, however, that Holocene sand systems (table 1) are generally less voluminous than their ancient counterparts (table 2) because relative sea-level changes have been minor and vertical stacking of multiple sand bodies has been minimized.

Table 1. Dimensions of late Quaternary Gulf Coast sand bodies.

Feature	Sand	Age	Thick. ft	Length ft x 10^3	Width ft x 10^3	Sand vol. x 10^9 ft^3	Reference
Mississippi River	point bar	H	75	26	21	41	Frazier and Osanik, 1961
Mississippi delta	distributary-mouth bar	H	100	21	5	11	Fisk, 1961
Mississippi delta	delta-front system	H	40	317	80	1,014*	Fisk, 1955
Rio Grande	fluvial channel	H	15	40	10	6	Fulton, 1975
Rio Grande	fluvial system	H	65	237	53	816*	Brown and others, 1980
Rio Grande delta	delta front	P	10	17	15	3	Figure 1, and Fulton, 1975
Rio Grande delta	transgressive marine	H	30	53	16	25	Fulton, 1975
Brazos River	point bar	H	55	6	3	1	Bernard and others, 1970
Brazos River	fluvial channel	H	40	53	8	17	Bernard and others, 1970
Brazos River	fluvial system	H	40	264	63	665*	Bernard and others, 1970
Brazos River	fluvial system	P	25	316	158	1,248*	Winker, 1979
Brazos Delta	delta system	H	25	8	10	2*	Figure 2, and Bernard and others, 1970
Padre Island	barrier	H	40	105	26	109	Fisk, 1959
Galveston Island	barrier	H	30	137	13	53	Bernard and others, 1970
Grand Isle	barrier	H	20	20	4	2	Conatser, 1971
South Padre Island	barrier	H	12	105	5	6	Morton and McGowen, 1980
Texas barrier islands	barrier system	H	40	1,056	15	633*	Morton and McGowen, 1980
Ingleside	strandplain system	P	60	528	53	1,679*	Winker, 1979

*system scale H - Holocene P - Pleistocene

Table 2. Dimensions of Tertiary Gulf Coast sand bodies.

	Area	Form.	Poros. %	Perm. md	Thick. ft	Length ft x 10^3	Width ft x 10^3	Sand Vol. x 10^9 ft^3	Reference
FLUVIAL	East Texas	Wilcox	--	--	300	106	53	1,685*	Fisher and McGowen, 1967
	Seeligson, TX	Frio	--	--	40	40	13	21	Nanz, 1954
	Central Texas Coast	Miocene	--	--	200	106	185	3,922*	Solis, 1980
	Central Texas Coast	Miocene	--	--	150	211	37	1,171*	Doyle, 1979
	Austin Bayou, TX	Frio	21	211	60	26	26	42	Morton and others, 1980
	Central Louisiana	Wilcox	--	--	130	32	8	33	Galloway, 1968
	Main Pass, LA	Miocene	34	3,000	35	16	2	1	Hartman, 1972
DELTAIC	South Cook, TX	Wilcox	25	242	60	74	16	71	Bebout and others, 1979
	Austin Bayou, TX	Frio	20	40	60	106	37	235	Bebout and others, 1978
	Austin Bayou, TX	Frio	--	--	400	106	53	2,247*	Bebout and others, 1978
	Central Texas Coast	Miocene	--	--	500	317	79	12,522*	Solis, 1980
	Central Texas Coast	Miocene	--	--	300	686	105	21,609*	Doyle, 1979
	South Texas	Wilcox	--	--	100	211	79	1,667*	Edwards, 1980
	E. White Point, TX	Frio	--	--	300	20	15	90	Martyn and Sample, 1941
	Upper Texas Coast	Vicksburg	--	--	30	700	150	3,150*	Gregory, 1966
	Louisiana Onshore	Miocene	--	--	300	370	105	11,655*	Curtis, 1970
BARRIER-STRANDPLAIN	S.W. Lake Arthur, LA	Frio	30	2,000	15	40	8	5	Gotautas and others, 1972
	Chandeleur Sound, LA	Miocene	33	1,680	60	7	5	2	Woltz, 1980
	Milbur, TX	Wilcox	34	600	15	35	10	5	Chuber, 1972
	Hardin, TX	Yegua	27	2,200	35	10	1	<1	Casey and Cantrell, 1941
	Jim Hogg, TX	Jackson	--	--	35	158	53	292	Freeman, 1949
	Central Texas Coast	Wilcox	--	--	400	400	158	25,280*	Fisher and McGowen, 1967
	Central Texas Coast	Frio	--	--	1,000	317	68	21,556*	Boyd and Dyer, 1966
	Central Texas Coast	Miocene	--	--	450	211	53	5,032*	Solis, 1980
	N.E. Thompsonville, TX	Wilcox	20	140	75	32	4	10	Young, 1966
SUBMARINE CHANNEL AND FAN	Katy, TX	Wilcox	12	~1	100	32	25	80	De Paul, 1980
	McAllen Ranch, TX	Vicksburg	15	~1	60	30	15	27	Berg and others, 1979
	Port Arthur-Port Acres, TX	Hackberry	29	275	450	23	16	165*	Halbouty and Barber, 1961
	N.E. Thompsonville, TX	Wilcox	15	28	50	22	15	17	Berg and Tedford, 1977
	Port Arthur-Port Acres, TX	Hackberry	--	--	300	32	11	105*	Weise and others, 1981

*system scale

Table 3. Dimensions of non-Gulf Coast sand bodies.

	Area	Age	Poros. %	Perm. md	Thick. ft	Length ft x 10^3	Width ft x 10^3	Sand Vol. x 10^9 ft^3	Reference
FLUVIAL	Elk City field, Okla.	Pennsylvanian	10-15	75-1,500	50	10	4	2	Sneider and others, 1977
	Rhone River, France	Holocene	---	---	7	10	8	<1	Oomkens, 1970
	Clinton delta, Ohio	Silurian	---	---	20	16	2	<1	Overby and Henniger, 1971
	Coyote Creek field, Wyo.	Cretaceous	15	200	50	20	4	4	Berg and Davies, 1968
	Fry area, Ill.	Pennsylvanian	14-25	10-1,200	30	12	3	1	Hewitt and Morgan, 1965
DELTAIC	Clinton delta, Ohio	Silurian	---	---	35	64	11	25	Overby and Henniger, 1971
	Rhone delta, France	Holocene	---	---	33	163	65	350*	Oomkens, 1970
	Bartlesville Sandstone, Okla.	Pennsylvanian	---	---	50	475	158	3,752*	Visher and others, 1971
BARRIER	Elk City field, Okla.	Pennsylvanian	16-24	10-1,000	40	8	7	2	Sneider and others, 1977
	Bell Creek field, Mont.	--	---	---	20	60	7	8	Berg and Davies, 1968

Fluvial Sandstones

Along the Gulf Coastal Plain, fluvial channels differ from distributary channels in that the former commonly meander, whereas the latter are relatively stable owing to lower gradients and the mud-rich delta-plain deposits that inhibit lateral migration of the channels. Either channel type may contain clay plugs as abandoned channel fill. The locations of such major discontinuities are largely unpredictable unless well control is fairly dense. However, as shown by Galloway (1968) and others, clay plugs are well documented and easily distinguished on electric logs. Within a fluvial system, grain size generally decreases downstream, but at the scale of most reservoirs, vertical and cross-channel changes in grain size are more important to reservoir performance.

Mississippi River

Point-bar deposits of this major river were described by Frazier and Osanik (1961). They reported that sedimentary structures for the middle and lower point-bar deposits of the Mississippi River were mainly festoon crossbeds or large-scale scour and fill features. Moreover, their diagrams show rapid lateral thinning of fluvial sands and replacement by silts and clays deposited as natural levees and abandoned-channel fill. These fine-grained discontinuities would disrupt fluid flow across the sand body but would not necessarily interfere with fluid movement parallel to the channel axis.

The Mississippi River point-bar deposit described by Frazier and Osanik (1961) is 75 ft thick, about 5 mi wide, and contains approximately 40 billion ft^3 (Bcf) of sand. As expected, the dimensions and volume are large by comparison in other individual fluvial sands (table 1).

Rio Grande

Frequent discontinuities in fluvial sands were also recognized by Fulton (1975), who utilized numerous borings and electric logs to delineate the geometry of sandstone facies of the Rio Grande fluvial system. A cross section

(fig. 1) through the same stratigraphic interval studied by Fulton (1975) illustrates the thickness and continuity of Holocene and Pleistocene fluvial sands in a downstream (dip) direction.

Channels of the Holocene Rio Grande average 15 to 30 ft thick (table 1), progressively younger channels being thinner. Such chronological relationships are common where thin but areally extensive alluvial plain and upper delta-plain sediments were deposited over older and more stable fluvial deposits. Channel sands of late Pleistocene age vary widely in thickness owing to the abundance of clay plugs that separate thick fluvial sands (fig. 1). Channel sands up to 65 ft thick and containing about 800 Bcf of sand represent a major river system that built a relatively large delta (70 to 160 ft thick) that extended more than 50 mi along strike and more than 20 mi across the inner shelf. Because of their depositional setting, the late Pleistocene channels are probably good analogs for many of the Tertiary fluvial sandstones associated with stable platform deposits.

Brazos River

The Blasdel point bar of the Brazos River (Bernard and others, 1970) displays an upward-fining sequence accompanied by an upward decrease in scale of primary sedimentary structures. The vertical succession of structures from lower point-bar to floodbasin deposits is as follows: (1) large-scale trough cross-stratified sand with some minor clay partings separating foreset units, (2) horizontally stratified sand with interlaminated silt and clay, (3) small-scale trough cross-stratified sand and silt with clay drapes, and (4) laminated sandy clay and silt. The Blasdel point bar and the Wallis point bar, described by Morton and McGowen (1980), show that the thickness and frequency of mud partings increase toward the top of the deposit, and the proportion of mud to sand increases in a downstream direction. Correlation of the SP responses in these deposits (Bernard and others, 1970) indicates that most of the shale breaks are

discontinuous, but a few extend as much as several thousand feet normal to the channel axis.

Although individual point-bar deposits contain less than one Bcf of sand, the channel segments of which they are a part contain considerably more sand owing primarily to the greater length of the channel segment. One channel segment of the Modern Brazos River contains about 17 Bcf of sand, whereas the fluvial system contains about 600 Bcf of sand (table 1). By comparison, a part of the Pleistocene Brazos River system contains nearly twice as much sand (1,200 Bcf) because of greater meanderbelt width and slightly greater length (table 1).

Deltaic Sandstones

Sediment dispersal within a delta system is controlled largely by the interaction of astronomical tides, fluvial processes, oceanic waves, and littoral currents. In addition to these physical processes, the depth of water and the nature of underlying sediments also control the lateral extent of deltaic sand bodies. For example, sheetlike sand bodies are typical of shallow-water deltas (Fisk, 1955) deposited on shelf platforms with relatively stable substrates. Shallow-water deltas are also characterized by thin prodelta muds and relatively thick delta-plain sequences that contain numerous alluvial and distributary channels. These fluvial facies commonly account for the greatest volume of sand preserved in shallow-water deltas (Morton and Donaldson, 1978).

In contrast, sandstones deposited by deep-water deltas typically parallel the fluvial axes and are highly elongate. Thick bar-finger sands (Fisk, 1961) are protected from lateral reworking as they subside into the underlying prodelta/shelf and slope muds, which are unstable because of their great thickness, high water content, and relatively steep gradient. Under these conditions, sandstone continuity is disrupted by slumping, growth faulting, shale diapirism, and sediment deformation within the sand itself (Coleman and Garrison, 1977).

Patterns of sedimentation and their control on the distribution of sandy sediments within modern deltas are well known. Periods of active delta growth are interrupted by intervals of nondeposition or local mud deposition as distributaries become inactive and minor reworking of abandoned lobes begins. Subsequent reactivation of distributaries or renewed outbuilding marks the beginning of another delta construction cycle. The largest deltas of the northwest Gulf of Mexico (Mississippi, Brazos-Colorado, Rio Grande) are lobate to elongate, attesting to fluvial dominance, abundant sediment supply, and relatively low wave energy. Except for the Mississippi bird's-foot delta, which is building into deep water near the shelf edge, these deltas were deposited in shallow water following the Holocene transgression. Each of these fluvial-deltaic systems is fed by a large drainage area. These systems are analogous to the high-constructive deltas that prograded basinward throughout the Tertiary period. They are also substantially larger than the coastal plain rivers and deltas located between major depocenters.

Mississippi delta

The primary subdeltas of the Mississippi River are some of the most intensively studied deltaic deposits in the world. Areally extensive and closely spaced borings (Fisk, 1955, 1961; Scruton, 1960; Frazier, 1967, 1974) provide abundant control on the thickness, lateral extent, and textures of major deltaic sand bodies. Delta-front sands of the shoal-water Lafourche subdelta are relatively thin (25 to 50 ft) but widespread (>15 mi) along depositional strike and contain about 1 trillion ft^3 of sand (table 1). Delta-front sands grade upward from prodelta clayey silts with sand laminae to well-sorted sands. They are typically crossbedded, bioturbated, and interlaminated with thin layers of organic detritus as well as silt and clay (Gould, 1970).

In contrast, distributary-mouth bars of the bird's-foot delta are relatively thick (100 to 200 ft) but narrow (1 mi) ribbons of sand that parallel the distributary channel. Distributary-mouth bars coarsen upward and exhibit an upward decrease in thickness and frequency of silt and clay interbeds. Bar sands grade from interlaminated silts and sands with organic detritus to clean cross-bedded sand near the bar crest (Gould, 1970). As shown by Frazier (1967, 1974), the offlapping arrangement of deltaic facies causes physical disruptions in sand continuity even though delta-front and distributary-mouth bar sands appear at the same stratigraphic horizon.

Rio Grande delta

Similar disruptions in sand continuity occur in the ancestral Rio Grande delta complex. However, in contrast to the Mississippi delta, sand bodies within the elongate-lobate Rio Grande delta are thinner and less extensive. The largest delta-front sands are 5 to 15 ft thick and 2,500 to 4,500 ft wide, whereas other lenticular sands are less than 5 ft thick and 500 ft wide (fig. 1).

The underlying transgressive marine sand is thicker and laterally more continuous than any of the deltaic sands. It extends a minimum of 3 mi in a dip direction (fig. 1) and 10 mi along strike and contains about 25 Bcf of sand (table 1). This widespread unit may be partly a marine deposit and partly a reworking of the sandy fluvial facies of the preceding progradational cycle. Regardless of its origin, this sand body exhibits the greatest continuity of any individual sandstone within the Rio Grande system.

Brazos delta

Although naturally occurring wave-dominated deltas are absent in the northwestern Gulf of Mexico, the new Brazos delta (fig. 2) embodies many of the properties that are attributed to intensive marine reworking. The delta exhibits an upward-coarsening sequence of textures beginning with shelf and prodelta muds

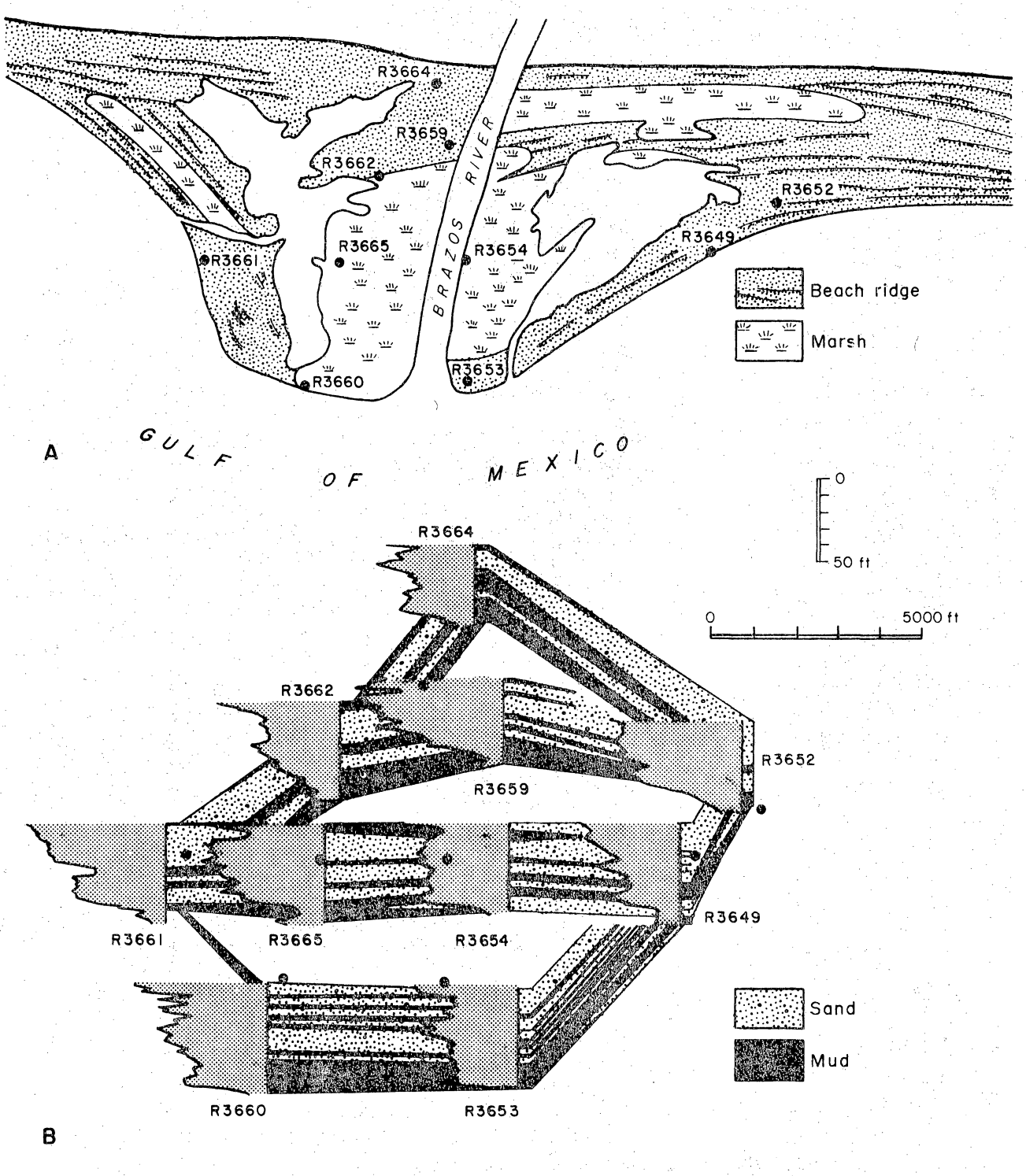

Figure 2. Subaerial distribution of subenvironments and subsurface distribution of sediment types in the new Brazos delta. SP patterns and boring locations from Bernard and others (1970).

and ending with shoreface and beach ridge sands that are products of winnowing by waves. On closer examination the SP curves and grain-size analyses (Bernard and others, 1970) show upward coarsening in the lower progradational facies followed by upward-fining aggradational sediments deposited in natural levee, marsh, and back-bar subenvironments. Ponds and swales between the beach ridges also trap mud that covers the delta plain during coastal flooding. Along some segments of the delta margin a thin, upward-coarsening sequence overlies the fine-grained delta-plain deposits where transgressive beach and washover sands were laid down during shoreline retreat. In plan view, the delta-plain environments occur in parallel and broadly arcuate-to-cuspate patterns that are characteristic of wave-dominated deltas (Fisher and others, 1969).

Successive periods of rapid sediment influx followed by wave reworking and sediment sorting give rise to clean, well-sorted sands that are interlaminated and interbedded with muds that disrupt the overall sand continuity. Because of the orderly arrangement of beach ridges and intervening swales, these zones of lower permeability may be laterally persistent, especially near the river mouth. The influence of high silt and clay concentrations introduced by riverine flooding progressively diminish away from the river mouth, where marine processes dominate over fluvial processes.

The new Brazos delta is a small geological feature, and yet it contains nearly 2 Bcf of sand. Naturally occurring wave-dominated deltas are substantially larger and have sand volumes which are several orders of magnitude greater. The Rhone delta, for example, contains about 350 Bcf of sand (table 3).

Barrier and Strandplain Sandstones

Barriers and strandplains are similar in environmental setting except that lagoons separate barriers from the mainland shoreline. These delta-flank or interdeltaic deposits are composed of sediments reworked from active and abandoned

deltas and transported away from the delta headlands and distributary mouths by littoral currents. Hence, barrier and strandplain sands are composed of well-sorted sands that grade seaward into shoreface sands and muds and landward into (1) washover sands and lagoonal muds (barriers) or (2) delta-plain sands and muds (strandplains). A feature common to barriers, strandplains, and wave-dominated deltas is the upward-coarsening shoreface profile of textures and sedimentary structures. Apart from this shared characteristic, barriers and strandplains are morphologically different landforms although one may grade into another.

Barrier and strandplain sediments with the greatest potential for preservation are deposited on the shoreface that extends from submarine depths of 30 to 45 ft to the intertidal zone. Landward increases in physical energy across the shoreface are reflected in slope, morphology, and sediment textures. The seafloor of the lower shoreface is composed of muds and sandy muds that are featureless and merge seaward with muddy slopes of the inner continental shelf. The upper shoreface, however, is a dynamic area where bars are constructed and destroyed or driven landward by wave processes in conjunction with tidal and wind-driven currents. Upper shoreface sediments are typically composed of fine to very fine sand with local shell concentrations. If preserved, the sedimentary structures are low-angle, parallel-inclined laminations, irregular scour and fill, and stratification types formed by vertical accretion and migration of breaker bars and troughs. These include horizontal parallel laminations of the bar crest as well as ripple cross-laminations and foresets. On high-energy coasts that experience seasonal changes, physical structures are commonly preserved; however, on low-energy coasts, such as the Gulf Coast, abundant nearshore infauna effectively rework the sediments and destroy much of the stratification.

Along many coastal areas, erosional (transgressive) and accretionary (regressive) barriers occupy orderly positions relative to active and abandoned delta lobes. More often than not, delta headlands grade laterally into transgressive barriers, which in turn grade into regressive barriers. The transition from transgressive to regressive landforms can cover a shoreline distance from a few thousand feet to tens of miles. Transgressive and regressive barriers can be distinguished on the basis of geologic history, surficial morphology, and lateral facies relationships. This distinction is important for predicting the sedimentary properties and inferred reservoir characteristics of preserved barrier deposits. The spectrum of barrier settings and associated sand facies is represented by Padre Island, Galveston Island, and South Padre Island in Texas and Grand Isle in Louisiana.

Padre Island

Barrier sands of Padre Island stretch unbroken from the Rio Grande to the central Texas coast, a distance of over 100 mi. The central and northern parts of the barrier are 3 to 10 mi wide. Sand thicknesses of 35 to 60 ft have been reported (Fisk, 1959; Dickinson and others, 1972) from areas where the barrier has been stable for the past few thousand years. According to Fisk (1959), Padre Island grew vertically as sea level rose, and grew seaward after sea level stabilized. Regardless of the vertical aggradation, total thickness of the barrier sands is similar to that of other Gulf Coast barriers that accreted seaward much greater distances than did Padre Island.

A large volume of laterally continuous sand composes Padre Island and the other barrier islands between the Holocene Brazos-Colorado and Rio Grande deltas (table 1). Barrier chains of comparable length occur elsewhere, but the Texas barriers are probably unsurpassed in content of clean, well-sorted sand. Recurrence of this barrier system in the same geographic area throughout the Tertiary

is attributed to the San Marcos Arch, an area of lesser subsidence between the Rio Grande and Houston Embayments.

Galveston Island

Borings and SP logs through Galveston Island (Bernard and others, 1970) show distinctly different vertical sequences for eastern (regressive) and western (transgressive) segments. A classical offlap sequence is preserved on east Galveston Island where accretion ridges are prominent. Along this segment, lower shoreface and shelf deposits of bioturbated and interlaminated shelly sand and mud grade laterally and upward into horizontal and low-angle cross-stratified barrier and upper shoreface sand containing thin shell beds. On west Galveston Island, the Pleistocene-Holocene unconformity is overlain by Brazos River prodelta mud which, in turn, is overlain by a thin interval of barrier-island and shoreface sands and muds.

Barrier sands beneath Galveston Island range in thickness from 15 to 50 ft. Sand thickness progressively increases eastward from the Brazos delta. The lenticular sand body is 1 to 2.5 mi wide and about 26 mi long (Bernard and others, 1970). Of the total volume of sand in the barrier, Bernard and others (1970) estimated about 50 Bcf is clean sand.

The depositional model of Galveston Island suggests that barrier sands are best developed progressively farther away from the delta with which they are associated. This appears to be supported by field evidence along the Texas coast and elsewhere.

Grand Isle

Like Galveston Island, Grand Isle is a delta-margin barrier with both transgressive and regressive features. Moreover, the lens of fine-grained sand beneath Grand Isle thickens eastward from 10 ft to nearly 60 ft (Fisk, 1955) in a pattern remarkably similar to that seen at Galveston Island (Bernard and others, 1970). However, the greatest thicknesses of sand beneath Grand Isle are

actually a composite of individual sand lenses, each between 20 and 30 ft thick (Conatser, 1971). Individual sand lenses each contain about 2 Bcf of sand, whereas the aggregate volume of sand for the vertically stacked lenses includes about 8 Bcf.

South Padre Island

Barrier islands fronting the Rio Grande delta represent delta destruction and transgressive marine deposition that followed delta abandonment. On South Padre Island, barrier sands 10 to 15 ft thick overlie delta-plain deposits (fig. 1). The subaerial part of the barrier is 2,000 to 15,000 ft wide and extends a minimum of 20 mi along depositional strike.

Typical sedimentary structures of the barrier sands are horizontal and low-angle parallel-laminations with subordinate scour and fill and rare foresets, and small-scale ripple cross-laminations. Sands are mainly fine to very fine grained, and textural changes within the sands are primarily related to the presence or absence of shell fragments. The thin sand facies interfingers with and overlies lagoon muds and interbedded algal-bound sands and muds deposited on wind-tidal flats and washover fans.

Ingleside Strandplain

During the late Quaternary Period, abundant sand was supplied to the Texas coast by coalescing deltas with broad sand-rich meandering streams. Accumulation of the sand along a stable aggrading coastline formed a 10-mi wide strandplain system that extended more than 100 mi along strike and contained slightly more than 1.5 trillion ft^3 of sand (table 1). The Ingleside strandplain occupied an area that is currently the site of several modern barrier islands that are separated from the Pleistocene strandplain by lagoons. This present-day example of stratigraphically juxtaposed or stacked barrier sequences produces a sand body greater than 60 ft thick beneath San José and Padre Islands. The Ingleside strandplain is of comparable thickness where it is buried and

unmodified by surficial erosion. This suggests that the Ingleside itself may be a composite of vertically aggraded and laterally accreted barrier-strandplain deposits (Winker, 1979).

Shelf-Slope Sandstones

Unlike those of the other sandstone facies, sedimentary models of shelf and slope sandstones were not developed from the northwestern Gulf Coast region mainly because submarine canyons and fans are not presently active along the continental margin of the area.

Short cores from the Mississippi fan and deeper parts of the central Gulf of Mexico contain mostly mud; the few sands present exhibit turbidite characteristics (Bouma, 1968). Classical turbidites described by Bouma (1962) have been interpreted by Walker (1979) as being outer suprafan deposits. The sand sequences are usually widespread but thin bedded (1 to 3 ft) and fine upward. The sands themselves can be either well sorted by high velocity turbidity currents or contain considerable mud owing to gravity-induced slumping and high concentration of suspended sediment. Thick sand sequences deposited by coalescing and aggrading submarine channels provide the best reservoirs in deep-water sediments. Although they are well documented in the rock record, these channel sands have not been cored in Quaternary sediments of the Gulf of Mexico.

Tertiary Sediments

Direct comparison of modern sand bodies with ancient examples is difficult owing to a paucity of detailed core descriptions and other sedimentological properties for the Tertiary sandstones. Nearly all the published studies rely principally on stratigraphic cross sections, isopach maps or both; some also include fence diagrams or grain-size analyses. Remarkably few include core descriptions or plots of sedimentary structures and pore properties.

The environmental groupings of Tertiary sandstones (table 2) are tentative. For example, Wilcox sands in the Katy field have been interpreted as delta fronts (Fisher and McGowen, 1967; Williams and others, 1974) and as turbidites (Berg and Findley, 1973; DePaul, 1980), whereas Wilcox sands in the Northeast Thompsonville field have been interpreted as barriers (Young, 1966) and as submarine fans (Berg and Tedford, 1977). Furthermore, Hackberry sands in the Port Acres-Port Arthur area have been interpreted as deltaic deposits (Halbouty and Barber, 1961) and as submarine channels (Berg and Powers, 1980). The interpreted deep-water origin of the Hackberry sandstones appears valid on the basis of regional depositional setting (Paine, 1971); however, recent work (Edwards, 1980, 1981) confirms that sandstones of the Wilcox Group were deposited primarily in shallow water.

Although the depositional environment of the Tertiary sandstones is uncertain, table 2 provides reasonable estimates of ancient sandstone dimensions and volumes. The volumetric estimates agree with estimates for modern analogs at the same hierarchical level. Individual sand bodies (third level) contain from 10^9 to 10^{11} ft^3 of sand, whereas sand systems (first level) contain from 10^{11} to 10^{13} ft^3 of sand.

Fluvial Sandstones

Tertiary sandstones interpreted as fluvial deposits characteristically have dendritic and elongate isopach patterns oriented normal to depositional strike. Many of these sand bodies exhibit upward-fining textures and upward increases in shaliness as shown by SP log patterns. In plan view, grain size also tends to decrease toward the channel axis (Nanz, 1954), probably reflecting the presence of fine-grained abandoned channel fill.

Individual fluvial channels are a few thousand feet to a few miles wide, 3 to 8 mi long, and 35 to 60 ft thick (table 2). Greater thicknesses may develop

near distributary mouths where unstable prodelta muds promote sandstone subsidence and vertical aggradation (Fisk, 1961). Apparently, sand volumes of 20 to 40 Bcf are typical of meandering alluvial channels, whereas smaller coastal plain streams or minor, laterally restricted distributary channels are an order of magnitude smaller. The few dimensional data for fluvial systems suggest that differences in volume (1 to 4 trillion ft^3) result mainly from differences in meanderbelt width, which may vary from 7 to 16 miles.

Deltaic Sandstones

Despite their importance in the Gulf Coast Basin, only a few individual Tertiary sandstones of deltaic origin have been described in the literature, none in detail. Most published examples of deltaic sandstones are partial or complete delta systems (table 2) rather than individual sandstones. Progradational sequences recorded on electric logs contain 10 to 40 percent sandstone. The sandstones are arranged in elongate to lobate patterns that reflect sediment dispersal by fluvial and marine processes. The sandstones grade updip and laterally into shales and thin sandstones deposited in delta-plain and interdistributary bay environments. They also grade downdip into prodelta shales.

Upward increases in sand-bed thickness and upward decreases in shaliness are typical of these regressive deposits. The sandstones are laminated and crossbedded, and carbonaceous material is common.

Individual sandstones deposited in delta-front and delta-fringe environments are typically 3 to 7 mi wide, and 14 to 20 mi long (table 2) with corresponding sand volumes of 100 to 200 Bcf. In contrast, deltaic systems are 100 to 500 ft thick, 10 to 30 mi wide, and 20 to 130 mi long. Sand volumes for these deltaic systems range from 2 to 20 trillion ft^3, a range similar to that of the barrier-strandplain systems. The similarity in range may be explained by

the depositional similarities between barrier-strandplain systems and wave-dominated deltas.

Barrier and Strandplain Sandstones

Tertiary barrier and strandplain sandstones are identified mainly by elongate and lenticular isopach patterns that parallel depositional strike. Other corroborating evidence includes well-sorted sands with uniform or upward-coarsening textures and concomitant upward or central increases in permeability. Some sand bodies interpreted as barriers grade landward into fine-grained sandstones and carbonaceous mudstones and shales that probably represent marsh deposits. These same sand bodies grade seaward into fine-grained shelf deposits.

The dimensions of individual barrier and strandplain sands cover a broad range, even though the volumes of both sand types are 10 Bcf or less (table 2). Barrier sands are 15 to 75 ft thick, a few thousand feet to a few miles wide, and 2 to 8 mi long, although the latter dimension is arbitrary because of map boundaries. Barrier systems are 450 to 1,000 ft thick, about 10 mi wide, 40 to 60 mi long, and contain from 5 to 25 trillion ft^3 of sand. Variable thicknesses of the barrier system are largely responsible for the differences in sandstone volume.

Shelf-Slope Sandstones

Outer shelf and upper slope sediments formed by turbidity currents are widely recognized in deep-water deposits such as the Hackberry sandstones. These submarine channel and fan deposits typically have narrow, dip-trending, elongate to digitate patterns in areas of maximum net sandstone. Considering the entire depositional interval, sandstone thickness diminishes upward and shale bed frequency and thickness increase upward. The sandstones also grade laterally into shale with thin interbedded sandstones and siltstones that

comprise the fan deposits. Both massive sands with abrupt bases and thin-bedded sandstones show textural gradations. Grain sizes range from coarse to fine; the average grain size is fine-grained sand. Internal stratification varies greatly, and the sandstones are typically laminated, rippled, or contorted and occasionally bioturbated. These sedimentary structures are not unique to deep-water deposits; hence, turbidite interpretations should also be supported by faunal evidence.

Available data suggest that the outer-shelf and upper-slope sandstones are remarkably uniform in size considering the limited number of examples (table 2). The individual sandstones are 3 to 5 mi wide, 4 to 6 mi long, and 50 to 100 ft thick; corresponding sand volumes are 30 to 80 billion ft^3. The dimension that distinguishes shelf/slope systems from individual sandstone units is thickness. Genetically related turbidite systems are 300 to 450 ft thick and contain about 100 to 150 billion ft^3 of sand-size sediment. These volumes are 2 to 3 orders of magnitude less than sand volumes estimated for other depositional systems (table 2).

Sediments of Other Ages

A brief examination of the literature indicates that some sandstones from the Appalachian, Rocky Mountain, and mid-continent regions of the United States are not unlike Tertiary Gulf Coast sandstones. In fact, sandstones of Paleozoic and Mesozoic age have dimensions (table 3) and sedimentary properties that are similar to Cenozoic sandstones of comparable origin (tables 1 and 2). Sand volumes of individual sandstones and sandstone systems are within the same ranges as Tertiary examples, albeit on the low end, suggesting somewhat smaller sand bodies; however, the number of examples is too small to be conclusive.

FAULT COMPARTMENT AREAS

The volumes of Gulf Coast reservoirs are, as mentioned above, determined by depositional sand-body geometries, the areas of fault compartments, and by internal permeability barriers. The second of these factors, the size and geometry of fault compartments, can be further examined as a function of position within the Gulf Coast geopressure trends.

To examine data for the second hierarchical level (fault area), published and unpublished regional structure maps at depths of interest for geopressured sediments were assembled. For the Wilcox fairways of South and Central Texas, the structure maps presented by Bebout and others (1979) for top of Wilcox (for Zapata, Duval, and Live Oak fairways) and top of lower Wilcox (for De Witt and Colorado fairways) were used with slight modification. A structure map for the Bee delta system (top of Wilcox) was taken from Weise and others (1981). For the Frio fairways of the central Gulf Coast (Nueces, Matagorda, and Brazoria fairways), commercial structure maps (Geomaps) of the top of the Frio were used in conjunction with published structure mapping of Bebout and others (1978) in the Brazoria fairway.

On each of these regional structure maps, fault compartment areas were measured by planimeter for all the fault compartments shown. This amounted to 90 compartments in the Wilcox fairways and 116 compartments in the Frio fairways.

The Wilcox data are presented in table 4 and figure 3a. A wide range of compartment areas is represented, ranging from 0.4 mi^2 to 52 mi^2. Seventy percent of all the compartments lie between 1.5 mi^2 and 29 mi^2. The distribution of areas is highly skewed toward small areas, but the distribution of log area is nearly uniform. The median area is 9.3 mi^2 and the mean is 15 mi^2.

Table 4. Areas of fault compartments in Wilcox geopressured fairways.

	Zapata fwy.	Duval fwy.	Live Oak fwy.	Bee delta	DeWitt fwy.	Colorado fwy.	Overall
Small							
Number	3	2	8	2	13	1	29
Percent of all	21	11	42	18	59	17	32
Mean area	2.0	1.7	1.5	3.1	1.5	0.8	1.7
Medium							
Number	6	7	8	4	7	5	37
Percent of all	43	39	42	36	32	83	41
Mean area	9.7	8.6	10.4	13.1	7.0	16.5	10.4
Large							
Number	5	9	3	5	2	0	24
Percent of all	36	50	16	45	9	0	27
Mean area	43.8	28.3	26.4	38.8	29.0	--	36.9
Overall							
Number	14	18	19	11	22	6	90
Mean area	20.2	17.6	24.1	23.0	5.8	13.9	14.7
Median area	13.0	18.1	6.1	16.7	2.6	16.3	9.3
84% greater than	2.5	3.7	1.2	3.3	0.8	0.8	1.5
84% less than	44.0	32.3	17.5	29.2	7.8	18.5	28.6

All areas in mi^2. Small blocks are less than 4 mi^2 (10 km^2); medium blocks are 4 to 20 mi^2, and large blocks are more than 20 mi^2 (50 km^2).

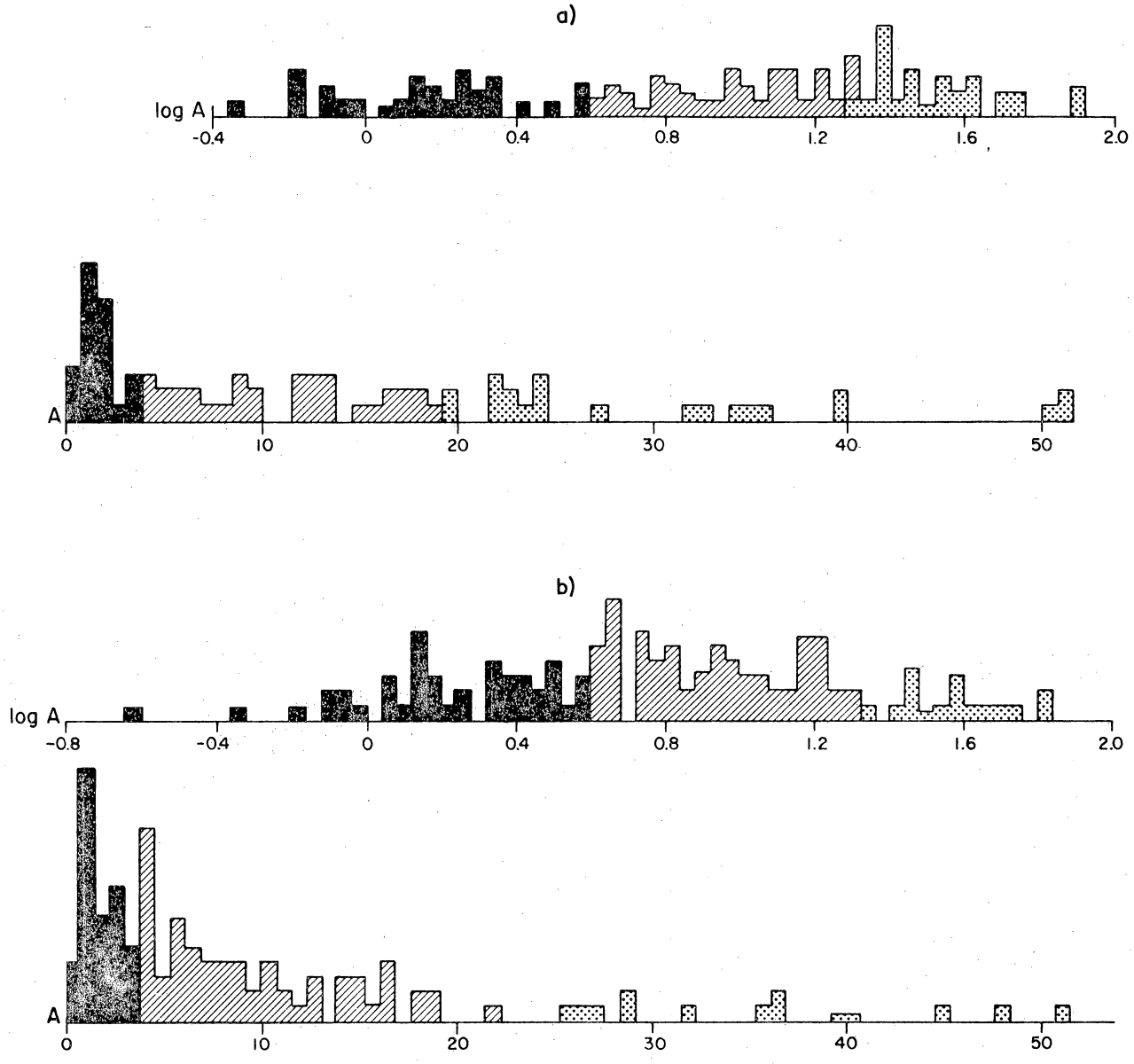

Figure 3. Histograms of fault compartment areas, showing the lognormal distribution of (a) Wilcox compartments, Lower and Middle Texas Gulf Coast, and (b) Frio compartments, Middle Texas Gulf Coast (between Corpus Christi and Brazoria fairways). Area in mi^2.

The distribution of fault compartment areas along the growth fault trend shows no distinct variations. The percentage of large compartments seems to be greater south of the Bee delta than in the De Witt and Colorado fairways, but this may be due to the smaller scale and the different datum of the structural maps in South Texas. The distribution of areas in each Wilcox fairway is skewed toward small areas, the mean being greater than the median in all except the Duval and Colorado fairways. The range of areas is generally similar; the higher limit is greatly dependent on definition of the closure of large fault blocks.

The Frio data are presented in table 5 and figure 3b. Again, there is a wide range of values from 0.3 mi^2 to 52 mi^2. The overall distribution is skewed toward small areas, and the mean area of 12 mi^2 is significantly greater than the median area of 5.8 mi^2. The histogram of areas plotted as log area (fig. 3) shows that the distribution is close to lognormal.

The Frio data, like the Wilcox data, show no distinct variations with respect to position on the growth fault trend within the area studied. Percentages of large fault compartments fluctuate widely, owing largely to the problems of defining closure of large compartments. The area distribution in each part of the trend is skewed toward small areas and is probably lognormal.

The overall values for Wilcox and Frio fault compartment areas are similar, with a median of 9.3 mi^2 for the Wilcox, as compared to 5.7 mi^2 for the Frio. The somewhat smaller size of Frio compartments is in part due to the smaller scale of most Wilcox structure maps used. The irregular distribution of Wilcox areas differs from the lognormal Frio distribution only by the lesser occurrence of areas of about 4 mi^2.

There are limitations to estimating the area distribution by the means used here. First, the compartment areas measured are the result of the construction of the structure maps. This is an uncertain process whose accuracy is dependent

Table 5. Areas of fault compartments in Frio geopressured fairways.

	Kleberg	Nueces	San Patricio	Refugio Aransas	Calhoun Jackson	Matagorda	Brazoria	Overall
Small								
Number	3	5	5	8	0	3	8	32
Percent of all	30	33	62	50	0	10	27	28
Mean area	3.0	2.2	1.2	2.0	--	2.6	2.2	2.2
Medium								
Number	6	7	3	8	7	19	17	67
Percent of all	60	47	38	50	86	66	56	58
Mean area	11.1	9.3	4.9	5.9	11.2	9.7	9.0	9.3
Large								
Number	1	3	0	0	1	7	5	17
Percent of all	10	20	0	0	13	24	17	15
Mean area	40.0	41.5	--	--	64.9	34.7	42.1	42.7
Overall								
Number	10	15	8	16	8	29	30	116
Mean area	11.5	13.4	2.6	3.9	18.0	15.6	12.7	11.9
Median area	10.6	6.5	1.5	3.9	12.8	10.9	6.3	5.7
84% greater than	2.9	1.4	0.7	1.1	4.5	4.1	2.3	1.5
84% less than	15.6	21.9	4.5	6.7	18.9	27.7	20.7	17.6

All areas in mi^2. Small blocks are less than 4 mi^2 (10 km^2); medium blocks are 4 to 20 mi^2, and large blocks are more than 20 mi^2 (50 km^2).

on adequate well control. Further, the degree to which fault blocks are differentiated (that is, which faults are considered significant) depends on the scale of mapping; smaller scale maps yield larger fault blocks. Finally, the largest fault blocks are not closed but are part of large indeterminate areas of unfaulted terrain. In general, however, the mean and median values derived here are approximations of the most probable size of fault compartment to be found in the Texas Gulf Coast geopressure trends. Note the order-of-magnitude similarity to the areas covered by typical sand bodies.

COMPARISON OF PRODUCTION AND GEOLOGIC ESTIMATES OF AQUIFER VOLUME

Nine geopressured gas fields were studied in detail to obtain volumetric estimates of reservoirs within a fault-bounded sandstone (fourth hierarchical level) and to gain additional insight into reservoir continuity in the geopressured zone. Eight of these fields were selected and analyzed by C. K. GeoEnergy (Boardman, 1980) to give estimates of aquifer volume and area from gas production and pressure data (fig. 4). Similar calculations were made for a ninth field (Mobil David "L" block, Nueces County). The fields represent three water-drive and four pressure-depletion reservoirs in the Wilcox Group and two depletion-drive reservoirs in the Frio Formation.

The distribution of these nine reservoirs (fig. 5) is less than ideal for a regional study of reservoir parameters. They were chosen largely because they: (1) contained a small number of producing wells and (2) are close to geothermal prospect areas. Five of the nine are from a single Wilcox fairway, the De Witt fairway. Given this erratic distribution, the studies presented here should be considered as case histories. They serve largely to provide insight into possible factors affecting reservoir continuity and as a check on the accuracy of geologic estimates of reservoir volume.

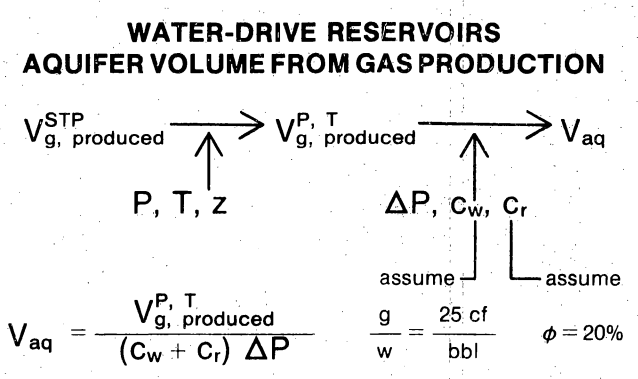

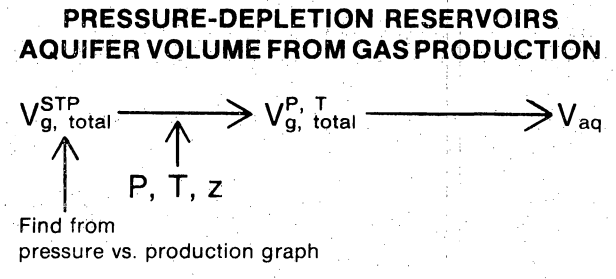

Figure 4. Calculation procedures for estimating aquifer volume from production data for (a) water-drive reservoirs, and (b) pressure-depletion reservoirs.

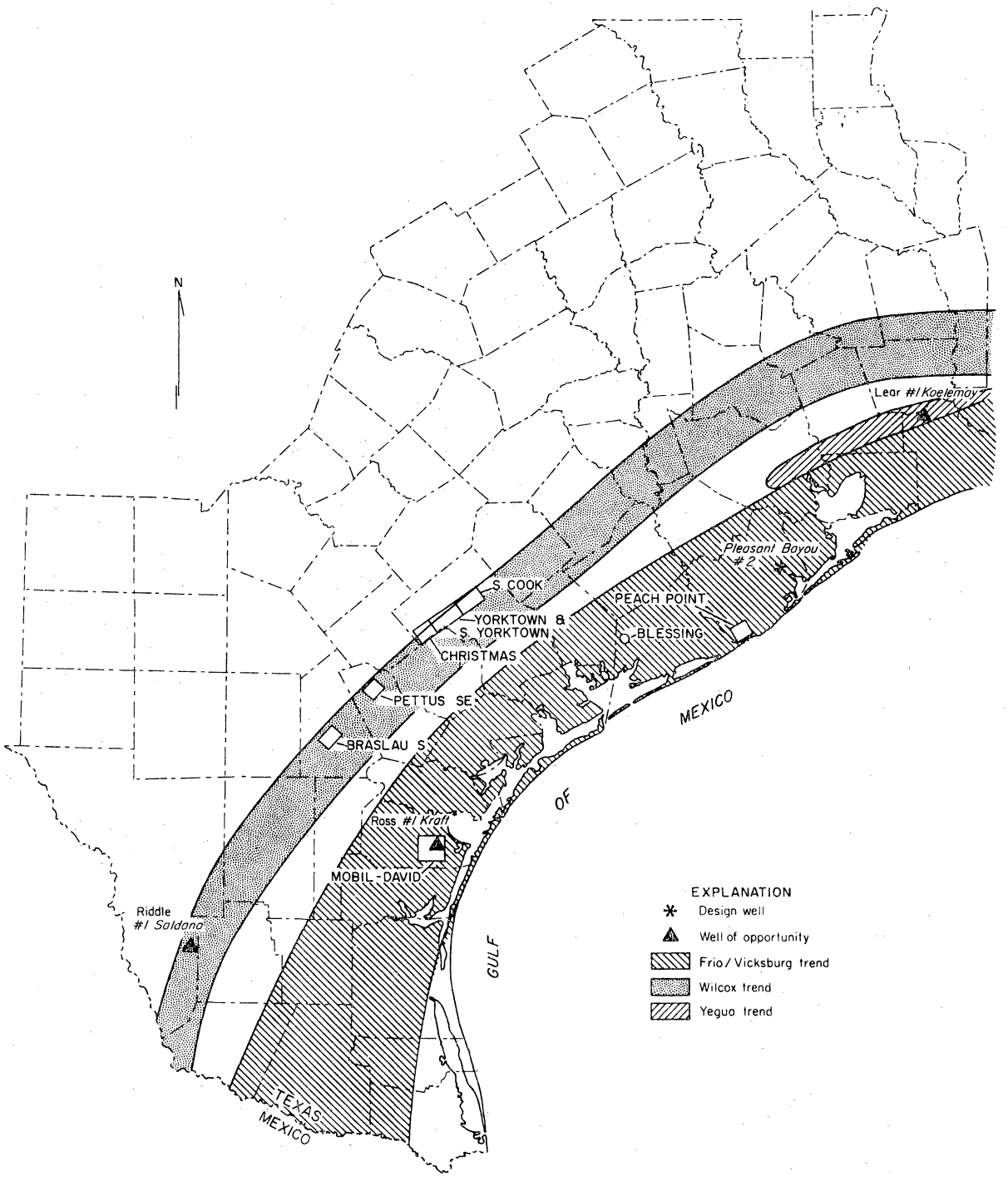

Figure 5. Location of geopressured trends, geothermal test wells, and areas studied for this report, Texas Gulf Coast.

Calculation of Aquifer Volume from Production Data

The procedures for calculation of aquifer volume from production data have been briefly summarized by Boardman (1980). Information for that study was obtained from semiannual 24-hour shut-in wellhead pressures reported to the Texas Railroad Commission; only annual readings were used. After the data were obtained, it was decided whether the reservoir is driven by water or pressure depletion. This was done largely on the basis of consultation with the companies concerned.

For water-drive reservoirs (that is, large reservoirs with a gas/water contact), the technique developed by Stuart (1970) was used to calculate water volume (Vaq) (fig. 4a). In this method the produced gas volume is first converted to gas in place. Then, assuming a gas saturation of 25 ft^3/bbl of water at a standard temperature and pressure and a porosity of about 20 percent (needed to determine the rock compressibility, Cr), the aquifer volume is estimated by a simple equation.

For pressure-depletion reservoirs (that is, smaller reservoirs with no water contact which are produced by gas pressure only, figure 4b), the decline in bottom-hole pressure as corrected for compressibility (BHP/z) with gas production should be linear. An extrapolation to zero pressure gives an estimate of total gas volume in the reservoir. This volume is corrected to gas in place. Then, assuming a water saturation of 25 percent, the aquifer volume is obtained (Craft and Hawkins, 1959, p. 40-43).

The estimates obtained by these methods (table 6) are sensitive to the assumptions and values used. If a reservoir is misclassified, an order-of-magnitude difference in aquifer volume can result. However, such misclassifications are unlikely in the cases presented here. Other variations that could affect production estimates are inaccuracies in pressure and temperature of the

Table 6. Volume estimates for geopressured gas reservoirs, Texas Gulf Coast.

Name, county sand, depth	Primary geologic estimates				Production ests.		Comparison	
	Area (mi^2)	V_{res}(Bcf)	V_{aq}(MMbbl)	Porosity	V_{aq}(MMbbl)	Drive	Eff. %	Revision:
Pettus SE, Bee Co. First Massive, 9,000'	2.04-4.26	4.56-9.52	130-270	16%	28±2	pd	23-10	thin shale breaks V_{aq}=60-120MMbbl
Braslau S, Live Oak Co. First Tom Lyne, 9,000'	2.82-3.92	5.15-6.99	139-212	16%	61±14	pd	71-27	thin shale breaks
S. Cook, De Witt Co. 'B' sand, 10,850'	7.35-14.71	9.84-32.14	351-794	20%	588	w	168-74	none
S. Cook, De Witt Co. 'C' sand, 10,900'	8.75-26.01	17.9-58.0	638-2066	20%	207	w	32-10	thin shale break
Yorktown, De Witt Co. Migura, 11,000'	3.71	9.8-10.5	284-302	14%	576	w	203-191	connection to S V_{aq}=565-606 MMbbl
Yorktown S, De Witt Co. Migura, 10,800'	1.96-2.87	4.2-5.0	151-180	14%	82±14	pd	56-47	breaks?
Christmas, De Witt Co. Migura, 10,800'	2.35	4.0-8.0	100-250	14%	49±1	pd	50-19	poor control
Peach Point S, Brazoria Co. Frio 'A', 11,250'	0.61	0.72	19	15%	33±3	pd	175	connection to S
Mobil-David "L", Nueces Co. Anderson, 11,100'	1.22	4.25-4.75	182-203	24%	185-290	pd		none

Production estimates for water-drive reservoirs from C. Boardman (1980), using the method of Stuart (1970).
Area is area of fault compartment or equivalent. V_{res} is sand volume; V_{aq} is aquifer volume.
Drives: pd is pressure depletion, w is water.
Eff. is ratio of production estimate to geologic estimate of V_{aq}, and is a measure of that part of the sand connected with the wells.

reservoir (affecting the conversion to gas in place), scatter of points on a BHP/z versus production graph, changes in the gas/water ratio or water saturation, and porosity variation.

The production estimates reported by Boardman (1980) for pressure-depletion reservoirs (that is, for six of the nine reservoirs studied) were recalculated for several reasons:

(1) to incorporate all of the semiannual shut-in data since 1972, thus providing a more accurate picture of pressure decline;

(2) to study the behavior of individual wells in the fields;

(3) to use porosity values more appropriate to the reservoirs considered; and

(4) to provide error limits on the projected total gas in the reservoir, as derived from a least-squares linear regression on the data points.

All of the results presented in this report for pressure-depletion reservoirs (table 6) are recalculated values.

South Cook Field

The South Cook field contains the type well of the Cuero study area of Bebout and others (1979). The producing sands are the B and C correlation intervals of the lower Wilcox Group. Temperatures in the reservoirs are about 275°F. Shut-in pressure was originally 7,100 psi, giving a pressure gradient of 0.65 psi/ft. Porosity in the reservoir is about 20 percent, as measured in the Atlantic #1 Schorre well (Bebout and others, 1979).

Stratigraphy of Producing Sands

The B and C (10,850 ft and 10,900 ft) sands occur at the top of the lower Wilcox Group and form the upper units of the Rockdale delta system in the area. The geometry of the sand facies is influenced by syndepositional faulting. In

the fault block of interest, the sands are dip-oriented and were deposited by distributary channels extending southeast from the delta plain. These channels may or may not have been interconnected.

Four dip-oriented sand thicks in the B sand can be identified (fig. 6). The westernmost, the producing sand in the South Cook field, runs nearly north-south across the southwestern part of the fault block. Interpretation of whole core from the Atlantic #1 Schorre well suggests that the sand formed in a distributary-channel setting (Winker and others, 1981).

There are two dip-oriented depocenters in the C sand (fig. 7); only the western one is under South Cook field. Interpretation of core from the Atlantic #1 Schorre well suggests that the lower part of the sand formed in a distributary-channel setting and the upper part in a channel- and distributary-mouth-bar setting (Winker and others, 1981). The two parts are separated by a thin (2 to 3 ft) shale break. The E-log characters of the B and C intervals at the Atlantic #1 Schorre well are shown in figure 9.

Structure of the South Cook Area

The South Cook area lies within the trend of lower Wilcox growth faulting. The field is located on a slight rollover anticline within an elongate fault compartment up to 25 mi^2 in area. Large, well-defined faults to the northwest, south, and southeast isolate the compartment. The northeastern boundary of the fault compartment is less well determined. The eastern extremity of the compartment shown on figures 6 and 7 may be separated by a smaller fault (not shown) from the South Cook compartment proper. More information on the structure of the area is given in Bebout and others (1979) and Winker and others (1981).

Reservoir Volume - B Sand

The sand volumes for each channel (fig. 6) are (from west to east) 5.05 billion ft^3 (Bcf), 4.8 Bcf, 12.5 Bcf, and 15.8 Bcf. Estimated aquifer volume

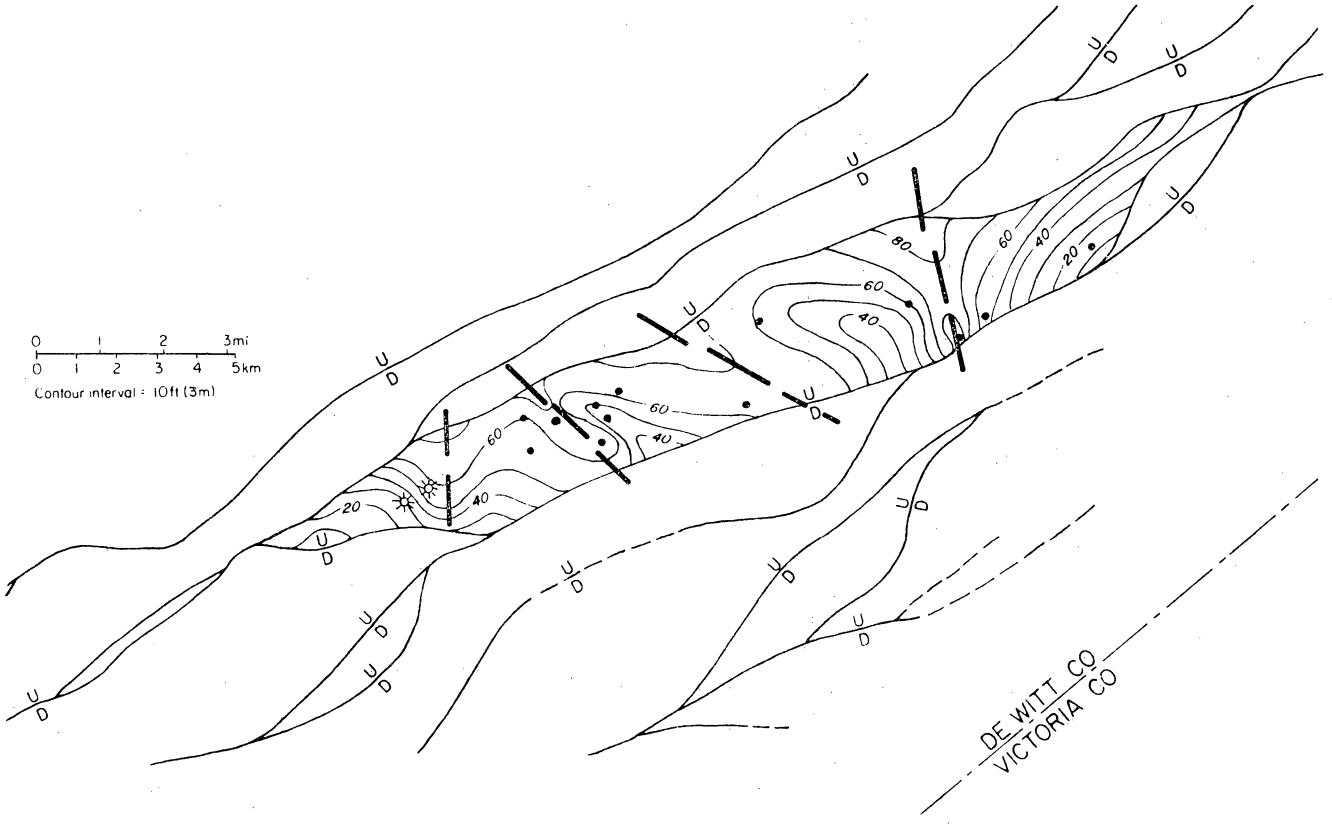

Figure 6. Net-sand map, "B" sand, South Cook field. Channel axes shown. From Bebout and others (1979).

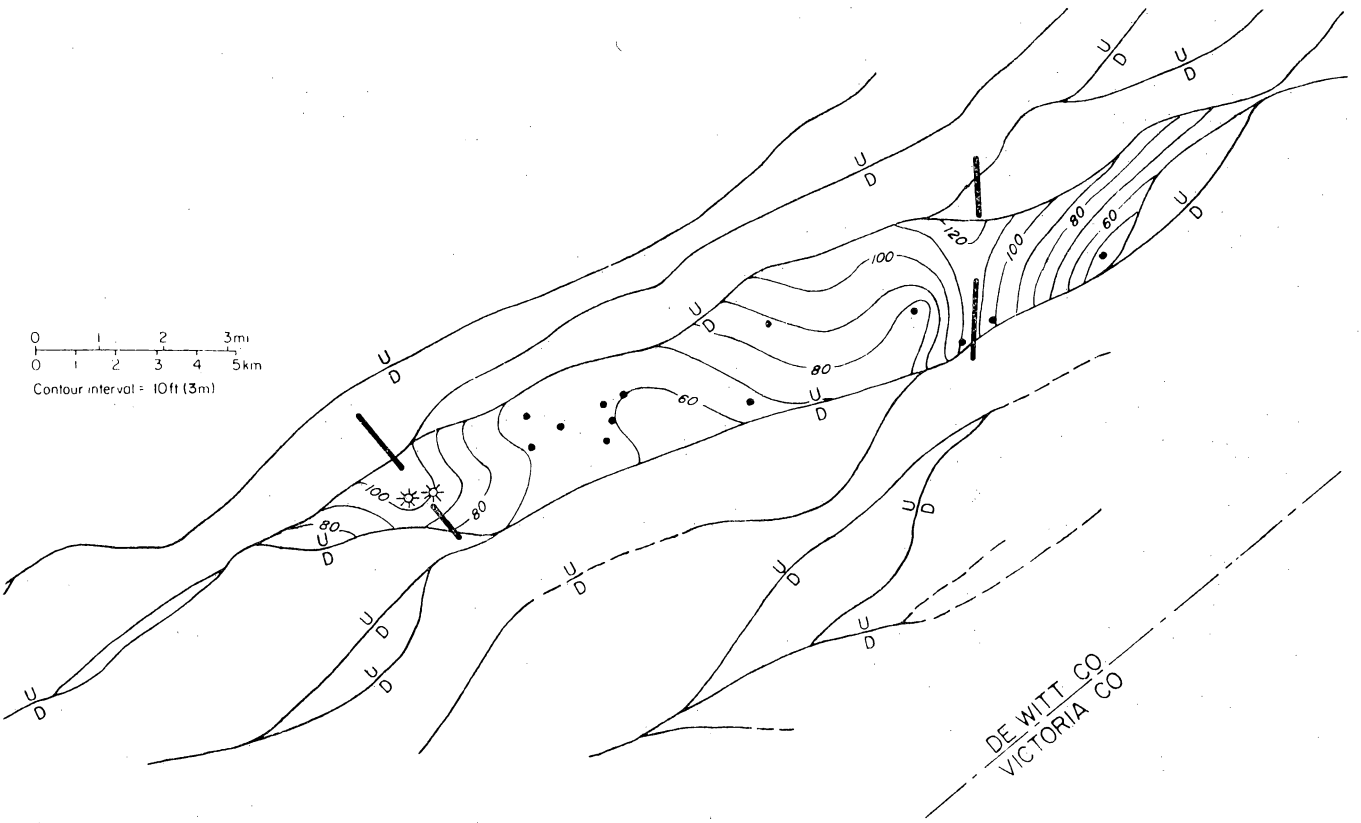

Figure 7. Net-sand map, "C" sand, South Cook field. Channel axes shown. From Bebout and others (1979). Channel axes shown.

(at 20 percent porosity) for these channels is 180, 170, 440, and 560 million barrels, respectively. The aquifer volume estimate from gas production from the B sand in this water-drive reservoir is 588 million barrels. This value is within the range of values of geologic estimates.

The production estimate, if correct, requires that several of the B sand thicks are being produced. The western channel, in which South Cook field is located, must be connected with at least the next channel to the east and probably the next, as well. In the latter case the ratio for production estimate to geologic estimate would be 75 percent. Possibly, thin sands in the B interval are not connected to the main sand body.

Reservoir Volume - C Sand

Sand volumes measured for each channel (fig. 7) show that the western (South Cook) channel contains about 18 Bcf of sand, giving an aquifer volume of 638 million barrels. The eastern channel contains 40 Bcf of sand, giving an aquifer volume of 1,430 million barrels. The production estimate of aquifer volume for this water-drive reservoir is 207 million barrels. Production volume is less than one-third of the geologic estimate for this sand, even if only the western channel is considered.

The discrepancy can be explained by the thin shale break noted above in the Atlantic #1 Schorre well. This break can be correlated throughout the area of the western channel. The three producing wells from this interval tap only the distributary-channel sand below the shale break. This lower sand pinches out within a short distance northeast of the field; its volume is about one-third of the western channel sand volume taken from figure 7. The production estimate, therefore, indicates that the upper and lower parts of the C sand are not connected.

Summary

The B and C sands at South Cook represent distributary-channel and related sands that prograded across a growth-faulted zone. The B sand has good lateral continuity between channels, while the C sand shows poor lateral continuity, and vertical continuity limited by a thin shale.

Yorktown and South Yorktown Fields

The Yorktown and South Yorktown fields (fig. 5) are located southeast of Yorktown in De Witt County. Production in the fields (and from two other wells in the immediate vicinity) is from the "11,000 ft" or "Migura" sand of the lower Wilcox Group. Temperatures in the Migura sand range from 245° to 260°F. Original shut-in pressures were 8,316 psi in the South Yorktown field and 9,272 psi for the Yorktown field, giving pressure gradients of 0.75 and 0.83 psi/ft, respectively.

Stratigraphy of the Migura Sand

The Migura sand lies about 700 ft below the top of the lower Wilcox Rockdale delta system of Fisher and McGowen (1967). The Migura interval is from 150 ft to 400 ft thick with sandstone percentage varying from over 90 percent to less than 10 percent. The sand isolith contours (fig. 8) outline a large dip-oriented sand with a maximum thickness of over 300 ft. The sand grades into a thick shale sequence to the southwest within 1.3 mi of the channel axis (fig. 9) and pinches out northeastward in an area of poor well control. To the northeast, in the South Cook field, the Migura interval (H) is composed of shaly sand (fig. 9), which is part of a larger interbedded sand and shale sequence. Updip, the Migura sand appears to become one of several upward-fining sequences. The sand has not been penetrated downdip of the Yorktown area.

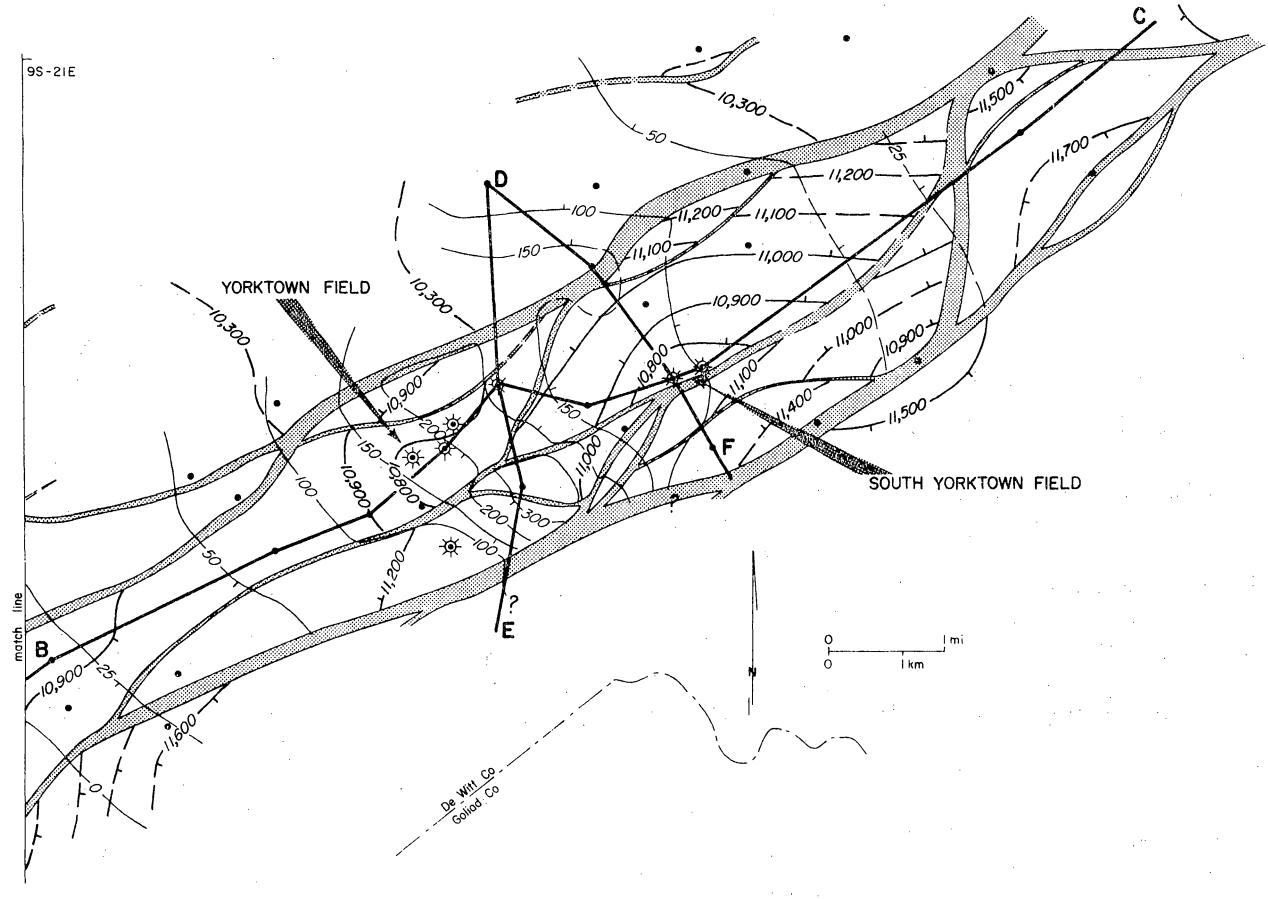

Figure 8. Structure and net-sand map, Yorktown area. Heavy contours are structure on the Migura sand; light contours are net-sand isoliths of the Migura sand. Shading indicates sand greater than 200 ft.

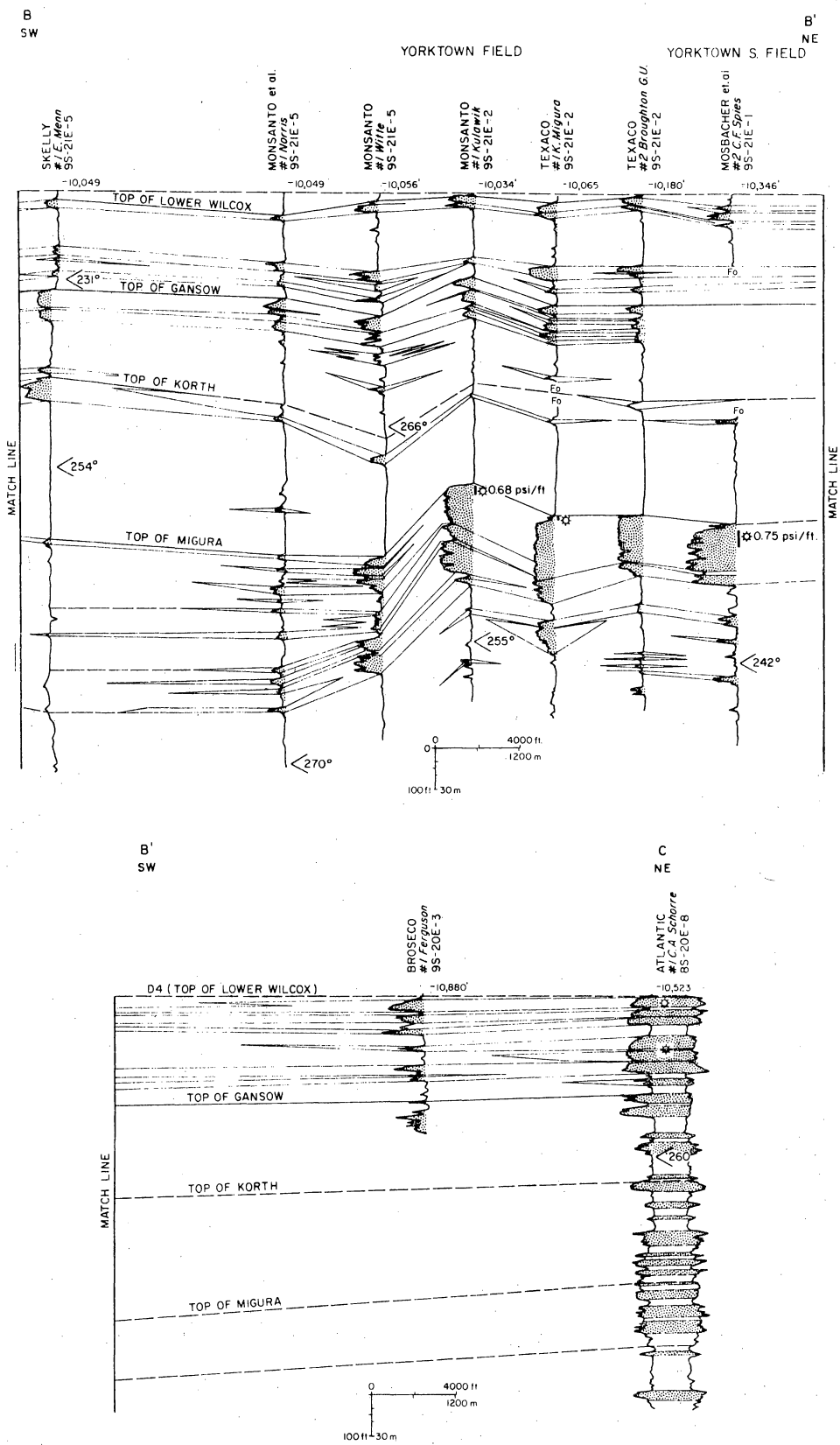

Figure 9. Stratigraphic section of lower Wilcox Group sands, Yorktown area. Datum is top of lower Wilcox (D4'). Match line, left, is to figure 12. Letter intervals in South Cook field from Bebout and others (1979). Sands are stippled in each well; producing zones, pressure gradients (psi/ft) and temperatures (in °F) are indicated. All cross sections show SP logs unless indicated.

The Yorktown field is located on the main axis of the Migura channel. The sand in this area is 150 to 240 ft thick and contains three upward-coarsening sequences, as seen in the Monsanto #1 Kulawik well (fig. 9). The interval gives a high, sawtooth SP response, suggesting numerous thin intervals of less permeable sand or silt.

The South Yorktown field is located on the northeastern edge of the Migura channel; sand thickness in the Mosbacher et al. #1 Spies and #2 Spies is 95 ft and 130 ft, respectively. The character of the sand is similar to that in the Yorktown field with little increase in shale content.

Structure of the Yorktown Area

The structure of the Yorktown area is a complex of strike-oriented normal faults (fig. 8). Most faults are downthrown to the Gulf; two antithetic faults of small displacement are postulated. Individual fault blocks are slightly tilted, and small rollover anticlines are developed. Most of the faulting occurred during lower Wilcox deposition, although upper Wilcox strata thicken over the southernmost faults.

The shape of the Yorktown fault compartment is fairly well determined. It is open to the southwest, although small cross-faults may be present. The antithetic block mapped to the north of the field is displaced only slightly from the main block. The South Yorktown fault compartment, on the other hand, is poorly delineated. No wells have penetrated the Migura sand east and north of the Mosbacher #1 Spies well. The shape of the eastern and northeastern margins of the fault block is therefore speculative, constrained by the known northern growth fault and the low elevation of the lower Wilcox horizon in the Broseco (La Gloria) #1 Ferguson well. Minimum and maximum extents of the fault compartment were therefore chosen in this direction. The compartment boundary west of the field is questionable; Geomap places a small antithetic fault just west of

the field. Such a fault might be sufficient to break continuity in this direction.

Reservoir Volume - Yorktown Field

The volume of the Yorktown reservoir was calculated by using a cutoff in the southwestern direction of 50 ft of net sand for the minimum case and 25 ft of net sand for the maximum case. The sand volume calculated is 9.8 Bcf for the minimum case and 10.5 Bcf for the maximum case. In addition, the antithetic block has a volume of 1.8 to 2.3 Bcf. If we assume a porosity of 20 percent as at South Cook, pore water volumes of 350 million barrels, 375 million barrels, and 65 to 85 million barrels, respectively, are calculated. However, 20 percent porosity is probably too high for this depth; in the De Witt fairway, porosity at 11,000 ft is typically about 14 percent (Bebout and others, 1979). Using this more realistic porosity, volumes are 245 to 260 million barrels plus about 35 to 40 million barrels for the antithetic block. The estimate of pore water volume in this water-drive reservoir is 576 million barrels. Thus, if these estimates are correct, more water drives this gas field than is contained in the Yorktown block.

This discrepancy may be due to nonsealing faults (fig. 10a). Along the main axis of the Migura channel, sand thickness is 250 to 300 ft. The faults that bound the Yorktown field on the south, however, have only 150 to 250 ft of throw. It is therefore plausible that the sand to the south of the Yorktown block Y is continuous with the Yorktown field. Reservoir rock volumes for the two blocks mapped south of the field are 2.85 Bcf for the smaller block A and 8.4 Bcf for the larger block B. Pore water volumes at 14 percent porosity are 70 million barrels and 210 million barrels, respectively. The production volume estimate could then be matched (with the assumptions outlined previously) if all of the above-mentioned blocks are connected along the Migura channel axis.

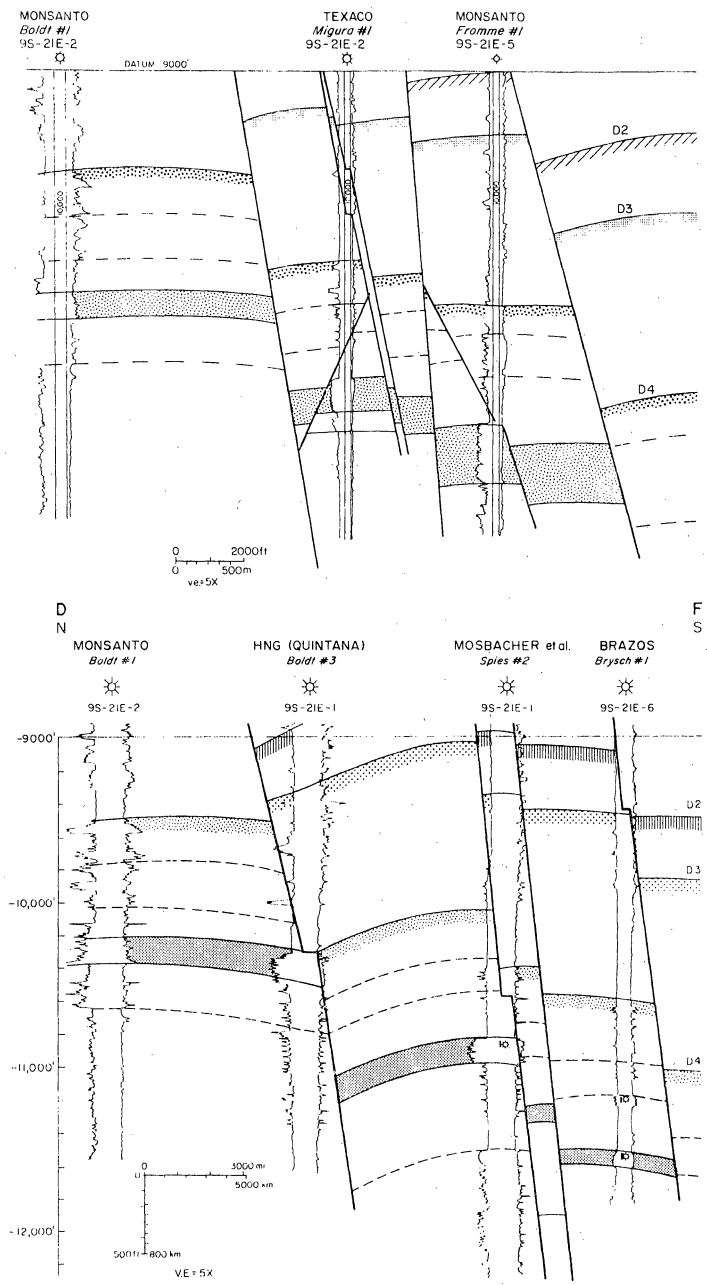

Figure 10. Structure sections, Yorktown area: (a) through Yorktown field, showing sand connections; (b) through South Yorktown field, showing sand isolation. Migura sand is stippled; lines of section are shown in figure 8.

Block B contains gas. If this block is connected with the Yorktown block Y, both blocks should show similar pressure histories. The limited pressure data available support this hypothesis. It would seem that the fault east of the Yorktown field is nonsealing, as it has small displacement; yet the South Yorktown field is separated from the Yorktown field, possibly because the sand thins to the east.

Reservoir Volume - South Yorktown Field

The volume of the South Yorktown block was calculated for several cases. For the minimum northeastern extent of the block, sand thinning to the northeast and an antithetic fault just west of the field, sand volume is 4.24 Bcf and water volume (at 14 percent porosity) is 150 million barrels. For the maximum extent of the block, rock volume is 5.0 Bcf and water volume is 180 million barrels. If there is no antithetic fault west of the field, these figures are 8.3 Bcf and 205 million barrels for the minimum case, and 10.1 Bcf and 250 million barrels for the maximum case. The water volume estimated from production figures is 82 $\pm$ 14 million barrels for this pressure-depletion reservoir. All the geologically estimated volumes are much higher.

This discrepancy may be resolved in several ways. Possibly the poor well control in this block has allowed some faults to go unrecognized; or the thinning assumption may be too generous. A revised minimum figure is 106 million barrels, which is similar to the production estimate. Alternatively, current production is coming from only part of the sand. Production efficiency (assuming 14 percent porosity) is 80 percent for the minimum case. Perforations in the two producing wells are in the top third of the sand. As mentioned before, small silty breaks are abundant in the sand throughout the area. One or more of these breaks may be continuous throughout the block, thus sealing off part of the sand. Other possibilities are that the porosity is markedly lower, or the

water saturation markedly higher, than the assumed values of 14 percent and 25 percent. The present data do not allow a decision between these possibilities.

Figure 10b shows that the thinner sand of the South Yorktown area is not continuous across the growth faults south of the field. The gas production from the well to the south is therefore from a separate reservoir. This conclusion is supported by pressure data.

Summary

The Yorktown and South Yorktown fields produce from the dip-oriented Migura sand. The Yorktown wells penetrate the channel axis where more than 250 ft of sand allows fluid flow between several blocks and production from a large reservoir volume. The South Yorktown field lies on the northeastern side of the channel; production is restricted to the block and may not be from the entire sand interval.

Christmas Field

The Christmas field is located 7.6 mi (12 km) southwest of Yorktown in De Witt County (fig. 5). Production in the field is mainly from the 10,800-ft sand of the lower Wilcox Group, which is equivalent to the Migura sand of the Yorktown area. Temperatures in the Migura sand are approximately 270°F. The original shut-in pressure for the field was 8,201 psi at the Hanson et al. #1 F. L. Altman, giving a pressure gradient of 0.76 psi/ft.

Stratigraphy of the Migura Sand

The Migura sand in the Christmas area (fig. 11) ranges in thickness from zero to 165 ft. The sand thins abruptly to the northeast; its southwestern limit is gradual with a strong strike-oriented component. Downdip to the southeast, sand percentage and net-sand thickness decrease rapidly; updip the sand is not

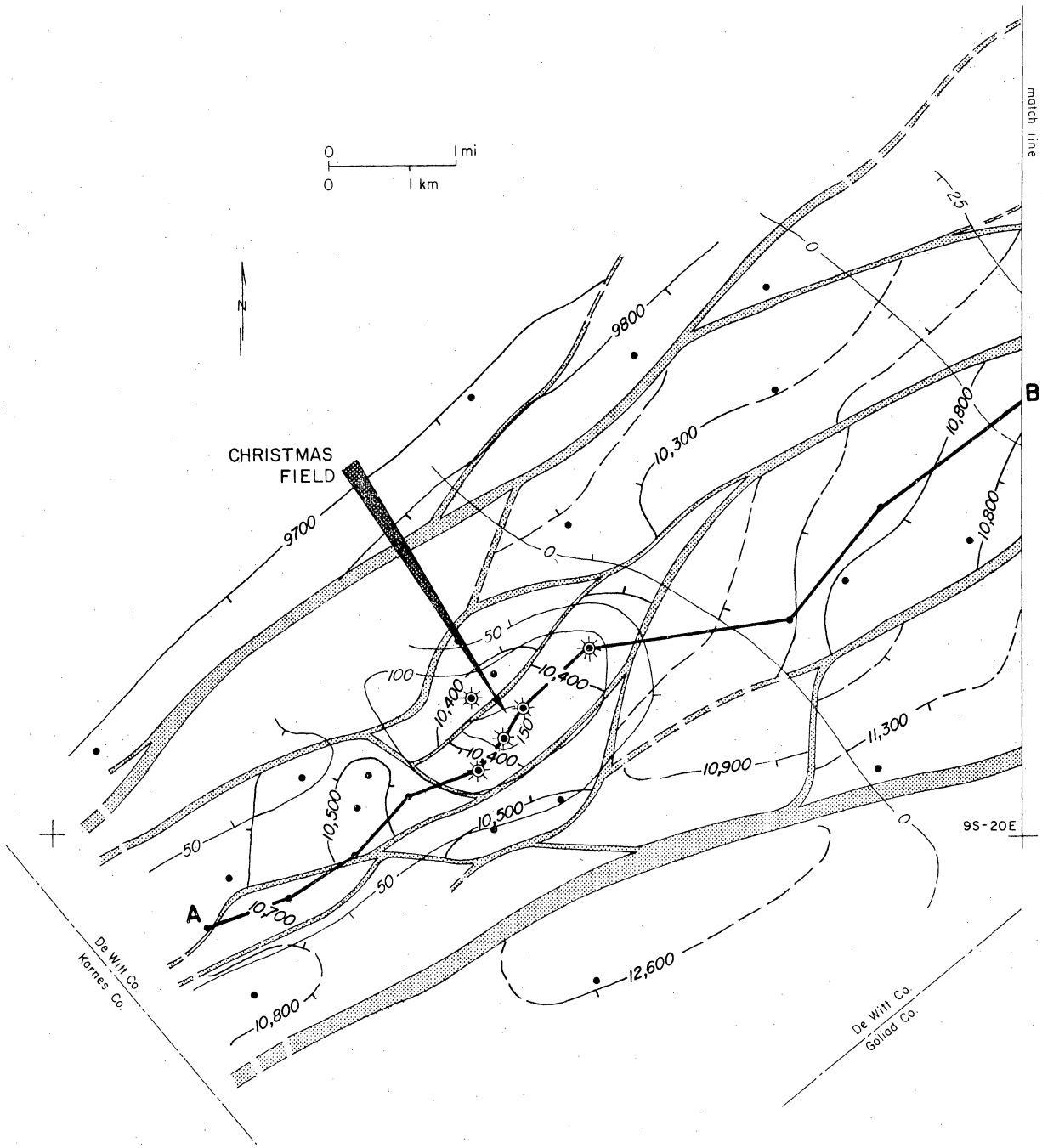

Figure 11. Structure and net-sand map, Christmas area. Datum is Migura sand. Match line is to figure 8. Shading indicates sand greater than 100 ft. All faults downthrown to southeast unless indicated.

correlatable. The Migura sand of the Christmas area is separated from that in the Yorktown area by about 3 mi of silt and clay.

From the well-log patterns (fig. 12), the Migura sand in this area can be divided into three facies. In the northern and northeastern part of the field, a large upward-fining sequence (seen in the Cox et al. #1 Kleine on fig. 12) suggests a thick sand and shale channel sequence. To the southwest the sand is divided into several parts by thin but correlatable shale breaks. Most of the sands in this facies show SP patterns typical of delta-front sands. The lower part of the upper sand in Hanson et al. #1 Altman, however, shows an upward-fining sequence possibly representing a thinner channel deposit. The sands of this facies thin and grade into shale to the southwest. Below these sands in the Nordheim field, fairly thick, blocky sands are found in the Getty #16 Nordheim and #13 Nordheim (fig. 12). These pinch out updip and are inferred to represent bar sands.

The five wells of the Christmas field penetrate the channel and delta-front facies of the Migura sand. One well (Cox et al. #1 Kleine, fig. 12) produces from the base of the channel sequence. Three wells produce from the upper sand of the delta-front facies; of these, one is perforated below a thin break, one above the break, and one straddles the break. The fifth well produces from a deeper sand.

Structure of the Christmas Area

The structure of the Christmas area is complex and not well determined (fig. 11). A network of normal faults divides the area into small fault compartments. The rapid facies changes in the Migura and overlying Korth intervals, together with the intense faulting make correlations unsure, especially to the southwest and northwest of the Christmas field.

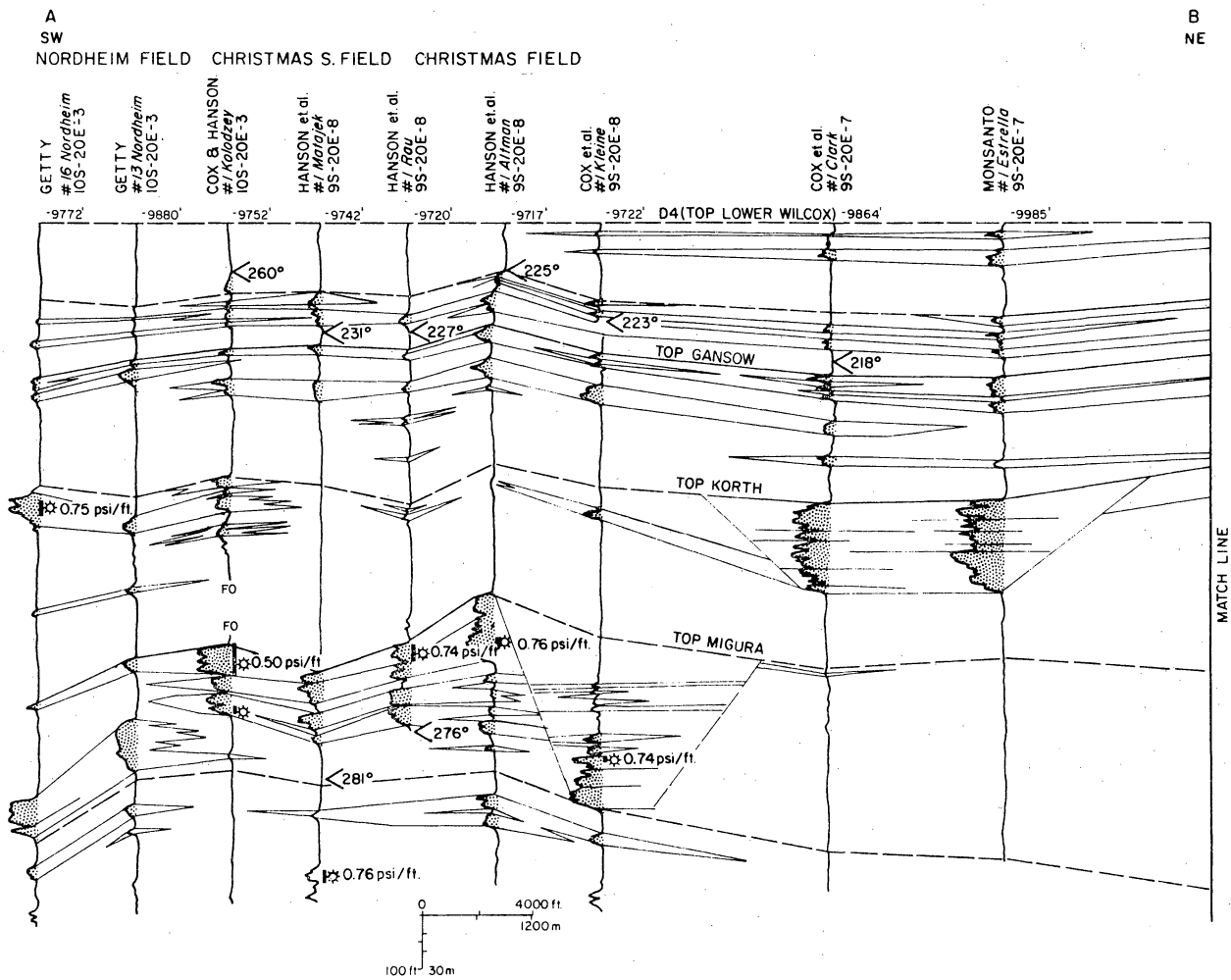

Figure 12. Stratigraphic section of lower Wilcox Group sands, Christmas area. Datum is top of lower Wilcox (D4'). Symbols as in figure 9; line of section shown in figure 11.

The Christmas fault compartment is poorly defined. Its southeastern fault is found in four of the producing wells and is adequately located. The northeastern limit is indefinite, but this does not affect the volume calculation, as the sand is not present in this direction. The southwestern boundary is inferred from the difference in elevation of the Migura sand to the southwest. The northwestern and northern boundaries are indeterminate. A small fault crosses between four Christmas wells and the Hanson #1 Buesing well to the northwest. The large northwestern fault has been tentatively identified below the Migura sand in the Buesing well. The lack of deep well control in the upthrown block makes its location uncertain.

Reservoir Volume - Christmas Field

The total volume of Migura sand in the Christmas fault compartment is calculated to be 6.3 billion ft^3 (Bcf), with an estimated uncertainty of about 30 percent. Assuming a reasonable porosity of 14 percent (as used for the Yorktown field), the aquifer volume is 160 million barrels. The volume estimate from production and pressure data for this pressure-depletion reservoir is 49 $\pm$ 1.2 million barrels. The overall production efficiency, therefore, is 25 percent.

Several factors may account for this low efficiency. The Hanson #1 Buesing does not produce from the Migura sand but has an identical pressure history. This suggests that the small faults between Buesing and the other wells are nonsealing. If so, the thinner sub-Migura sand should be used instead of the Migura itself; this would tend to reduce reservoir volume. The Cox et al. #1 Kleine produces a small amount of gas from the base of the thick channel sequence (fig. 12). Its connection to the other wells is doubtful. Also, as mentioned above, the remaining three wells produce from only the upper sand of the delta-front facies. The sand probably is separated from the lower unit of the Migura, which reduces the reservoir volume considerably. The thin shale break

within the upper sand may further fragment the reservoir. Finally, the indeterminate size of the fault compartment may lead to an inflated geologic estimate. Some combination of these factors, or deviation from the porosity and saturation assumptions, could give a geologic estimate more in line with the production estimate.

Pettus SE Field

The Pettus SE field is located 2 mi southeast of Pettus in Bee County (fig. 5). Gas production in the field is from the "Massive" or "First Massive" sand of the upper Wilcox Group. Temperatures in the First Massive sand average about 230°F. The bottom-hole shut-in pressure for the Hughes and Hughes #1 J. E. McKinney well in the field is 5,666 psi, giving a pressure gradient of 0.64 psi/ft.

Stratigraphy of the First Massive Sand

The First Massive sand lies within the Bee delta of the upper Wilcox Group, part of the Rosita delta system (Edwards, 1981). It occurs at the top of a sand-rich section of the Wilcox known collectively as the "Massive" sands about 200 ft below the Mackhank sand, which is the topmost unit of the Bee delta.

The area is transected by a large growth fault. Northwest of the fault the Massive sands are thin, and the First Massive sand is inseparable from lower sands. Downdip of the fault, the sand reaches a maximum thickness of over 100 ft immediately south of the Pettus SE field (fig. 13), but thins to the east, south, and southwest. Sand percentage is highest and the sand cleanest in the Pettus SE field. Downdip the shale content increases. Several shale breaks within the sand and overlying sands can be correlated throughout much of the area (fig. 14).

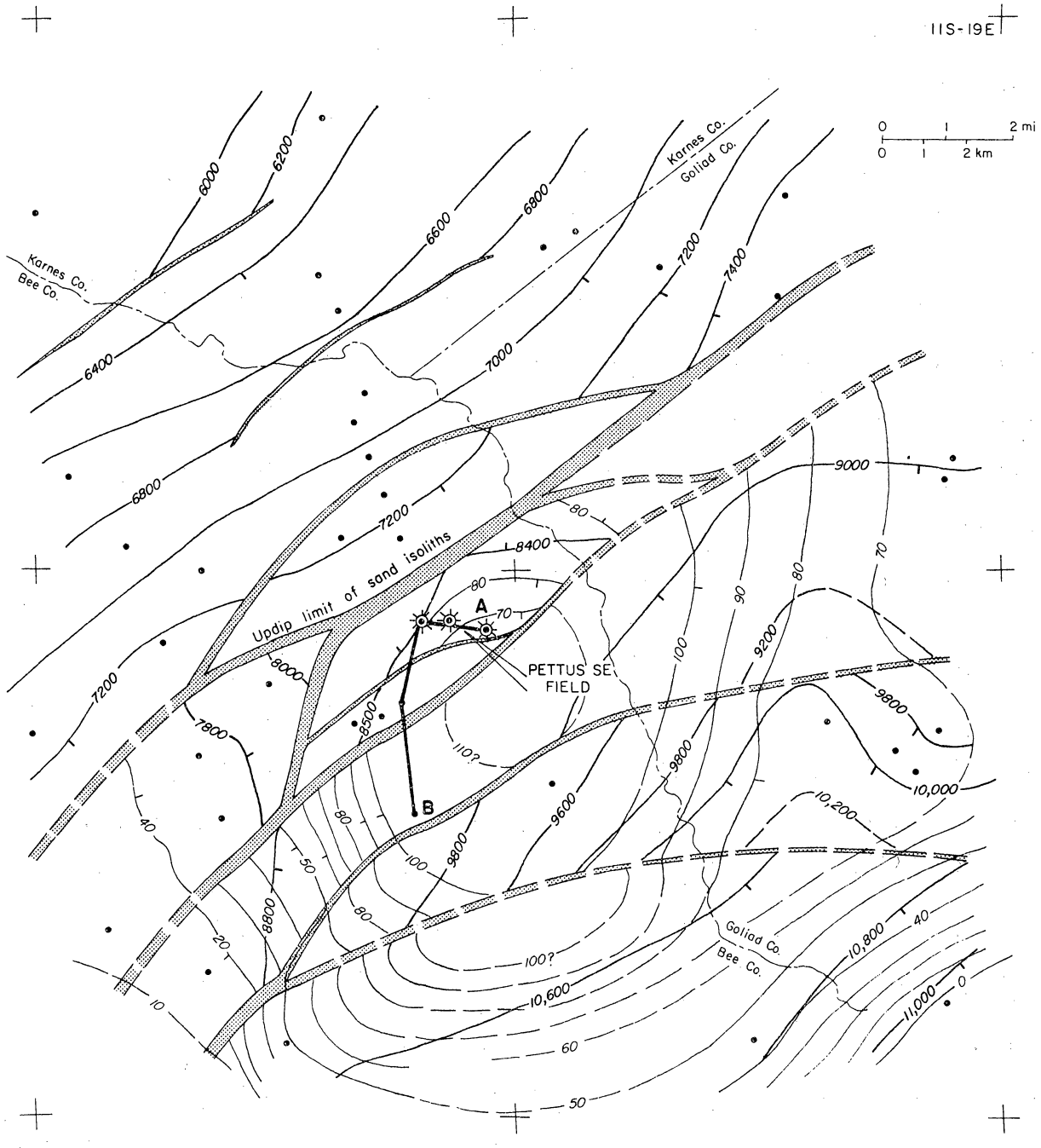

Figure 13. Structure and net-sand map, Pettus area. Datum is First Massive sand. Shading when sand is greater than 100 ft thick. All faults down to southeast unless indicated.

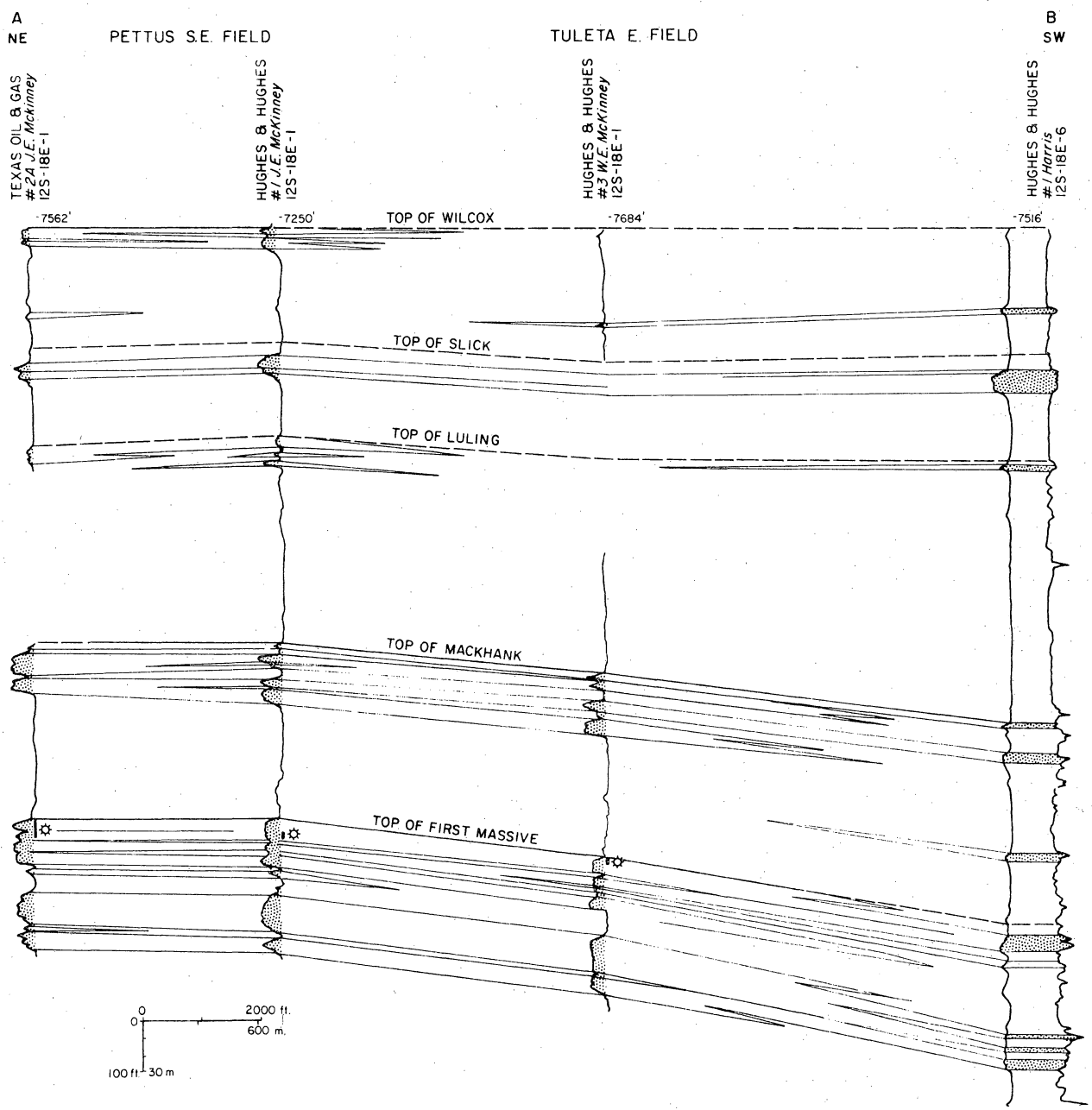

Figure 14. Stratigraphic section of upper Wilcox Group sands, Pettus area. Datum is top of Wilcox (TWX). Symbols as in figure 9; line of section is shown in figure 14.

From the net-sand map and the electric log character of the sand, the First Massive sand is inferred to represent a delta lobe of the Bee delta. The area northwest of the growth fault represents a condensed delta-plain facies. The blocky sands of the Pettus SE field area represent either delta-plain to delta-front sands or reworking of these sands into barrier bars. Downdip of Point B, upward-coarsening sequences are recognized in the First Massive sand interval, suggesting delta-front conditions. The relatively continuous shale breaks may represent short-lived lobe abandonments, preserved from later reworking by rapid subsidence along the growth fault.

Structure of the Pettus Area

The structure of the Pettus area (fig. 13) is marked by a uniform southeast dip in the northwest, broken only by minor faults, and a zone of closely spaced syndepositional normal faults to the southeast. The major growth faults during the deposition of the Massive sand occur in a belt trending northwest-southeast through the Pettus SE field area. The more southeastern faults also affected Massive deposition but appear to have experienced their greatest movement during Mackhank time.

The fault compartment within which the Pettus SE field is located is bounded by the major growth fault to the northwest and west. A fault of lesser displacement separates it from the Tuleta E field to the south. This small fault joins to the east with a larger growth fault, which continues beyond well control to the northeast. The northeastern limit of the fault compartment is not defined by existing well control.

Reservoir Volume - First Massive Sand

A volume for the First Massive sand reservoir at the Pettus SE field was calculated for two cases, a minimum area for the fault compartment, which includes only the producing area, and a maximum area (fig. 13). These two cases

yield reservoir areas of 2.0 and 4.3 mi^2, respectively. Combining these with an average sand thickness of 80 ft and a porosity of 16 percent derived from the regional study in the Live Oak fairway to the southwest (Bebout and others, 1979), the sand volume ranges from 4.6 Bcf to 9.5 Bcf, and aquifer volume in this pressure-depletion reservoir is 28 $\pm$ 2 million barrels. Thus, the producible volume is only 10 percent to 23 percent of the geologically estimated volume. This discrepancy may be ascribed to the presence of thin, laterally continuous shale breaks. All the producing wells in this field produce from the upper part of the First Massive sand. It is likely that the lower part of the sand is not in communication with the upper part within this small fault compartment. In support of this, resistivity logs from the Pettus SE field show two high-resistivity zones, indicating gas-filled sand within the First Massive. The lower gas zone is not being produced by the existing wells.

A revised geologic calculation of sand volume yields aquifer volume of 60 to 120 million barrels. The minimum figure is still too high for reasons unknown; possibly the assumed porosity is too high.

Braslau South Field

The Braslau South field is located 3.8 mi southwest of George West, Live Oak County (fig. 5). Four wells produce gas from the First Tom Lyne sand of the upper Wilcox Group. Reservoir temperature is approximately 240°F. The field had an original shut-in pressure of 6,652 psi, giving a pressure gradient of 0.73 psi/ft.

Stratigraphy of the First Tom Lyne Sand

The First Tom Lyne sand is located within the upper Wilcox Group between two larger sands, the Luling above and the Mackhank below. In the past it has been confused with the Mackhank sand in much of the area; recent work by Edwards

(1981) has demonstrated their separate nature. The Luling and the overlying Slick sands compose the Live Oak delta of the Rosita delta system (Edwards, 1981), while the underlying Mackhank and Massive sands are part of the newly defined Bee delta (Weise and others, 1981). The First Tom Lyne sand, also a deltaic sand, lies between the two previously defined deltas.

The sand varies from less than 25 ft to over 150 ft in thickness in the area (fig. 15) and is profoundly affected by growth faulting. Updip of a large growth fault the sand is not separable from the Mackhank sand, and both are under 25 ft thick. Thickening occurs over three structural levels to the main sand depocenter southeast of the field. Sand thickness decreases rapidly to the east and somewhat less rapidly to the west. The overall shape of the sand isoliths suggests a high-constructive, lobate delta sand.

The First Tom Lyne is a composite deltaic sand (fig. 16). Basal upward-coarsening sequences are overlain by delta-plain and channel sands with blocky to upward-tapering SP patterns. Shale breaks are remarkably continuous in this area, extending over 2.5 mi along strike. These may be delta-lobe abandonment shales preserved from later erosion by rapid subsidence, much as at the Pettus SE field. The shale breaks are thinnest in the Braslau South field area, but the lower delta-front sand is still separate from the rest of the sand sequence.

The depocenter of the First Tom Lyne sand lies between two depocenters of the immediately underlying Mackhank (Weise and others, 1981), and its main expansion faults are slightly Gulfward of the Mackhank faults. The expansion faults and depocenters of the Luling and Slick sands are still farther gulfward, as noted by Edwards (1981).

Structure of the Braslau South Area

The Braslau South field lies within a complexly growth-faulted area (fig. 15). A belt of small fault compartments lies southeast of a gently dipping

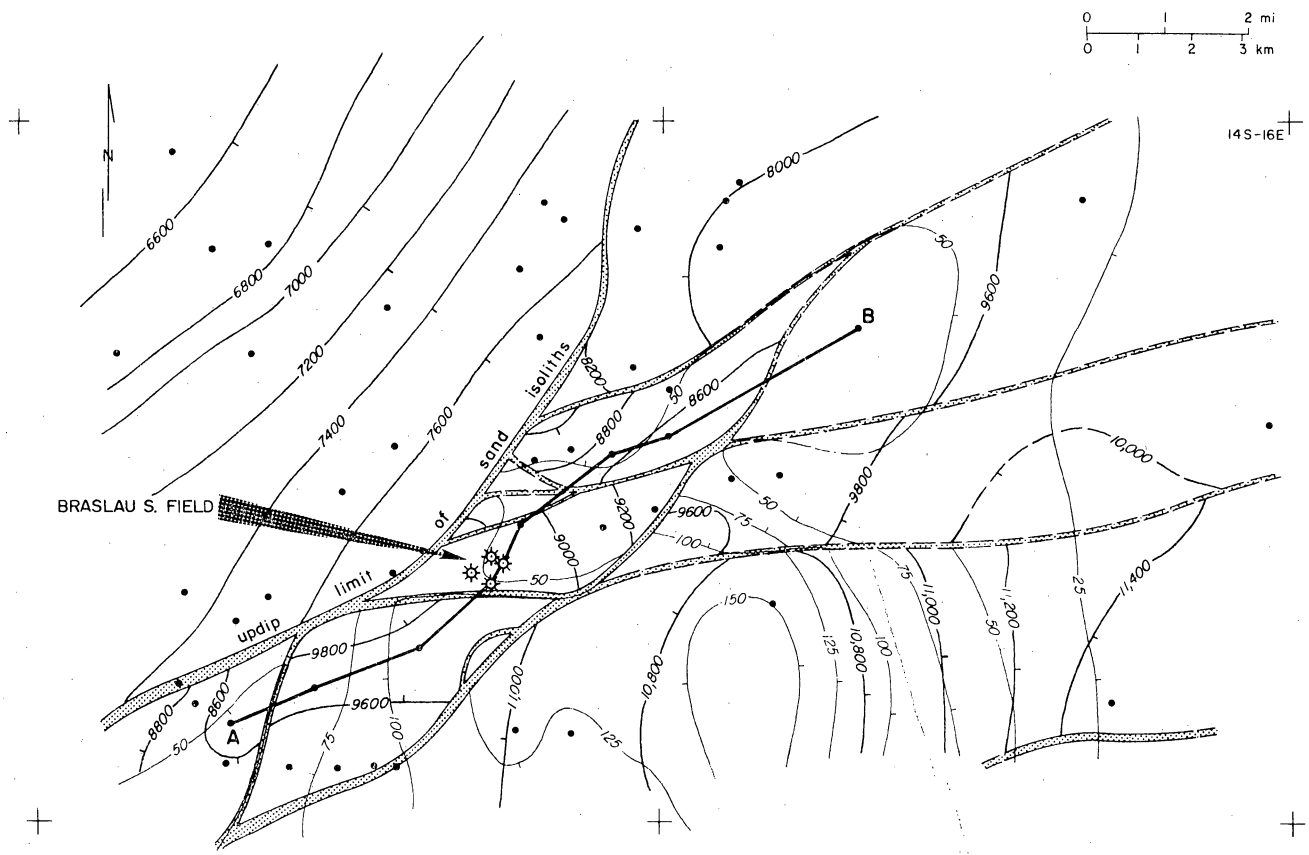

Figure 15. Structure and net-sand map, Braslau area. Datum is First Tom Lyne sand. Shading indicates sand greater than 100 ft thick. Faults downthrown to southeast unless indicated.

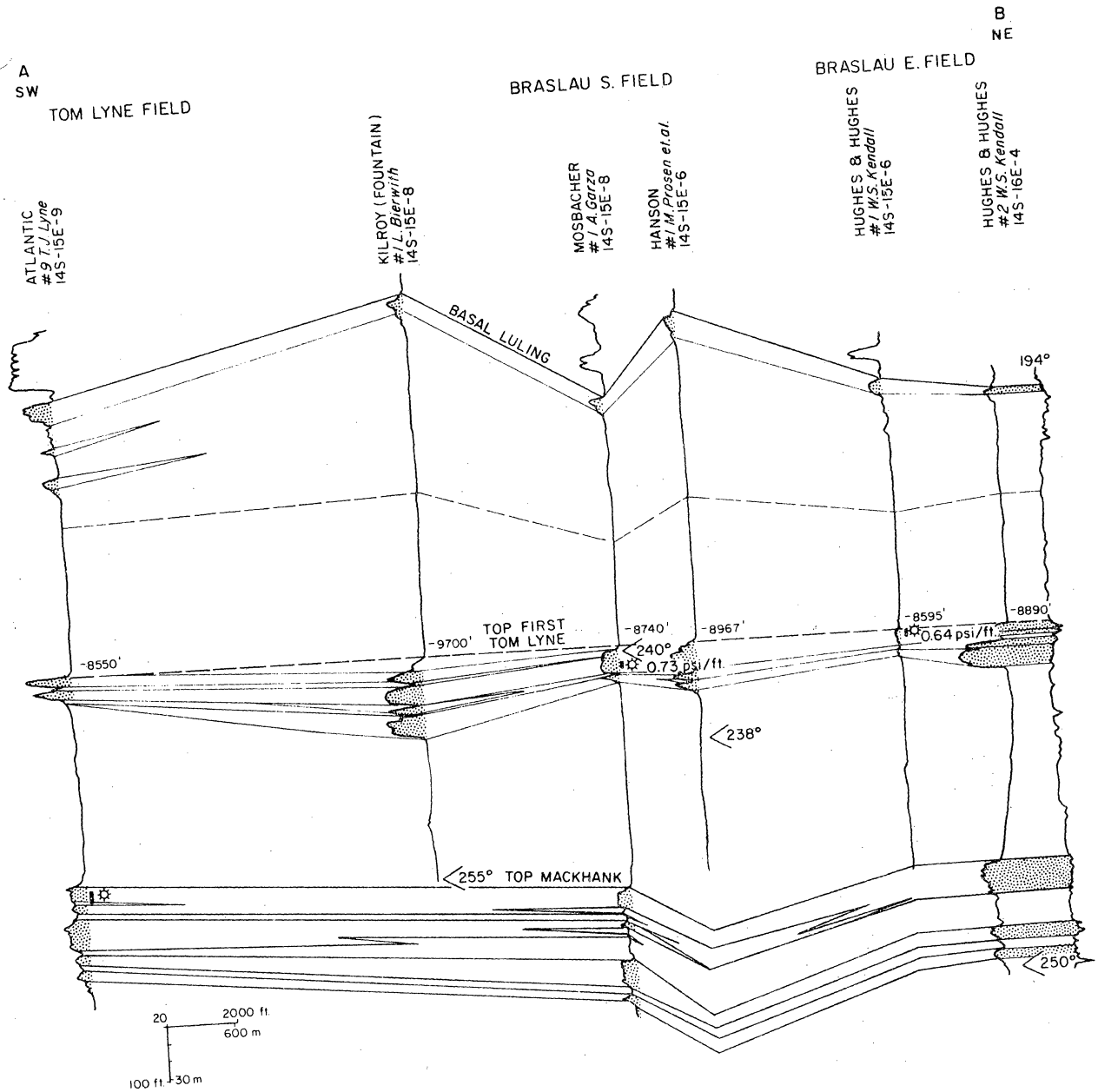

Figure 16. Stratigraphic section of upper Wilcox Group sands, Braslau area. Datum is top of First Tom Lyne sand. Symbols as in figure 9; section line shown in figure 15.

unfaulted area overlain by a thin Wilcox section. Southeastward of the belt, fault block size increases as well control decreases. The Braslau, Braslau South, and Tom Lyne fields occupy successive fault compartments along the belt from northeast to southwest.

Reservoir Volume - Braslau South Field

The Braslau South fault compartment (fig. 15) is bounded by major faults on all sides. A fault with 100 ft of throw is detected in the Hanson #1 Prossen well north of the field; it may or may not break reservoir continuity on the northwest. The eastern fault is poorly determined, as well control is not good. For calculating aquifer volume, the most westerly and most easterly locations for this fault yield minimum and maximum values.

Assuming that the entire net sand is produced in this compartment, and assuming that the small fault on the northwest does not break continuity, the area of the fault compartment is 2.8 mi^2 minimum and 3.9 mi^2 maximum. The sand volume in this compartment is 5.1 Bcf minimum and 7.0 Bcf maximum. At a porosity of 16 percent estimated from Live Oak fairway averages (Bebout and others, 1979), the aquifer volume is about 140 to 210 million bbl. The water volume estimated from production figures is 61 $\pm$ 14 million bbl. Hence, the producible volume is only 22 percent to 54 percent of the geologic estimate.

If the small fault disrupts continuity, the area of the fault compartment is between 2.2 and 3.2 mi^2, the reservoir volume is 3.7 to 6.0 Bcf, and the aquifer volume at 16 percent porosity is 105 $\pm$ 17 million bbl, giving an apparent efficiency of 27 to 71 percent. This low efficiency is probably caused by thin shale breaks. As noted above, shale breaks are remarkably continuous in the sand, and the lower delta-front sand is separated by 5 to 10 ft of shale from the rest of the sand. If this lower sand is not connected with the upper

sand, the two volume estimates are in good agreement. Alternatively, a much lower porosity assumption and a higher water saturation could be involved.

South Peach Point Field

The South Peach Point field is located 7 mi west-northwest of Freeport in Brazoria County (fig. 5). Two wells produce gas from the Frio A sand and one well produces gas from the underlying Frio A' sand. Reservoir temperature is approximately 250°F. The field had an original shut-in pressure of 9,572 psi, giving a pressure gradient of 0.85 psi/ft.

Stratigraphy of the Frio A Sand

The Frio A sand of the Peach Point area lies in the T3-T4 interval (Nodosaria blanpiedi zone) of the subsurface Frio. At Peach Point, three named sands are found in this interval, the A, A', and B sands. In the region studied, the A sand ranges in thickness from zero to over 60 ft. The sand is thickest and contains minimal breaks northwest of Clemens Dome, where it shows blocky SP patterns and some suggestion of upward-coarsening sequences. In the Peach Point fields, sands are less regular with numerous silty breaks (fig. 18); both upward-coarsening and upward-fining sequences are observed. Southeast and west of Peach Point, upward-fining sequences dominate and the sand is thinner. Sand isoliths (fig. 17) show that the thicker sand intervals are roughly dip-oriented. A sand-free area occurs northeast of the Peach Point fields.

This complex thickness pattern can be interpreted as a delta-margin sequence. Channel deposits form a thick, upward-fining sandy sequence through the Clemens Dome fields and a thinner one through Peach Point. Delta-front sands of irregular thickness occur at the ends and margins of these channels in the area southeast of Peach Point and in the Allen Dome area. Similar patterns of sand development characterize the other sands of the interval in this area.

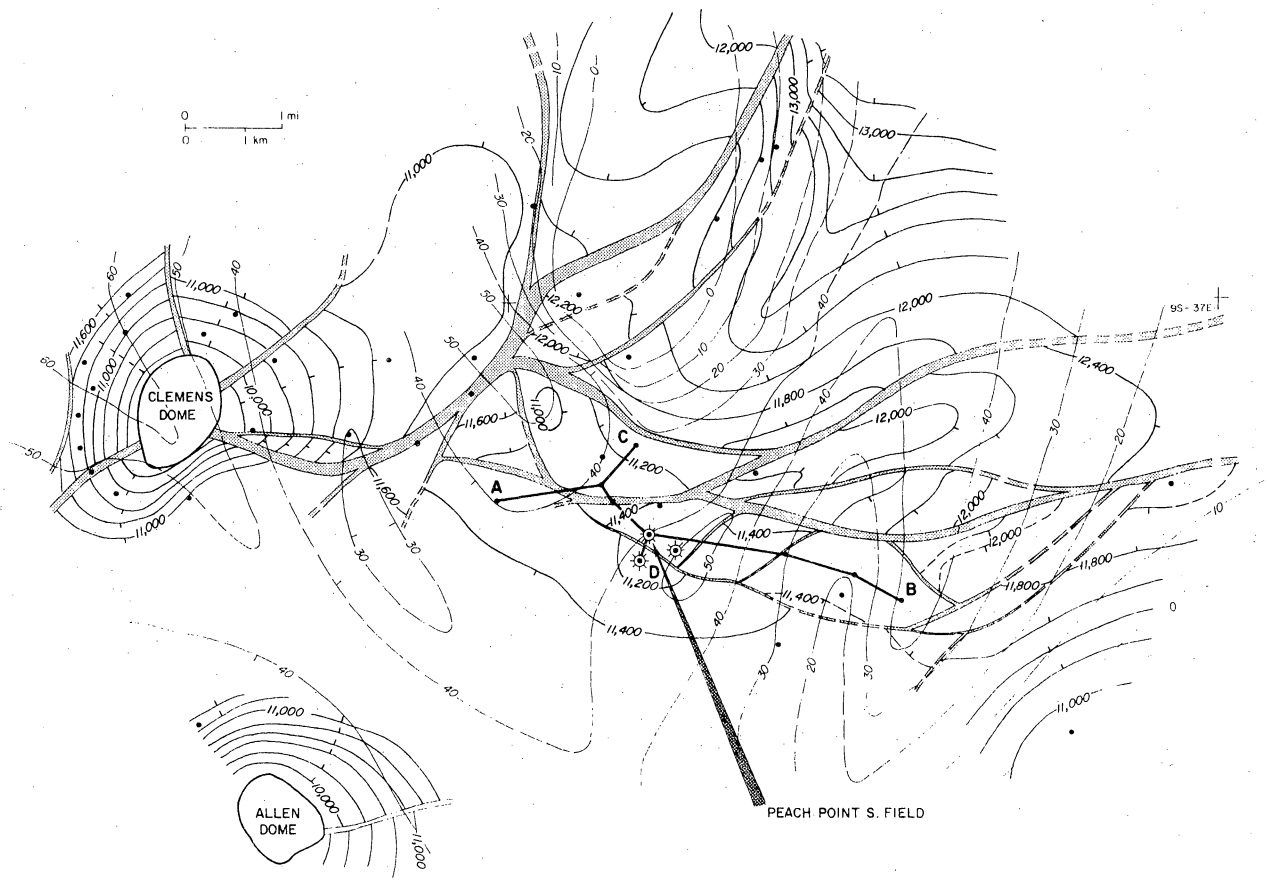

Figure 17. Structure and net-sand map, Peach Point area. Datum is the Frio A sand. Faults down-to-south unless indicated. Shading indicates sand greater than 40 ft thick.

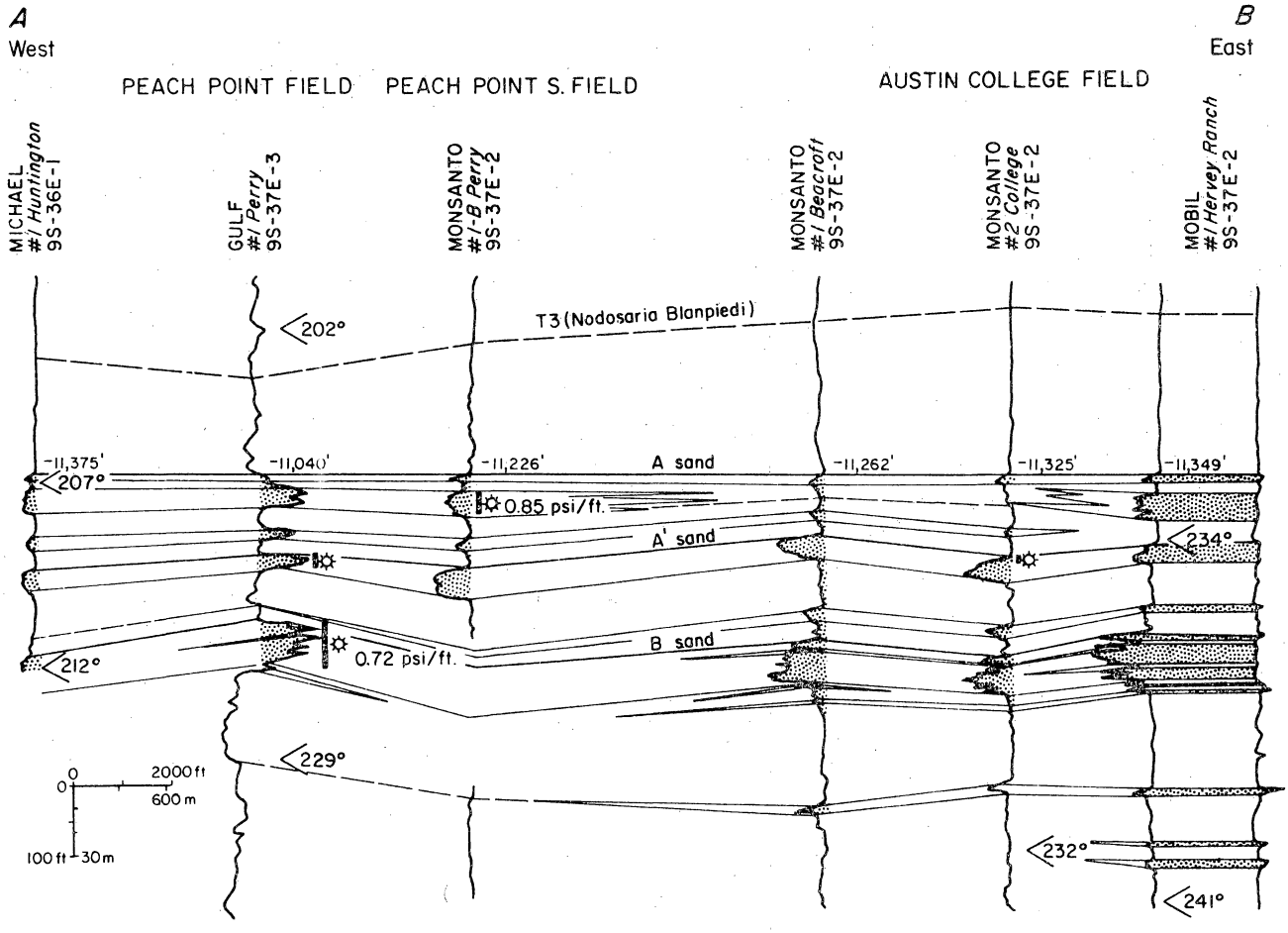

Figure 18. Stratigraphic section of T3-T4 sands of the Frio Formation, Peach Point area. Datum is top of the A sand. Note reversed SP in one well. Symbols as in figure 9; section line on figure 17.

The Peach Point area lies about 25 mi south of the main sand depocenter of the T3-T4 Frio interval (Bebout and others, 1978, fig. 18). The regional maps suggest that this area was at the seaward margin of the Houston delta system (Galloway and others, in press) during this interval. The sands represent the maximum progradation of that delta system in this area.

Structure of the Peach Point Area

The complex structure of the Peach Point area is primarily due to salt tectonics. The Peach Point fields lie atop an east-west-trending ridge (fig. 17) which is presumably salt-cored at depth. At the west end of the ridge is Clemens Dome, a piercement salt dome. At the east end, southeast of a sag in the ridge, is Bryan Mound salt dome. North of the ridge is a large salt-withdrawal basin. Another salt-withdrawal basin lies south of the ridge, in which Allen Dome is uplifted.

Faulting is complex and of several types. Radial fractures segregate fields around Clemens Dome and also occur at Allen Dome. Axial grabens dominate the Peach Point ridge (fig. 19). In the salt-withdrawal basin to the northeast, two growth-fault systems with numerous antithetic faults have been recognized from regional seismic data (Teledyne line 3F). These growth faults interfere with the Peach Point ridge, giving rise to complex, large-scale displacements of up to 1,000 ft. The extent of faulting in the Allen Dome withdrawal basin is unknown, due to lack of well control and available seismic data.

The productive blocks at Peach Point and South Peach Point fields are profiled in figure 19. The Peach Point field lies in a north-dipping section on the north side of the ridge. South Peach Point lies in the axial graben of the ridge (for the A sand production) and on the south side of the ridge (for the A' sand production). The A and A' sands are juxtaposed along the south fault of the graben (fig. 19).

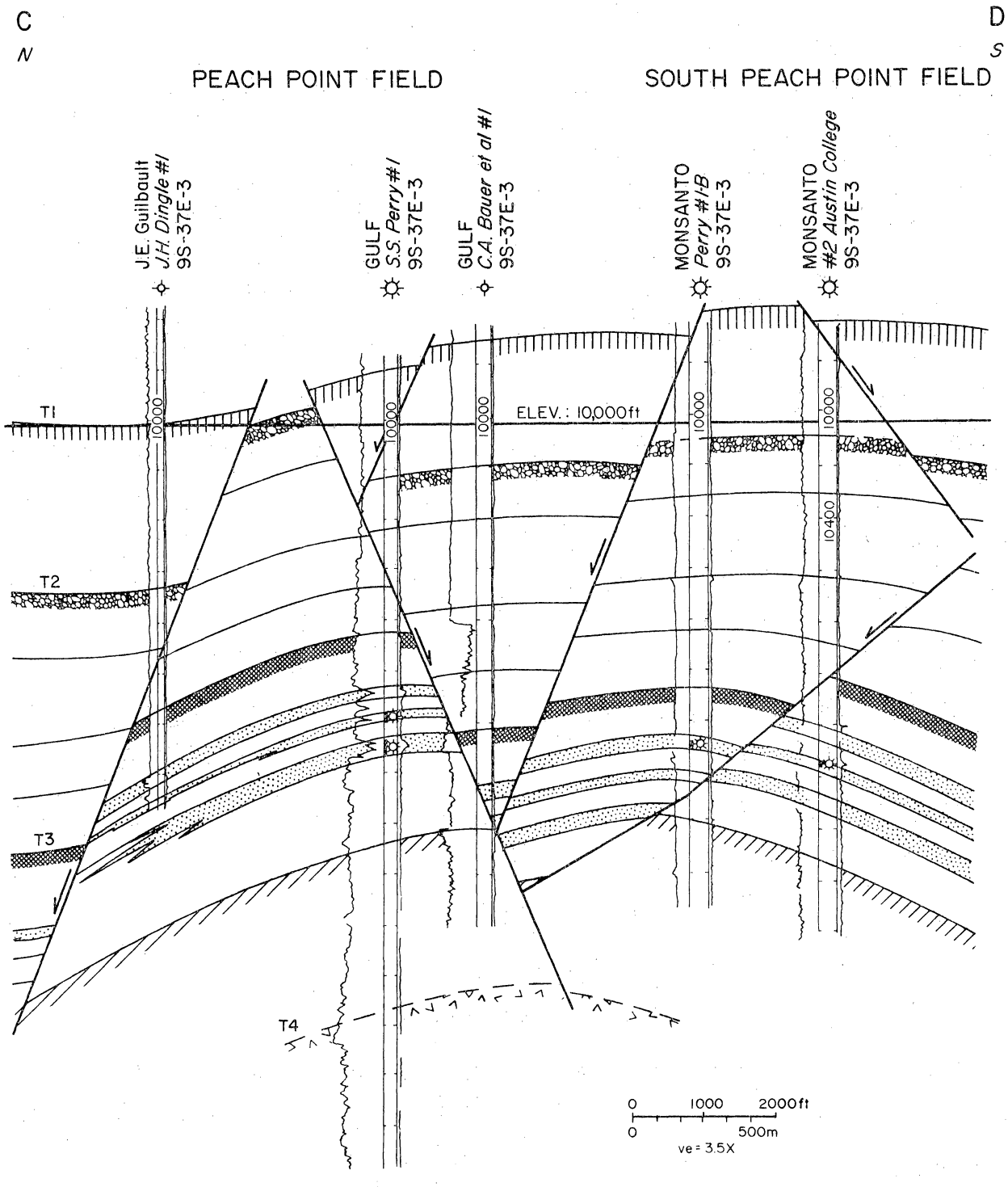

Figure 19. Structure section, Peach Point area. Section line on figure 17. Stipple indicates Frio sands; other patterns emphasize stratigraphic horizons.

Reservoir Volume - South Peach Point Field

The South Peach Point fault compartment (fig. 17) is bounded by minor faults on the south and east and a larger fault on the north. Assuming that the entire net sand is produced in this compartment, the sand volume is 0.72 Bcf (the fault compartment area is 0.61 mi^2). Assuming a reasonable porosity of 15 percent (from Brazoria fairway, Bebout and others, 1978), the aquifer volume is 19.2 million barrels; at a high porosity of 20 percent, the volume is 25.5 million barrels. The reservoir volume from pressure decline data is 33 $\pm$ 3 million barrels. Thus, the calculated aquifer volume is too small for the observed production for reasonable porosities.

As shown on the structure section (fig. 19), the A' sand to the south is juxtaposed with the producing A sand. The southern block A' sand is a likely candidate for providing the extra volume. If the two sands are connected, (1) the fault is nonsealing, and (2) the observed volume must be recalculated to include the production from the third well, giving 46 $\pm$ 6 million barrels. This connection is supported by the pressure history of the A' well. The extent of the A' fault compartment is unknown; therefore no volumes can be calculated. To match the observed and calculated values, a fault block area equal to 70 percent of the known fault compartment is needed.

Mobil-David L Field

The Mobil-David field lies southwest of Corpus Christi in Nueces County (fig. 5). Deep production in the area comes from the Anderson sand (Frio) approximately 11,000 ft below sea level. The field includes a number of fault compartments; one of these, the L compartment, is the reservoir of interest immediately southwest of the Ross (Coastal States) #1 Kraft well of opportunity. In the L reservoir the initial BHP was 9,507 psi, giving an initial gradient of 0.84 psi/ft. Reservoir temperature is estimated at 266°F (Duggan, 1972).

Stratigraphy of the Anderson Sand

The Anderson sand is one of a number of lower Frio sands in the Corpus Christi area. It occurs at the CC11 marker of Weise and others (1981), their deepest correlation marker, within the Anomalina bilateralis zone. In the area of interest the Anderson lies more than 1,000 ft below the CC10 (Harvey sand) marker.

In the Corpus Christi fairway, the Anderson sand is recognized in a belt between two major growth faults that form the western edges of the Nueces Bay and Corpus Channel fault blocks. In this area there are two major sand thicks. The northern one in San Patricio County ranges up to 100 ft in thickness and averages 50 to 60 ft. The southern one is larger and ranges up to 160 ft thick; this depocenter contains the Mobil-David field and the #1 Pauline Kraft well. Net-sand isopachs outline a combination of dip and strike trends, strike trends being dominant towards the Gulf. This pattern indicates a delta system with sand supplied from central Nueces and southern San Patricio Counties.

In the Mobil-David area, sand thickness is controlled by numerous small growth faults (fig. 20). The Mobil-David field produces gas from a thick, blocky Anderson sand (fig. 21). The sand becomes thinner and broken by shale partings to the southwest. Northeast toward the Kraft well, it becomes slightly less blocky in its SP response but thickens into a downfaulted block. North of the Kraft well the sands contain more shale and show a suggestion of upward-coarsening sequences. Westward, thickness variations are pronounced, possibly indicating a feeder channel; eastward, sand thickness and quality deteriorate toward a large growth fault.

Structure of the Mobil-David Area

The structure of the Anderson sand (fig. 20) is complex, although little of that complexity is mirrored at shallower depths. In the Mobil-David field,

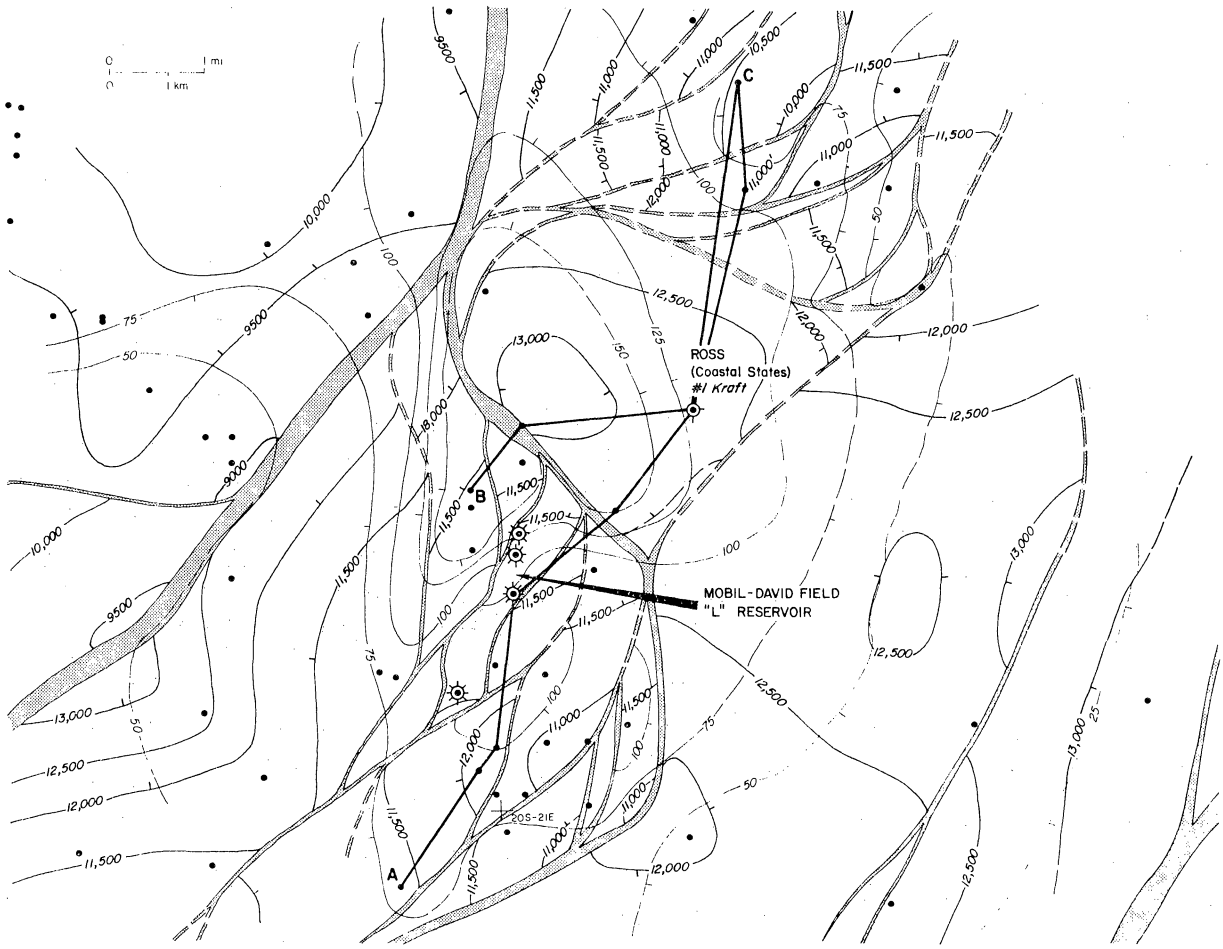

Figure 20. Structure and net-sand map, Mobil-David area. Datum is the Anderson sand (lower Frio). See also figure 27. Shading shows sand over 100 ft thick. All faults down to southeast unless indicated.

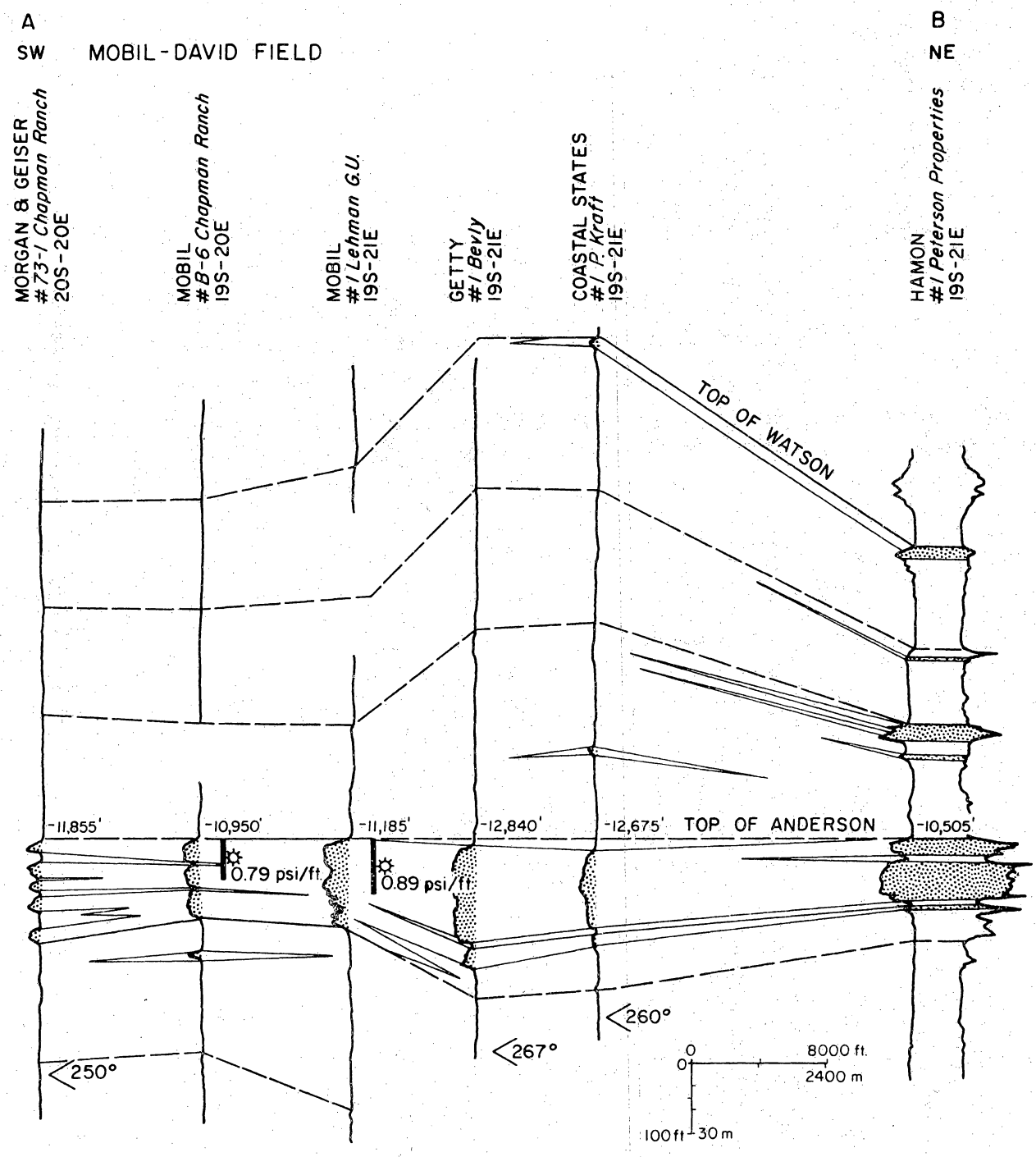

Figure 21. Stratigraphic section of lower Frio sands, Mobil-David area. Datum is top of the Anderson sand. Symbols as in figure 9; line of section shown on figure 20.

numerous growth faults with 100 to 200 ft of displacement divide the Anderson sand into small fault compartments, such as the L compartment described by Duggan (1972). These small faults are not clearly distinguishable on a seismic profile, which crosses the field (unpublished data). A similar structure occurs north of the Kraft well. In both of these areas the Anderson lies at 11,000 to 11,500 ft.

In contrast, a block between these two fractured areas is depressed over 1,500 ft. Five wells provide control within this block; two of the wells penetrate the Anderson sand itself. The depression is filled by a thick sequence of Anderson sand and post-Anderson shale and silt. In contrast to the Mobil-David wells, few minor growth faults can be found in the interval above the Anderson sand; apparently, this downfaulted block has been spared the extreme fragmentation seen in the structural highs to the north and south. This downdropped block is at nearly the same depth as the block east of the Mobil-David field, as interpreted from the seismic line, forming a landward embayment of the lower structural level inserted between two domes. This dome and basin structure, reminiscent of salt-tectonic features (but here probably shale-controlled) is mostly filled in by the top of the lower Frio.

Reservoir Volume - Anderson Sand

The Anderson sand in the L fault compartment ranges from 80 to over 100 ft thick. Shale breaks in the interval are minor and sand quality appears good. The fault compartment has an area of about 1.2 mi^2 and contains 4.25 to 4.75 Bcf of sand. Assuming a porosity of 24 percent (Duggan, 1972), the aquifer volume is 180 to 200 million barrels.

Production data for the Anderson L sand are given by Duggan (1972). Although a simple pressure-depletion drive was expected, the BHP/z versus production curve shows a negative deflection. Duggan attributed this to pressure

maintenance by the dewatering of adjacent shales. The gas-in-place estimate from early data was 112 Bcf, but approximately 70 Bcf was expected from volume calculation. More recent data (to October 1980) show cumulative production to be approaching 55 Bcf ultimate.

The data presented by Duggan (1972) suggest that the aquifer volume from production data ranges from 185 to 290 million barrels, the lower figure being indicated from the revised gas-in-place estimate. These figures (especially the minimum figure) agree with the geologic estimate. The actual near-ultimate gas production of 55 Bcf then indicates an efficiency ratio of 75 to 80 percent.

The concave-down production curve seen at Mobil-David L field has not been noted in the other production curves used for this study. If such an effect exists, the result would be to lower the production volume estimates. In most cases this would only increase the gap between production estimates and geologic estimates of aquifer volume.

Comparisons and Conclusion

Comparison of geologic and production estimates of aquifer volume for nine Texas Gulf Coast reservoirs (table 6 and fig. 22) shows a general tendency for geologic estimates to be higher than production estimates in small, pressure-depletion reservoirs (except where nonsealing faults are present). This tendency is largely due to thin (2 to 7 ft thick) shale breaks within the sand sequence, that seal off portions of the sand body within the small fault compartments. The larger (aquifer volume >100 MMbbl) reservoirs generally show a closer agreement between geologic and production estimates, although problems with shale breaks and nonsealing faults may still exist.

Nonsealing faults have been found in two, and possibly three, cases. In the Yorktown field, a small fault cuts a thick (300 ft) sand. The same sand is

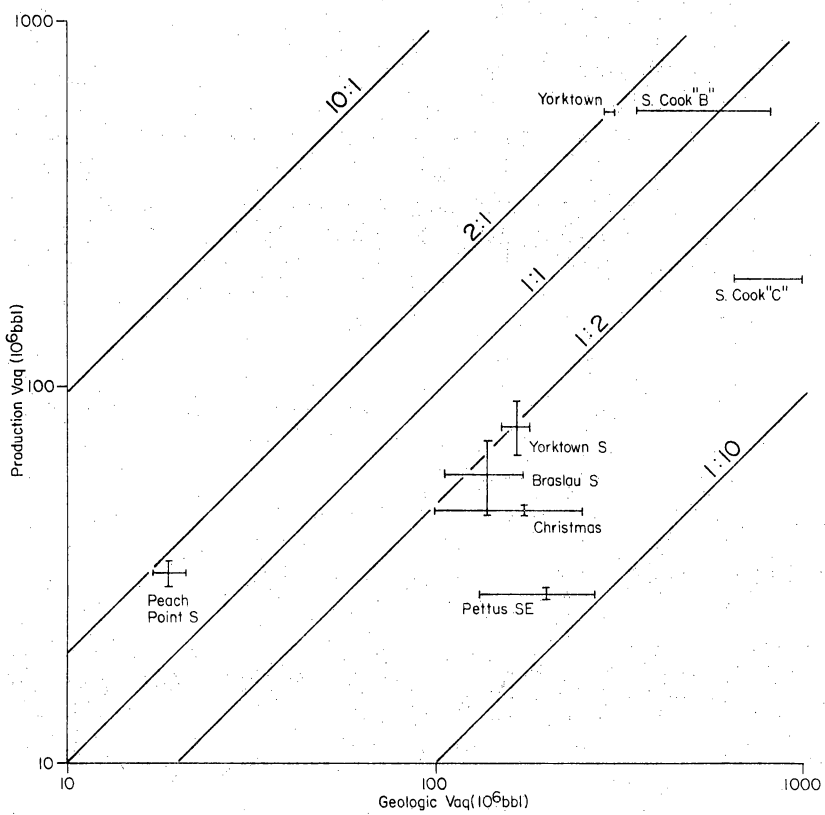

Figure 22. Comparison of production and geologic estimates of aquifer volume. Bars show the range of estimated volumes.

juxtaposed on both sides of the nonsealing fault. At South Peach Point, the thin A sand is juxtaposed across a small (100 ft) nonsealing fault with the smaller A' sand. At Christmas field the situation is less certain, but a nonsealing fault may be inferred, similar in magnitude and geometry to the one at South Peach Point. All other faults in the fields studied, especially those with large displacement or those which juxtapose sand on shale, are sealing.

In evaluating geopressured reservoirs, the reservoir continuity characteristics of the sand should be taken into account. Given adequate well control, it should be possible to recognize potentially nonsealing faults by their small displacement and juxtaposition of sands. If well control is not present, this recognition will be very difficult, as these small faults will generally not show up on seismic sections. Faults with small displacement can also be sealing, as in the Mobil-David L field. Such faults could seriously impair a prospective geopressured reservoir, but this problem is partially alleviated in areas of thick and numerous sands.

Thin, continuous shale breaks can be correlated within a fault block if there is sufficient well control. Breaks less than 5 ft thick may be hard to recognize. These permeability barriers are generally subtle and are not usually considered in sand correlation, but they do affect the potential production of the reservoir. Stratigraphic horizons at particular locations within the growth-fault systems may display a distinctive style of sedimentation. In particular, the Pettus SE and Braslau S areas in the upper Wilcox growth-fault trend of Bee and Live Oak Counties, an area of high expansion across closely spaced growth faults, show similar, continuous shale breaks in different sand units. The Frio sands, on the other hand, appear to have fewer shale breaks of significance. Such general knowledge could help to evaluate reservoirs in areas of poor well control.

GEOLOGIC SETTING AND RESERVOIR CHARACTERISTICS, WELLS OF OPPORTUNITY

Three deep wells on the Texas Gulf Coast (fig. 5, table 7) have been tested for their geopressured resource by Eaton Operating Company, under contract to the U.S. Department of Energy. To provide detailed geologic contexts for these wells of opportunity, the structure and stratigraphy of the areas adjoining them have been studied by the methods previously outlined for geologic estimation of aquifer volumes.

Riddle #2 Saldana

The Riddle Oil Company #2 Saldana well lies in the Martinez field in eastern Zapata County, Texas. The test reservoir, the First Hinnant sand in the upper Wilcox Group, is also the main reservoir of the Northeast Thompsonville field (Jim Hogg and Webb Counties) 10 mi to the northeast.

The Martinez field is located on a high-relief domal structure cut by three southeast-down normal faults that were active during Wilcox deposition (fig. 23). First Hinnant gas production occurs from two small gas caps, one in the western fault block, the other in the eastern. The Riddle #2 Saldana well tested the central fault block but yielded salt water; the gas cap in that block, if any, is small. In the test well, the First Hinnant sand had a bottom-hole shut-in pressure (BHSIP) of 6,627 psi (gradient of 0.68 psi/ft) and a temperature of 300°F. Reservoir properties were determined by Eaton Operating Company. The average porosity (from the sonic log) is 16 percent, the average permeability is 7 md, and measured water salinity is 13,000 ppm. Porosity is fairly uniform throughout the sand, whereas permeability shows two upward-decreasing cycles (fig. 24).

Table 7. Reservoir area and volume for Texas wells of opportunity.

Name, county sand, depth	Primary geologic estimates				Drive est.	Possible problems
	Area(mi^2)	V_{res}(Bcf)	V_{aq}(10^6)	Porosity		
Riddle #2 Saldana Martinez Wilcox area, Zapata Co. First Hinnant 9,120'	3.6	7.0	200	16%	w(?)	Compartment to N poorly determined Possible shale breaks
Coastal States #1 Kraft Mobil-David area, Nueces Co. Anderson 12,675'	4.77-8.34	17.9-28.6	638-1220	20-24%	no production	Poor compartment control on N,NW
Lear #1 Koelemay Doyle area, Jefferson Co. Leger 11,590'	2.5+	7	250	20%	w	Very poor compartment control

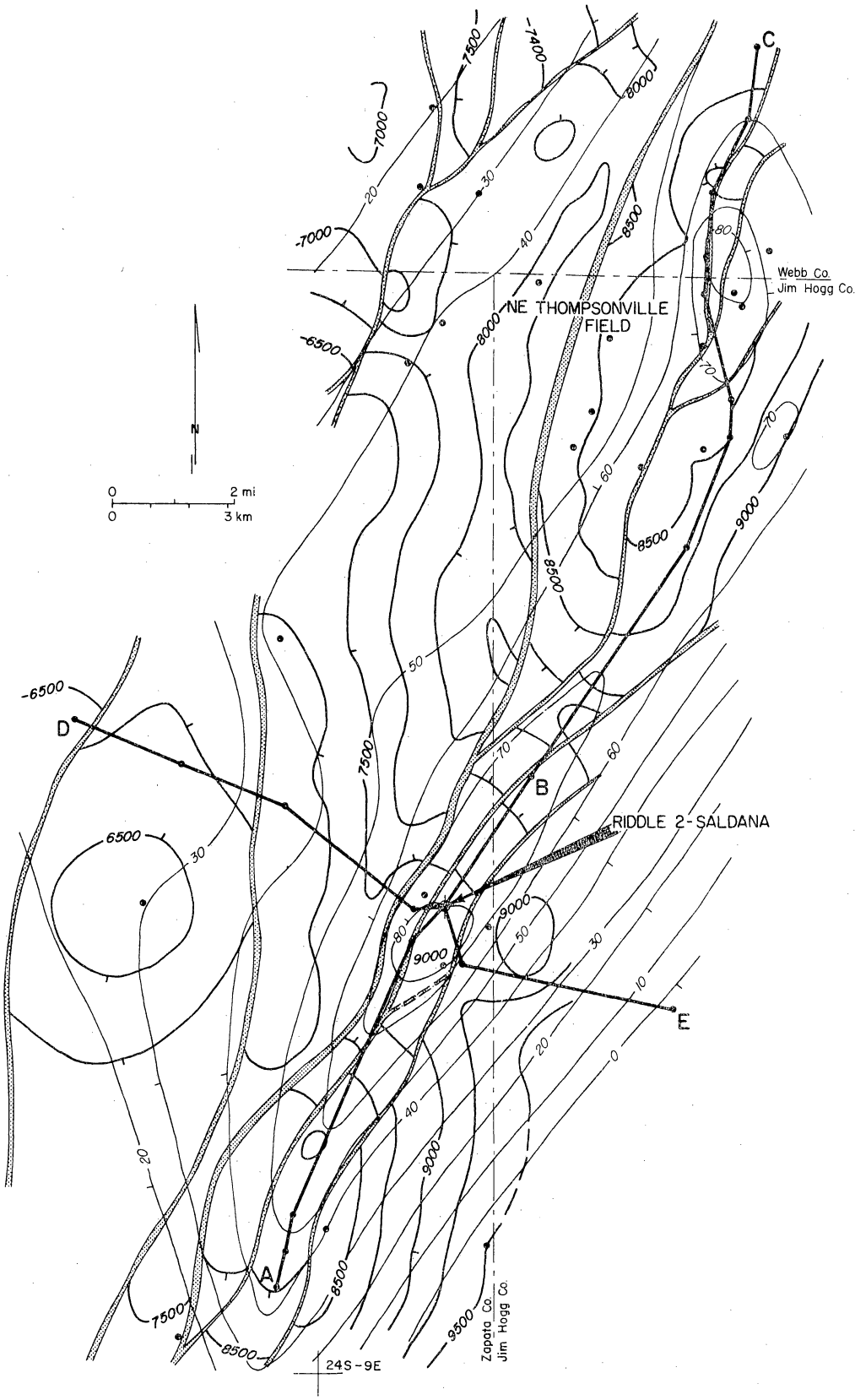

Figure 23. Structure and net-sand map, Riddle #2 Saldana area. Datum is top of the First Hinnant sand, upper Wilcox Group. Shaded area indicates sand thicker than 60 ft. Faults down to southeast unless indicated. Faults from Geomap.

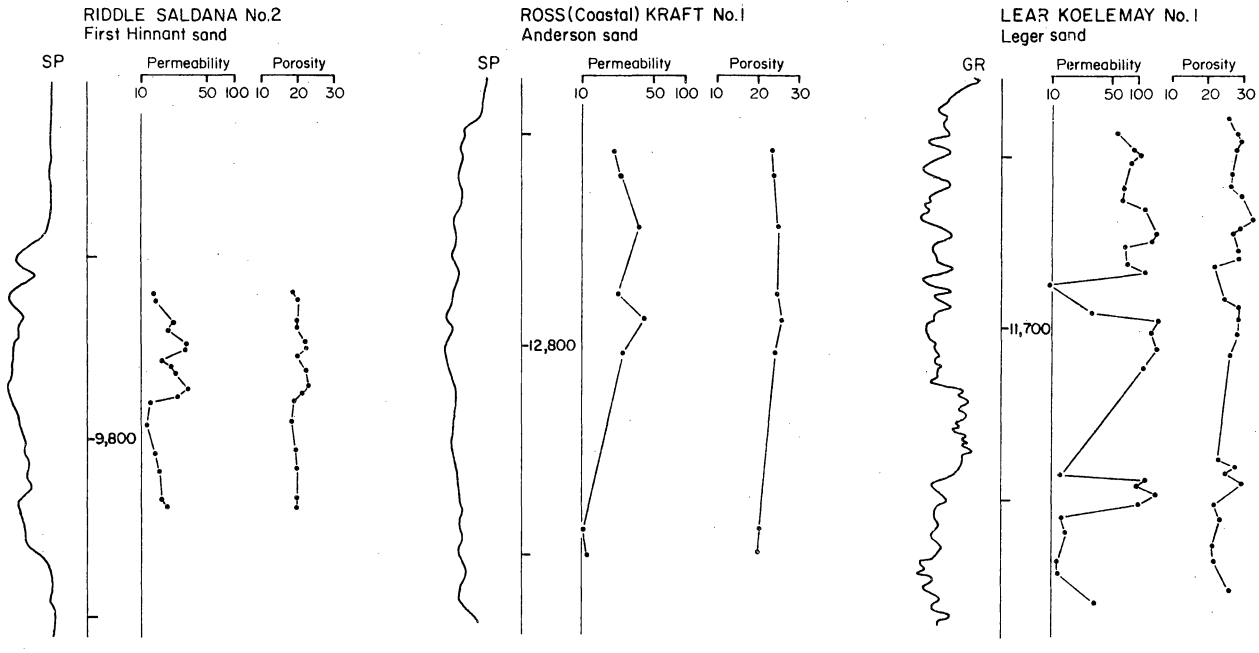

Figure 24. Porosity and permeability variations in three reservoirs tested by the well of opportunity program. For locations see figure 5.

Stratigraphy of the First Hinnant Sand

The First Hinnant sand occurs within the uppermost Wilcox interval, about 200 ft below the regional top of Wilcox. In the Martinez field, it is the topmost Wilcox sand and occurs within a dominantly shale sequence. The sand is more than 600 ft above the top of the Zapata delta complex (Edwards, 1981) and is correlative stratigraphically with the Live Oak delta complex in McMullen and Live Oak Counties 75 mi to the northeast.

The productive sand in the two fields is over 50 ft thick, with blocky SP and resistivity responses and minor shale breaks that can be correlated within each field. Despite the lack of well control between the two fields, the correlation is good (fig. 25). To the north and south, the sand merges into a mixed sand-shale sequence with subdued SP and resistivity response. To the south, this transition occurs over about 1.5 mi; to the north it is much sharper (less than 4,000 ft), occurring just north of Atlantic #1 Bruni (fig. 25).

The sand thins to both the east and the west (fig. 26). To the east the sand grades into silt within 2.5 mi. The sand thins markedly and migrates upsection to the northwest, where it overlies several upward-coarsening sequences, which increase in sand content westward. These sands are interpreted as delta sequences with a western source.

The First Hinnant sand has been studied previously in the Northeast Thompsonville field, where it was interpreted as a barrier-bar deposit by Wood (1962) and Young (1966); Berg and Tedford (1977) preferred a deep-sea fan origin. The sand exhibits a well-defined N30°E trend of maximum sand thickness with abrupt thinning to the southeast and gradual thinning to the west (fig. 23). This geometry is fully consistent with a barrier-bar origin for the First Hinnant sand but conflicts sharply with the dip-oriented fan model of Berg and Tedford (1977). The upward-coarsening sequences to the west represent small late-stage

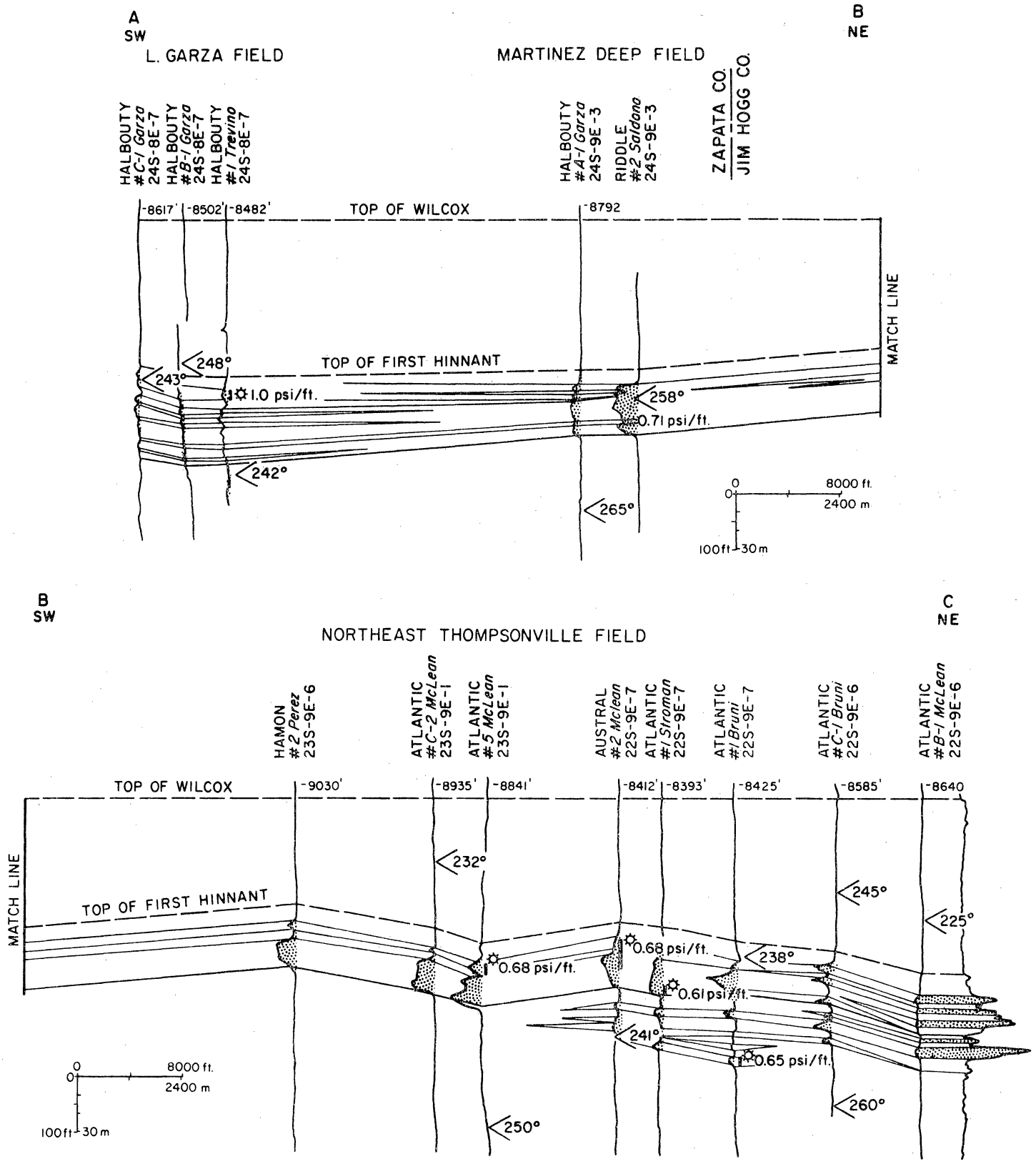

Figure 25. Stratigraphic strike section of First Hinnant sand, Riddle #2 Saldana and Northeast Thompsonville areas. Datum is top of Wilcox Group. Symbols as in figure 9; line of section shown in figure 23.

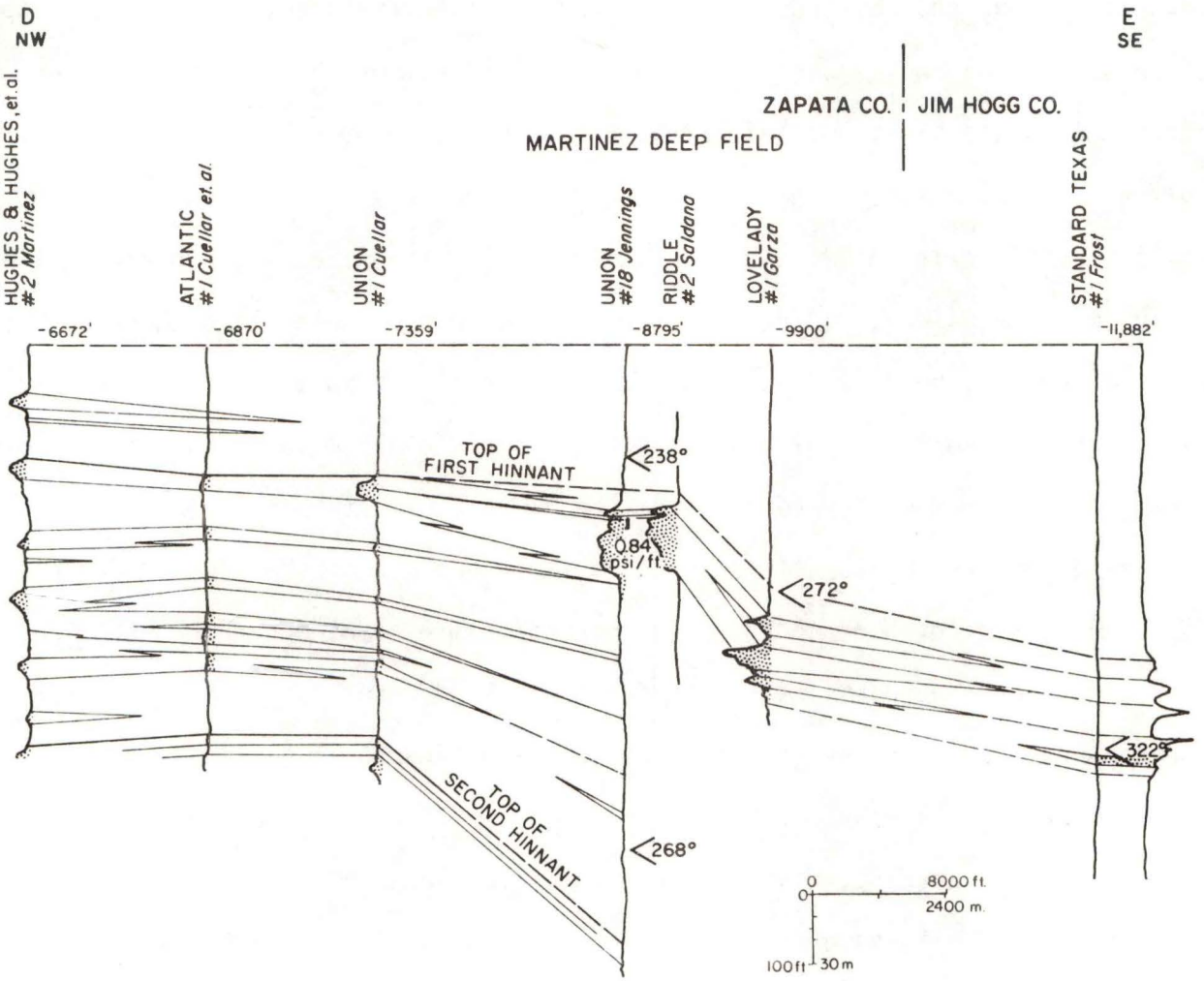

Figure 26. Stratigraphic dip section through Riddle #2 Saldana of uppermost Wilcox sands. Datum is top of Wilcox Group. Symbols as in figure 9; line of section shown in figure 23.

deltas, which in part formed as bayhead deltas behind the bar. The source of bar sand is unknown but may be the Live Oak delta to the northeast.

Reservoir Character and Volume

The character of the reservoir sand in the Martinez Deep field is shown on figures 24, 25, and 26. Four shale breaks can be correlated; two near the top of the sand, and two closer to the bottom. This raises the question whether continuous shale breaks may disrupt continuity within a fault compartment. The Gulf #1 Saldana well (northeast of the well of opportunity) provides some insight. It was originally completed in 1965 below the major shale break with a BHSIP of 8,882 psi. In 1974 it was recompleted above the shale break with a BHSIP of only 5,558 psi. The marked difference in pressure suggests that the two sands were connected within the small eastern block despite the large shale break, as no other well produces from the compartment at this interval.

Reservoir volume is difficult to estimate because of the lack of control for 2 mi to the north or south. A conservatively estimated compartment size, with a northern boundary just east of the Jim Hogg county line and a southern boundary near the Martinez field, gives an area of about 3.6 mi^2. With an average sand thickness of 70 ft, the rock volume is 7 Bcf. The measured porosity averages 16 percent, giving a pore water volume with an estimated range of from 100 to 800 million barrels. This volume is similar to that observed in the smaller water-drive geopressured reservoirs such as the South Cook field reservoirs.

The First Hinnant sand is a reservoir of good continuity (especially along strike) and poor to excellent reservoir quality (parts of the NE Thompsonville field range up to 22 percent porosity and 140 md permeability). Geopressure conditions are good (pressure gradient generally 0.7 to 0.8 psi/ft and temperatures of 240° to 260°F).

Ross (Coastal States) #1 Pauline Kraft

The Ross (Coastal States) #1 Pauline Kraft well lies on the northeastern fringe of the Mobil-David field in Nueces County, Texas (figs. 5, 20). The reservoir of interest is the Anderson sand of the lower Frio, which occurs at a subsea depth of 12,675 ft. The area lies within the Corpus Christi fairway of Weise and others (1981) and is immediately south of the Nueces Bay prospect. The Kraft well has a bottom-hole pressure of 10,986 psi at 12,805 ft, giving a pressure gradient of 0.86 psi/ft. Corrected bottom-hole temperature is estimated at 290°F.

Structure of the Mobil-David Area

The structure of the Mobil-David area has been previously described in relation to the Mobil-David L reservoir. Structural mapping indicates two domes, one of which localizes the Mobil-David field, separated by a downdropped block. A NE-SW structure section (fig. 27) shows that this transverse dome-and-trough structure is largely concealed by the time of CC9 deposition, but has over 1,500 ft of relief at the CC11 marker (the Anderson sand).

The Pauline Kraft well lies within the downdropped block (fig. 20). Its southwestern-bounding fault is precisely located. Its northwestern boundary probably occurs near the large fault to the northwest. The northern boundary is poorly known, but it must lie on the southwestern flank of the dome to the north. The southeastern-bounding fault probably cuts the Pauline Kraft well and is also inferred from a minor growth fault seen in a regional seismic line and from the regional study. This fault compartment is estimated to have a minimum area of 4.8 mi^2 and a probable maximum value of about 8.4 mi^2.

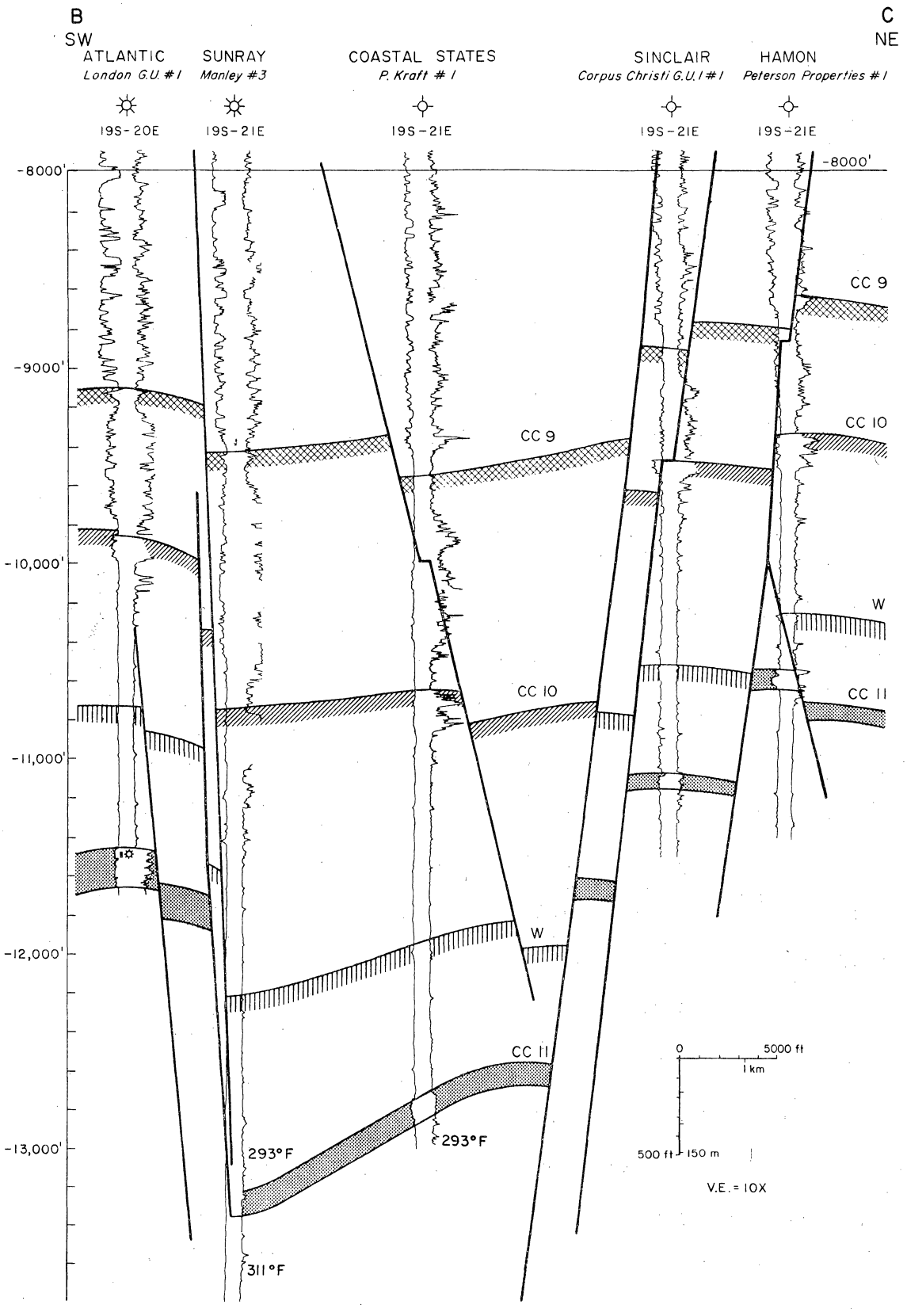

Figure 27. Structural section through Coastal States #1 P. Kraft well, Mobil-David area. Anderson sand (lower Frio) is at CC-11 (stipple); other patterns highlight stratigraphic markers. Line of section is shown in figure 20.

Reservoir Volume of the Anderson Sand

Within the fault compartment, the Anderson sand ranges from less than 10 ft to more than 150 ft thick (fig. 20). It is generally of good quality with minor shale breaks (fig. 24). Planimetry of the net-sand map over the minimum and maximum fault compartment sizes yields a minimum sand volume of 17.9 Bcf and a maximum volume of 28.6 Bcf. Porosity ranges from 20 percent to 24 percent, based on sidewall cores in the Kraft well and on estimates given for the Mobil-David field by Duggan (1972). For 20 percent porosity, the aquifer volumes for the minimum and maximum cases are 640 and 1,020 million barrels, respectively; for 24 percent, they are 700 and 1,200 million barrels. This can be compared with the C sand at the South Cook field, De Witt County (Cuero area), which has 588 million barrels. The aquifer volume is larger than the Texas water-drive geopressured gas reservoirs described above, but smaller than several calculated by Boardman (1980) for Louisiana. This reservoir might support 14,000 bpd for 10 years at 5 percent recovery, using 20 percent porosity and the larger fault compartment size.

The Pauline Kraft well of opportunity has a good sand thickness in an unusually large fault compartment. Unfortunately, insignificant quantities of fluids were produced during the short-term test because of very low permeabilities. Sidewall cores suggest that permeabilities are highest in the central part of the sand and lowest at the top and bottom of the sand (fig. 24). Such low permeabilities are common to many South Texas reservoirs (Loucks and others, 1981).

Lear #1 Koelemay

The Lear #1 Koelemay well was drilled as a wildcat in the Doyle area of northwestern Jefferson County (fig. 5). The test reservoir is the Leger sand of

the Yegua Formation, at 11,590 ft below sea level (fig. 28). The sands of this area lie within a geopressure trend which has been referred to previously as "Vicksburg" (Loucks, 1979); there are no sands in the Vicksburg interval in the immediate area. The Leger sand is geopressured in most of the area considered. In the Koelemay well, bottom-hole pressure was measured as 9,441 psi at 11,669 ft, giving a gradient of 0.81 psi/ft. Measured bottom-hole temperature is 257°F. Porosity and permeability trends within the sand are complex but they increase irregularly upward (fig. 24).

Stratigraphy of the Leger Sand

The Leger sand occurs about 700 ft below the top of the Yegua (Cockfield) in the study area, as correlated by paleontologic information from Texaco #1 Doyle and regional cross sections (Dodge and Posey, 1981). It is one of a number of lenticular, often shaly sands that occur in the shale-dominated Yegua section south and east of Sour Lake (fig. 29). Correlations in this sequence are generally unreliable, but the Leger sand is fairly persistent in most cases. Electric-log patterns of many of these sands suggest a deltaic origin; they were probably deposited as delta-front sands in a high-constructive delta.

The Leger sand shows two depocenters in the study area (fig. 28). The main depocenter of interest is south-southeast of Sour Lake Dome; in this area the sand is over 100 ft thick on the downthrown side of several growth faults. Immediately updip, this sand is only 15 to 40 ft thick, but thickens northward to 80 ft. The second depocenter, west of Sour Lake, is slightly younger. Its more dip-oriented sand reaches a thickness of 95 ft in Hathaway field, Liberty County. Sands in these two depocenters cannot be assumed to be connected.

The stratigraphic section (fig. 29) suggests a recurrent pattern of sedimentation in this area. The depocenter contains an upward-coarsening sequence

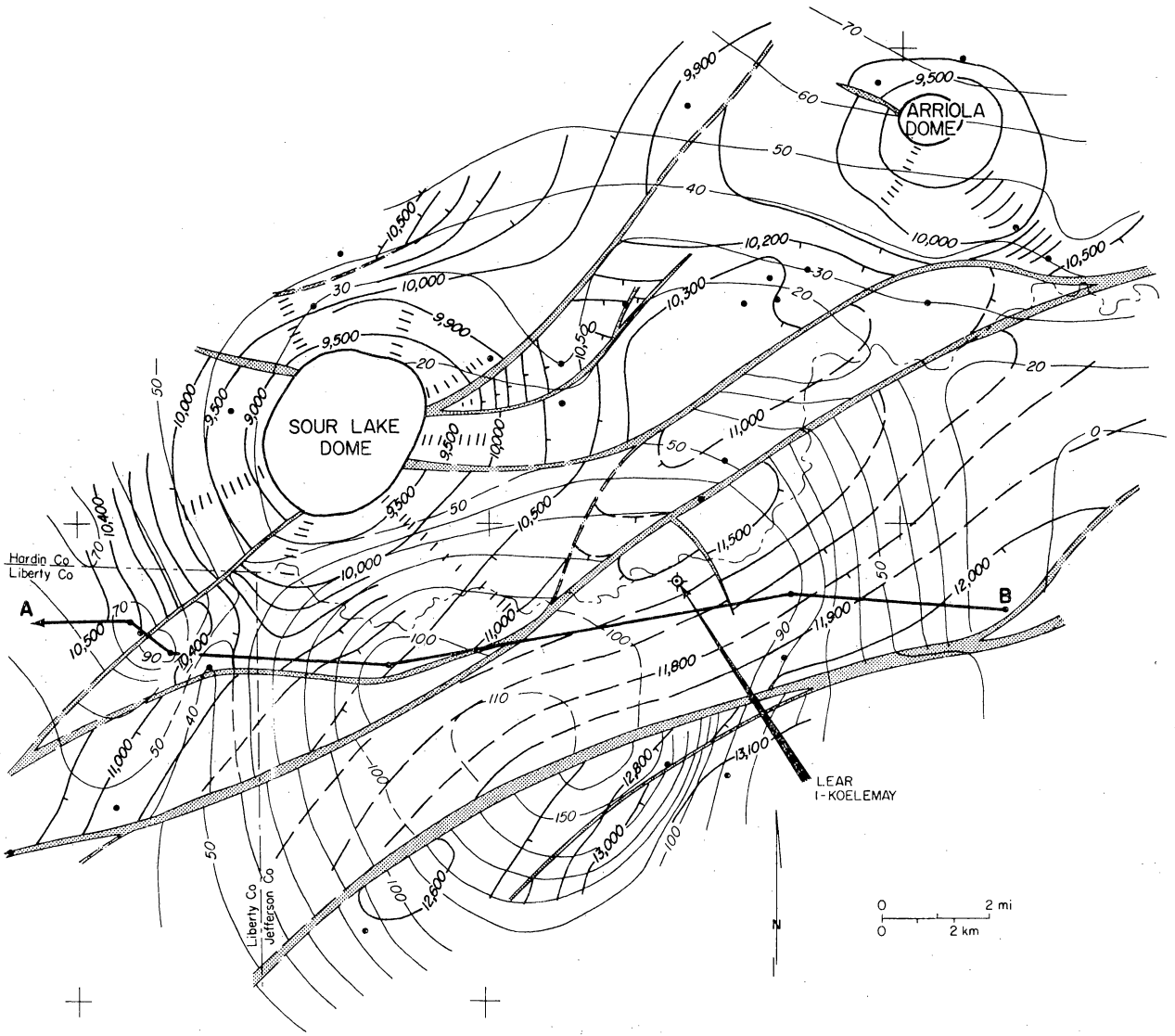

Figure 28. Structure and net-sand map, Lear #1 Koelemay area. Datum is top of the Leger sand, Yegua Formation. Shading indicates sand thicker than 90 ft. Faults downthrown to south unless indicated.

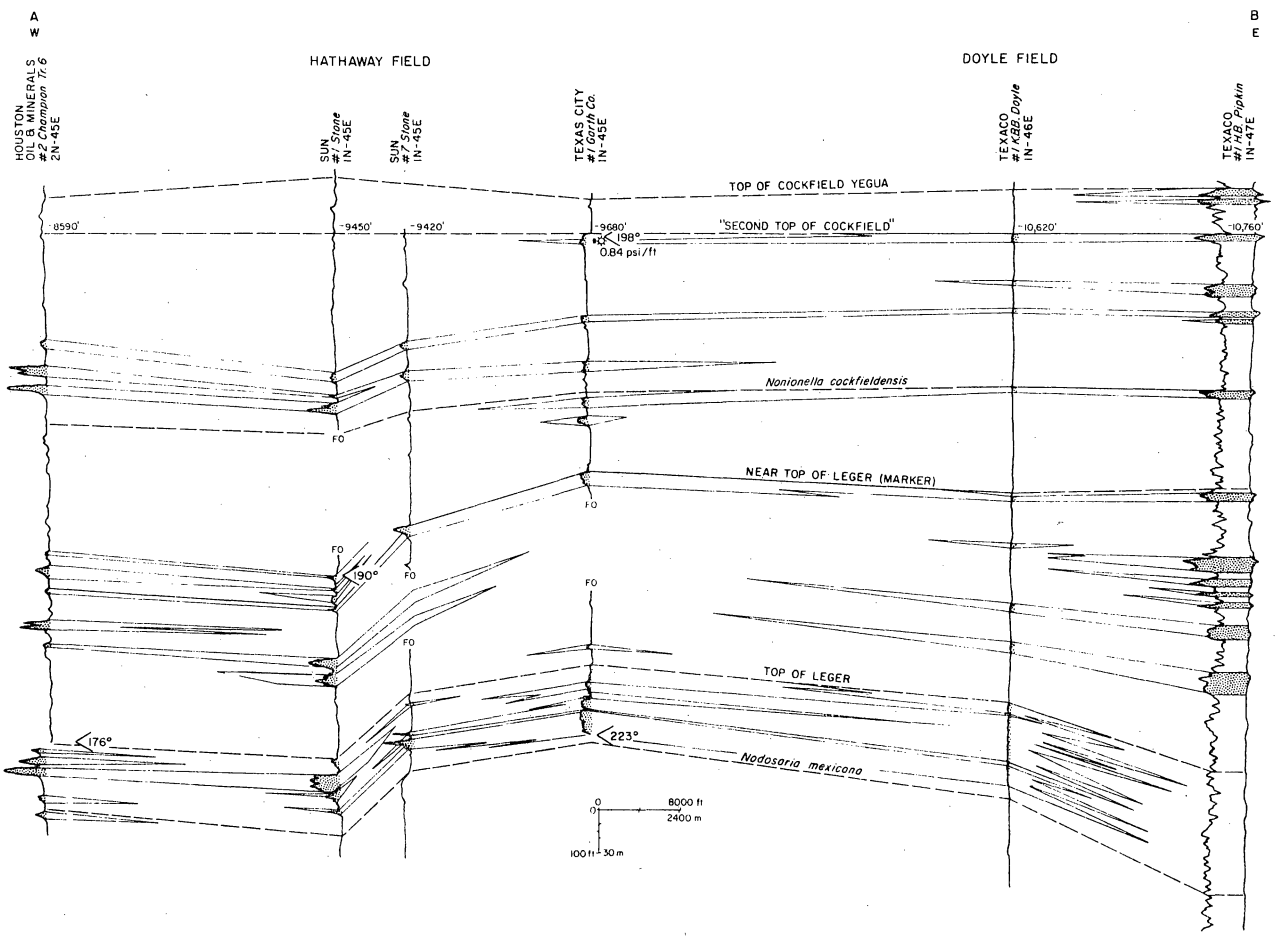

Figure 29. Stratigraphic section of Yegua sands, Lear #1 Koelemay area. Datum is "Second Top of Cockfield" of industry usage. Symbols as in figure 9; line of section on figure 28.

of shales to sands, presumably a delta-front sequence. Southwest of this depocenter are thinner, cleaner sands that have more blocky SP responses. These may represent bar sands reworked along strike from the delta front by longshore currents.

Structure

Well control at depth is sparse in this area; hence most of the major structures are not precisely located. Structure in the area consists of growth faults separating gently gulfward-tilting fault blocks, which are locally pierced by salt domes (fig. 28).

Expansion across the faults in this area is not large but did influence Yegua, Jackson, and Vicksburg sedimentation. Expansion factors across the faults suggest Yegua and Jackson movement for all faults (with greatest Jackson expansion on the most southern fault), Vicksburg movement on the southern faults, and slight Frio expansion on the most seaward fault. The long history of growth across these faults may be related to the low sedimentation rates in the shale-dominated Yegua-Jackson-Vicksburg sequence.

Three salt domes occur in the area: Hull (west of fig. 28), Sour Lake, and Arriola; the Yegua sands are uplifted to shallow depths around each salt stock. However, this does not appear to have relieved the geopressured condition of the Leger sand in the basin between Sour Lake and Arriola Domes, where the Sour Lake East field has a pressure gradient of 0.65 psi/ft.

Reservoir Volume and Continuity

The sparsity of deep well control in the area makes it impossible to estimate a meaningful compartment area or reservoir volume without seismic data. At least 2 to 3 mi^2 of reservoir area might be expected with a gross sand thickness of roughly 100 ft. This would give a sand volume of 7 Bcf, or (using

20 percent porosity) a pore volume of 250 million barrels. This is, however, only an order-of-magnitude calculation.

Continuity of this reservoir is difficult to estimate. No major shale breaks appear to be continuous through the area; however, minor shaly intervals are abundant in most wells and may interfere with vertical continuity in some cases. The fault on the north boundary of the area is marginally sealing. There may be connection to the Forest #2 Kirby well, but this is not likely.

The Leger sand in the Doyle area shows marginal geopressure conditions in an area of poor well control. The Lear #1 Koelemay test does, however, appear to be typical of the Yegua geopressure reservoirs in this area.

Conclusion, Well of Opportunity Study

Table 7 summarizes the reservoir volume estimates for three wells of opportunity. The wells of opportunity have sampled a Wilcox barrier sand, a Yegua distal delta-front sand, and a thick Frio delta-front or composite sand. Two wells have been located in South Texas and one in southeast Texas. All of the aquifers tested are similar in volume and fault-block area to water-drive gas reservoirs. Two of the aquifers (at Riddle #2 Saldana and Lear #1 Koelemay) have volumes similar to the Yorktown field of De Witt County. The aquifer at the Ross (Coastal States) #1 Kraft well is similar in volume to the South Cook sands of the Cuero area. For comparison, Blessing area sands (Winker and others, 1981) are larger, with aquifer volumes of 1,700 to 2,900 million barrels.

The greatest problem with determining aquifer volume for the wells of opportunity is the poor delineation of fault-compartment geometry. In all of these cases, seismic data is essential to properly evaluate fault-compartment area and, therefore, reservoir volume. This contrasts with the case histories for producing reservoirs in which lack of compartment control was important in

only a few cases. This difference is partly inherent in the data base; the case histories are of developed fields with production history, whereas wells of opportunity are generally wildcat holes, hence the structure is less well determined.

INTERNAL PROPERTIES OF SANDSTONES

The basic constructional elements of sand bodies (laminae, beds) may exhibit large grain-size variations over a space of inches. These textural differences may be enhanced during diagenesis and may result in major reductions in transmissivity after sandstone consolidation. Chemical precipitates that coat grains and fill pores serve to further restrict fluid flow. The small-scale inhomogeneities of reservoirs are controlled mainly by degree of cementation as well as by size and shape of grains (texture), their sorting and packing (texture), and arrangement (stratification). Predicting fluid flow through a reservoir using sandstone facies models depends largely on (1) whether or not original variations in pore properties are preserved in rocks, and (2) if vestiges of those trends are preserved, whether they are important in well completion and production strategies.

Porosity and Permeability of Modern Sands

Most modern Gulf Coast sands are typically fine to very fine grained because of their source and multi-cycle origin. Such fine-grained sands generally have higher porosities but lower permeabilities than coarse-grained sands from comparable environments elsewhere. In fact, some modern point-bar and beach sands from the Gulf Coast have original permeabilities that are five to ten times lower than those of equivalent sand types elsewhere (Pryor, 1973).

Pryor (1973) studied inhomogeneities associated with grain sorting and directional properties of modern sand bodies including several Gulf Coast beaches

and a Mississippi River point-bar deposit. He found that river sands have greater permeability variations than beach sands and that both sand types have well-organized directional permeabilities. The directions of greatest permeability are aligned parallel to the length of river bars and perpendicular to the long axis of beaches. Permeabilities for modern river and beach sands range from a few millidarcys to tens of darcys depending on grain size and sorting. This range of more than four orders of magnitude decreases as the sediments compact and are buried, but even ranges of three orders of magnitude (0.1 to 100 md) are common in consolidated sandstones.

Detailed Investigation of Vertical Changes in Porosity and Permeability

Cored intervals from the General Crude Oil/Department of Energy #1 and #2 Pleasant Bayou wells were selected for detailed analysis of vertical variation in porosity and permeability because of the excellent condition of the core and because the geology of the test well site (fig. 30) is well documented (Bebout and others, 1978, 1980).

All of the cored intervals examined occur between the T2 and T6 correlation units (Cibicides hazzardi through Anomalina bilateralis zones) of the Oligocene Frio Formation. A variety of depositional environments, ranging from distributary channel with associated subaerial levees to shallow-marine storm-related deposits on the shoreface toe, are represented. Over 300 ft of core were examined and described, selected intervals of which are presented in figures 32 through 35. Explanation of the symbols used in the detailed descriptions of the core is presented as figure 31.

Diagenesis, involving the reduction of pore voids through compaction and cementation, is an important modifier of initial porosities and permeabilities in ancient sandstones. The diagenetic history of the Frio Formation in the

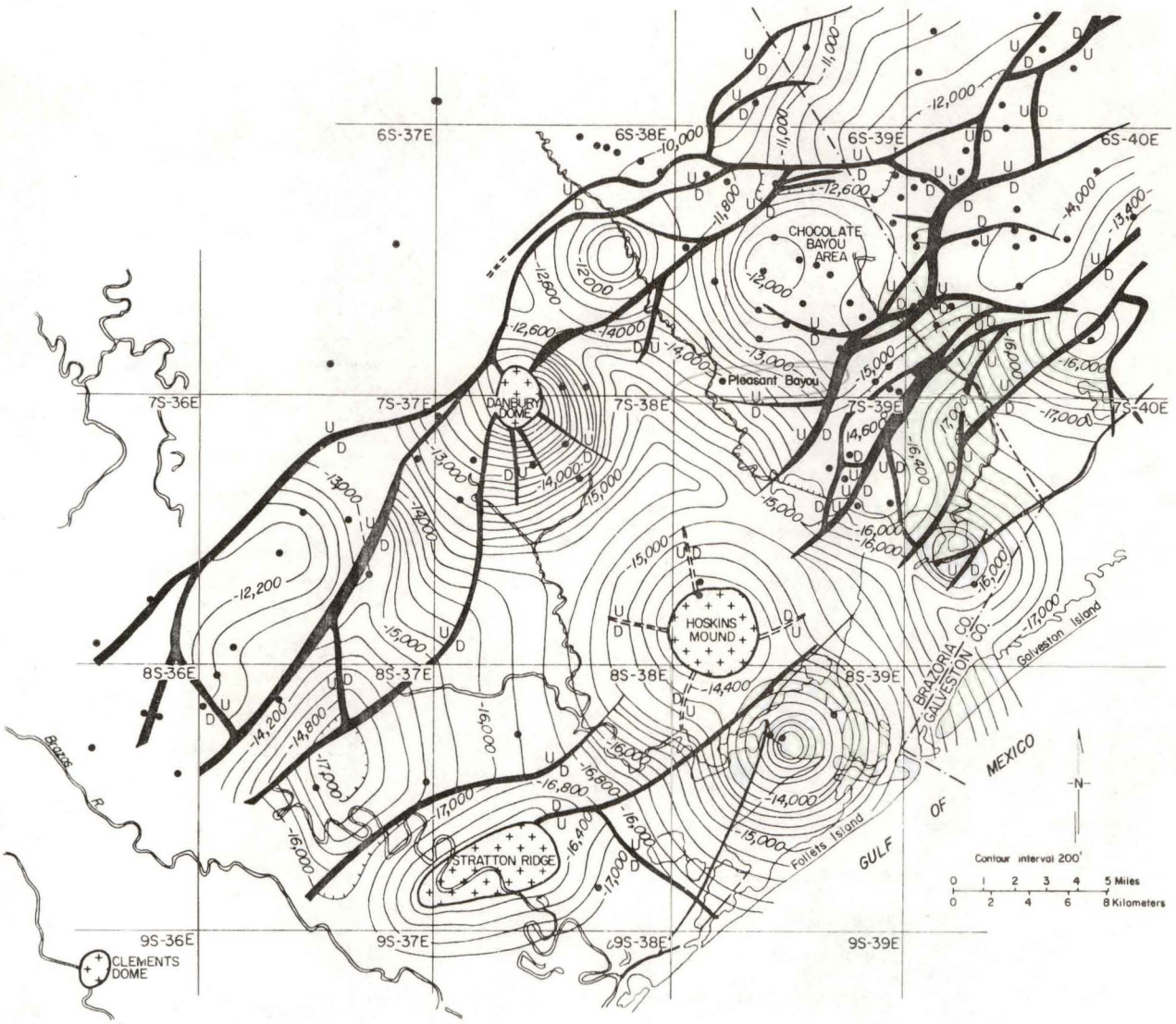

Figure 30. Location of the General Crude Oil/Department of Energy Pleasant Bayou No. 1 and No. 2 geopressured geothermal test wells (Pleasant Bayou) and structural fabric at the T5 marker (Anomalina bilateralis). The wells, which were drilled 500 ft apart, are located on the flanks of the Chocolate Bayou domal structure in a salt-withdrawal basin associated with the Danbury Dome. Northeast-trending faults are Frio-aged growth faults. [Modified from Bebout and others (1980)].

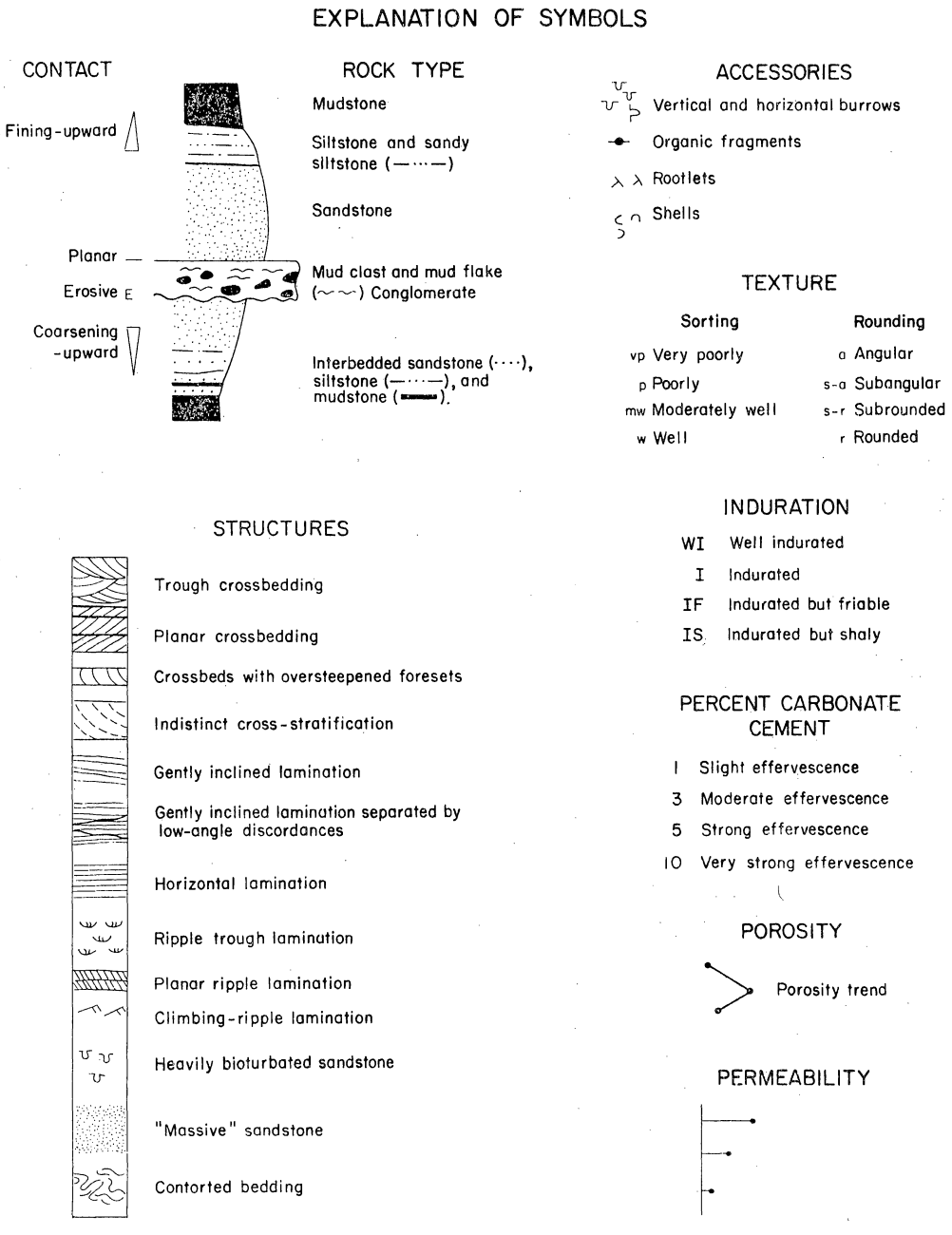

Figure 31. Explanation of symbols for figures 32 to 35. Porosity and permeability values obtained from whole-core analyses.

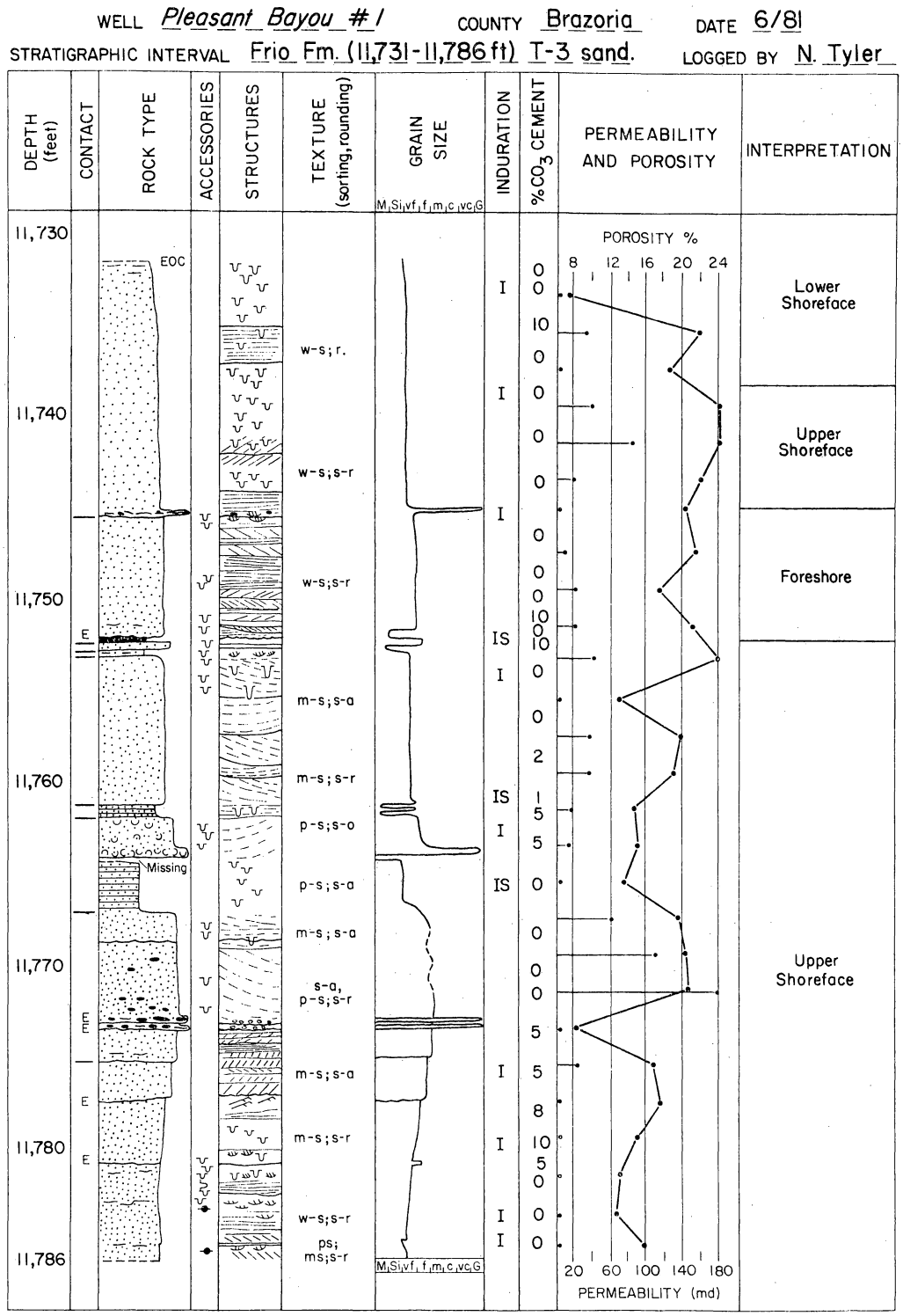

Figure 32. Detailed core description, core characteristics, and interpretation of the upper part of the Frio T3 correlation unit. Vertical changes represent a composite of several trends, the highest porosities and permeabilities being associated with large-scale crossbedding and the coarsest grain size present. Porosity and permeability data are derived from laboratory analysis of whole core.

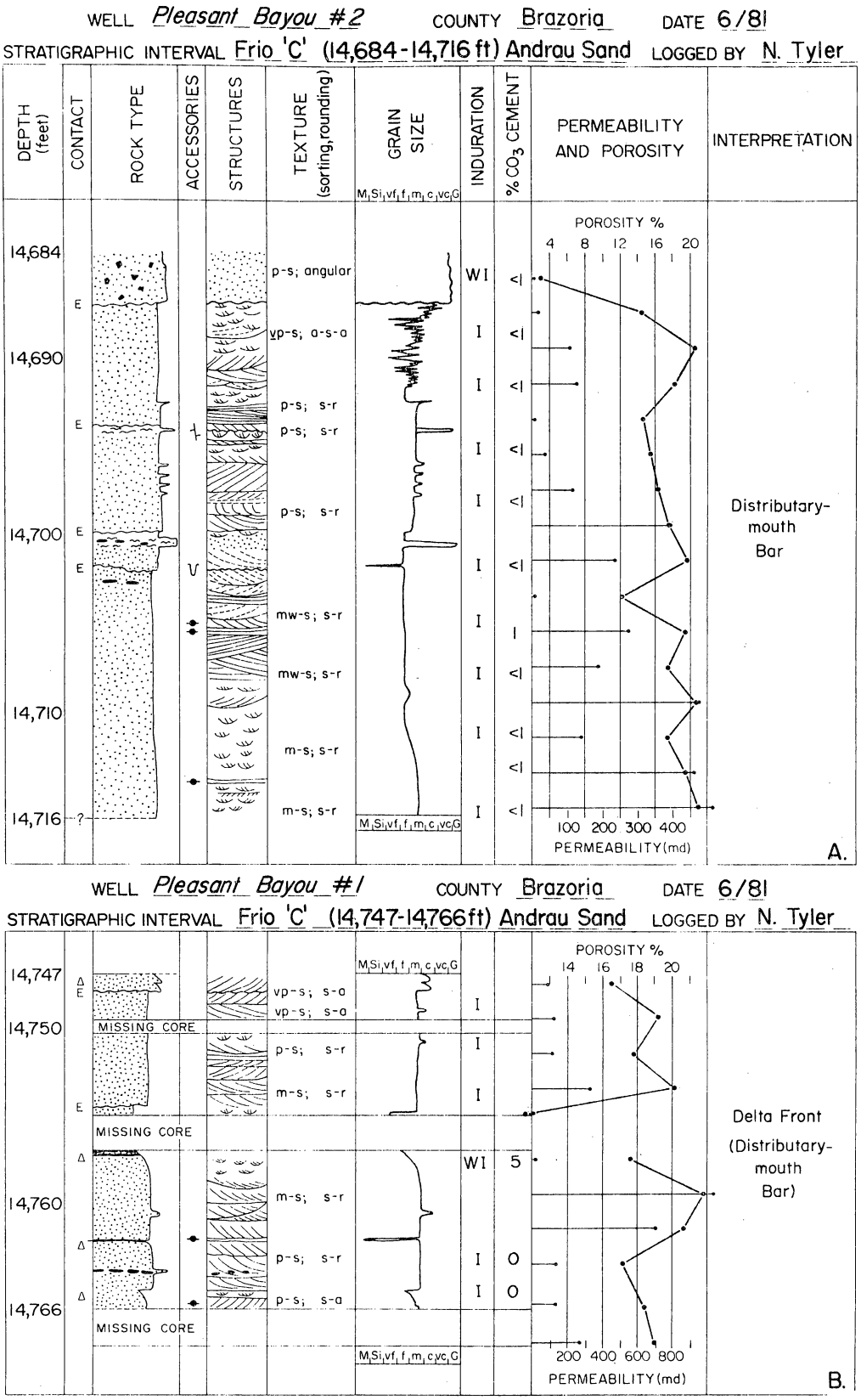

Figure 33. Detailed core description, core characteristics, and interpretation of the geopressured geothermal production interval (Andrau or C sand). Vertical changes generally show an upward decrease in porosity and permeability for both sections.

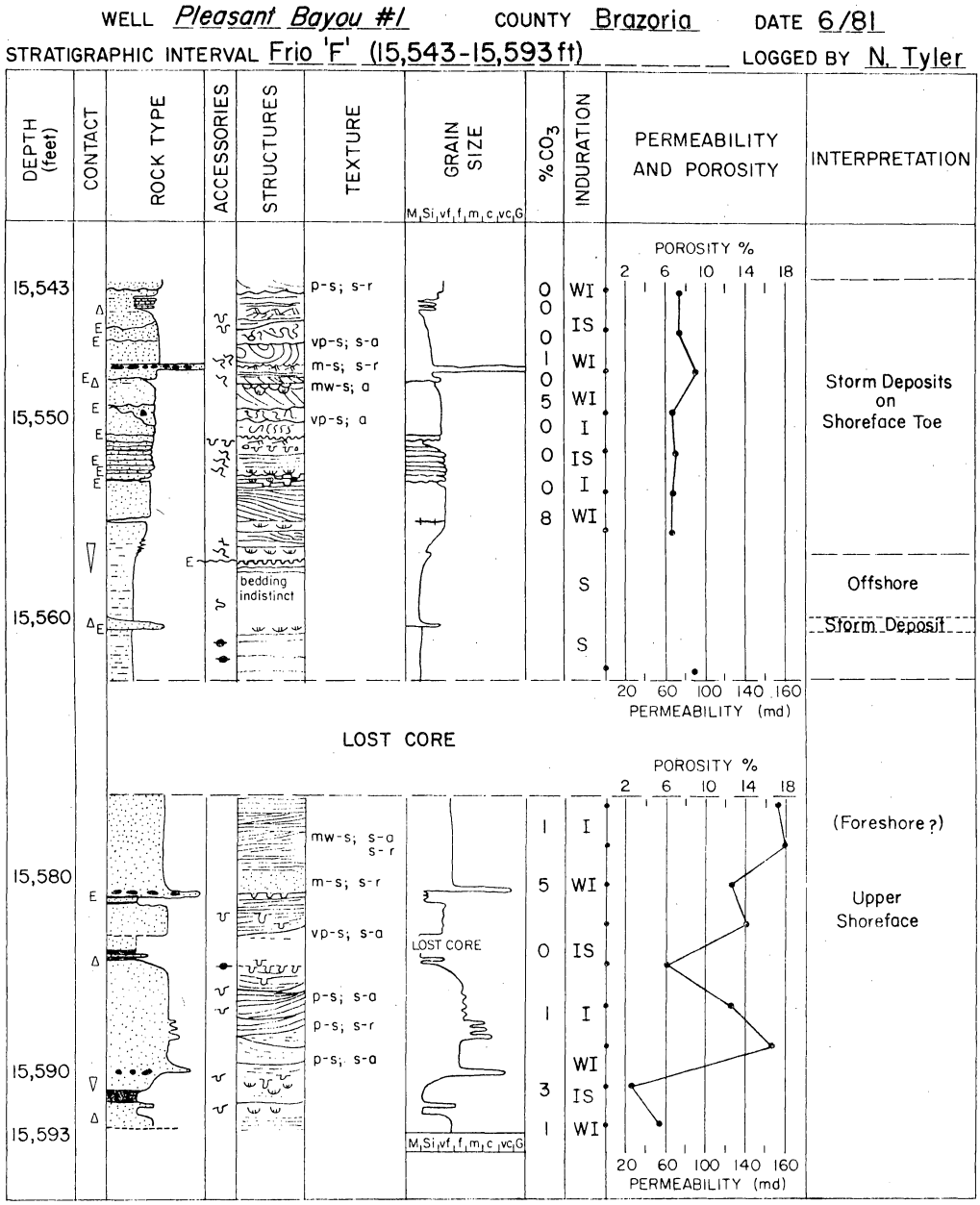

Figure 34. Detailed core description, core characteristics, and interpretation of a part of the Frio D correlation interval (sub T5). Upper sand exhibits uniformly low porosity and permeability. Contorted beds in this sand have lower porosities than adjacent undeformed beds (15,556 to 15,543 ft).

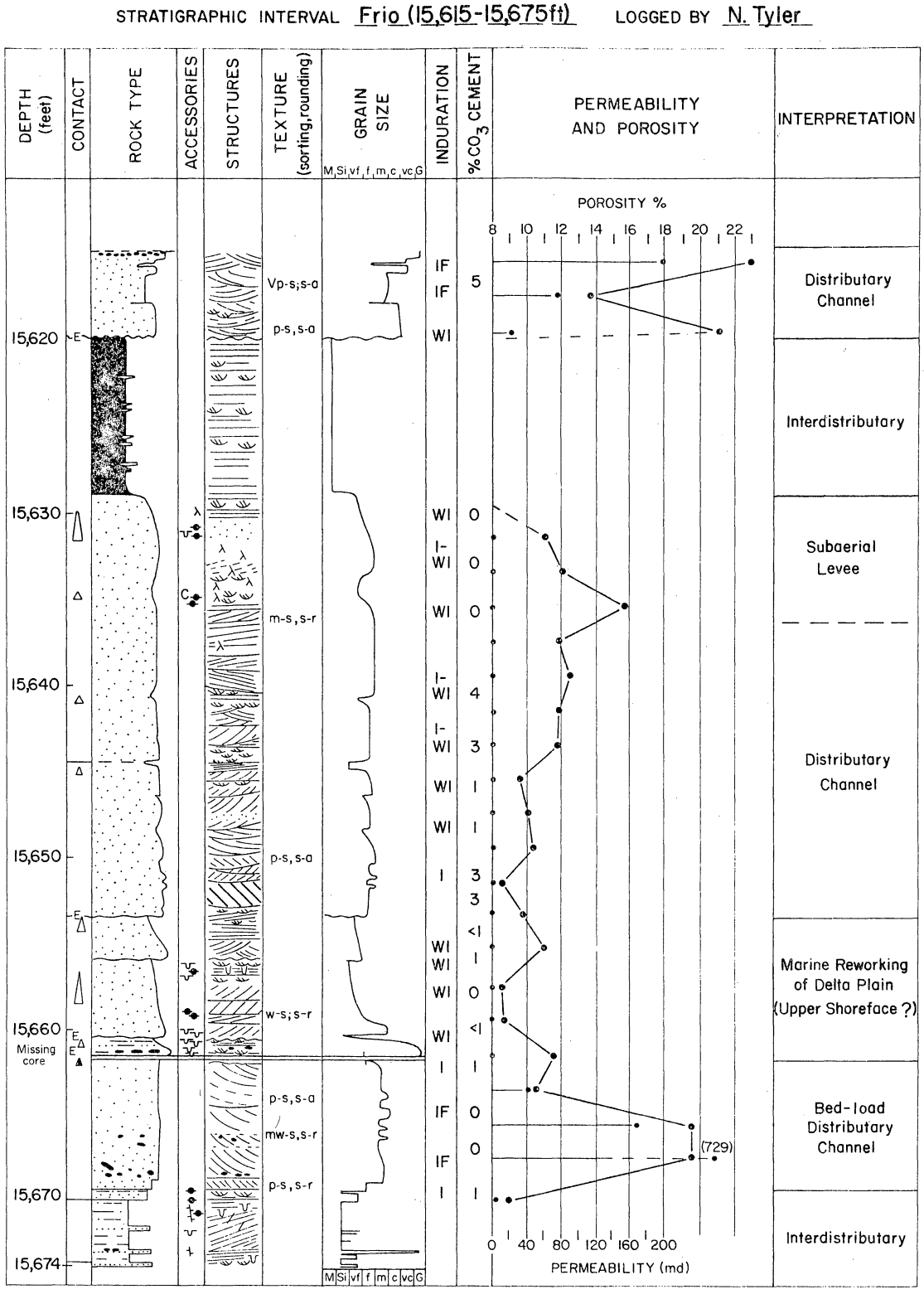

Figure 35. Detailed core description, core characteristics, and interpretation of a part of the Frio sub T5, F correlation interval. This composite sandstone shows a central decrease in porosity. On a smaller scale, large crossbeds (15,670 to 15,661 ft and 15,620 to 15,616 ft) have higher porosities and permeabilities than smaller scale crossbeds (15,653 to 15,640 ft).

Chocolate Bayou/Danbury Dome area has been described in detail (Bebout and others, 1978; Loucks and others, 1981; Milliken and others, 1981) and is briefly summarized here. Lithic arkoses and feldspathic volcanic arenites of the Frio Formation underwent early, near-surface leaching of feldspars accompanied by replacement and cementation by calcite. Compaction of the sediments, with concomitant generation of clay coats and feldspar overgrowths, was followed by precipitation of locally variable quantities of quartz overgrowths and a minor phase of sparry calcite cementation. This early phase of passive diagenesis took place to a depth of approximately 8,500 ft (Milliken and others, 1981) and reduced porosity to less than 15 percent (Bebout and others, 1978). Below 8,500 ft within the geopressured zone, leaching of the unstable lithic clasts (feldspar, volcanic rock fragments) and early calcite cement created secondary porosity, but this was somewhat reduced in the deep subsurface by precipitation of kaolinite and Fe-rich calcite cement (Bebout and others, 1978).

The primary objective of the present analysis was to "look through" the diagenetic imprint and examine the influence of variations in grain size, primary sedimentary structures, bioturbation, and texture (rounding and sorting of grains) on porosity and permeability trends in the geopressured Frio. In the Pleasant Bayou cores, porosity and horizontal permeability vary in direct relation to changes in these parameters. Generally, variation in one parameter is accompanied by a change in one or more of the remaining variables, e.g., a decrease in grain size is accompanied by an increase in bioturbation (fig. 32, 11,732 to 11,740 ft); therefore, considering these parameters individually places artificial constraints on the analysis. Because changes in grain size are commonly accompanied by changes in primary sedimentary structures, and because these two parameters exert the most influence on porosity and permeability, these parameters are discussed jointly.

Variations in Grain Size and Primary Sedimentary Structures

In the Pleasant Bayou cores a decrease in grain size is accompanied by a decrease in porosity and permeability (fig. 32, 11,732 to 11,741 ft; fig. 33B, 14,757.5 to 14,759 ft; fig. 35, 15,629 to 15,632 ft). This decrease is most marked where a decrease in grain size involves a change in lithology from sandstone to siltstone or mudstone (fig. 32, 11,765 to 11,772 ft, permeability decrease from an average of 100 md to less than 1 md, and porosity from 20 to 13.5 percent). However, even very subtle changes in grain size unassociated with changes in sedimentary structures result in dramatic changes in permeability. For example, in an interval composed of ripple cross-lamination (fig. 33A, 14,713 to 14,716 ft), a gradual decrease in grain size from medium to fine sand is accompanied by a threefold change in permeability (475 to 140 md). The coincident decrease in porosity is less dramatic (20 to 17.5 percent). The reverse also holds true, as an increase in grain size (fig. 32, 11,775 to 11,785 ft) results in a porosity increase from 13 to 17 percent.

Changes in grain size are generally accompanied by changes in primary sedimentary structures. A progressive increase in grain size from the base of the T3 cored interval (fig. 32) corresponds to a vertical gradation in the scale of structures from horizontal laminations and scattered rippled zones, through climbing ripples, to small-scale planar crossbeds, finally to a large-scale trough crossbed in the coarsest grain size present (11,771 to 11,785 ft). The highest permeabilities encountered in this interval occur in the large-scale trough crossbedded, medium-grained sandstone (fig. 32, average 118 md, 11,772 ft). Decreases in grain size are accompanied by a decrease in the scale of sedimentary structures as well as a reduction in porosity and permeability (fig. 32, 11,732 to 11,740 ft; fig. 33B, 14,757 to 14,759 ft; fig. 35, 15,653.5 to 15,662.5 ft).

Some of the sandstone intervals described do not exhibit a change in grain size but are characterized by variations in the scale and types of the primary sedimentary structures. These variations in bed thickness and configuration at constant grain size result from changes in water depth and/or current velocity (Simons and others, 1965; Southard, 1971). Porosity and permeability appear to be influenced by the scale and type of sedimentary structures. Generally, the larger the scale of the sedimentary structure, the higher the relative porosity and permeability. The term "relative" is used here as quantitative comparisons of the measured porosities and permeabilities from different intervals are not valid because of differences in diagenetic histories. Large-scale crossbedded sandstones (fig. 36A, right core slab) have higher porosity and permeability values than smaller-scale crossbedded sandstones (fig. 36A, left core slab, and fig. 36B), which, in turn, have higher values than rippled sandstones (fig. 36C). Horizontal (fig. 36C) and gently inclined laminated sandstones have variable permeabilities, probably as a result of fluids moving along bedding planes rather than between the sand grains (interstratal versus intrastratal flow). Non-biogenic, postdepositional structures also affect porosities and permeabilities. In an interval consisting of interbedded, undeformed and contorted upward-fining cycles, the undeformed beds have porosities significantly higher (2 to 3 percent) than the adjacent contorted beds (figs. 34 and 37A), that are of a similar grain size.

Bioturbation and Texture

The effects of bioturbation on permeability trends and, to a lesser extent, porosity in the Pleasant Bayou cores are well defined. In intensely bioturbated zones permeabilities are markedly reduced in comparison to adjacent slightly bioturbated horizons. This is partly because burrowing and feeding trails of trace fossils disrupt and destroy bedding, thereby inhibiting fluid movement

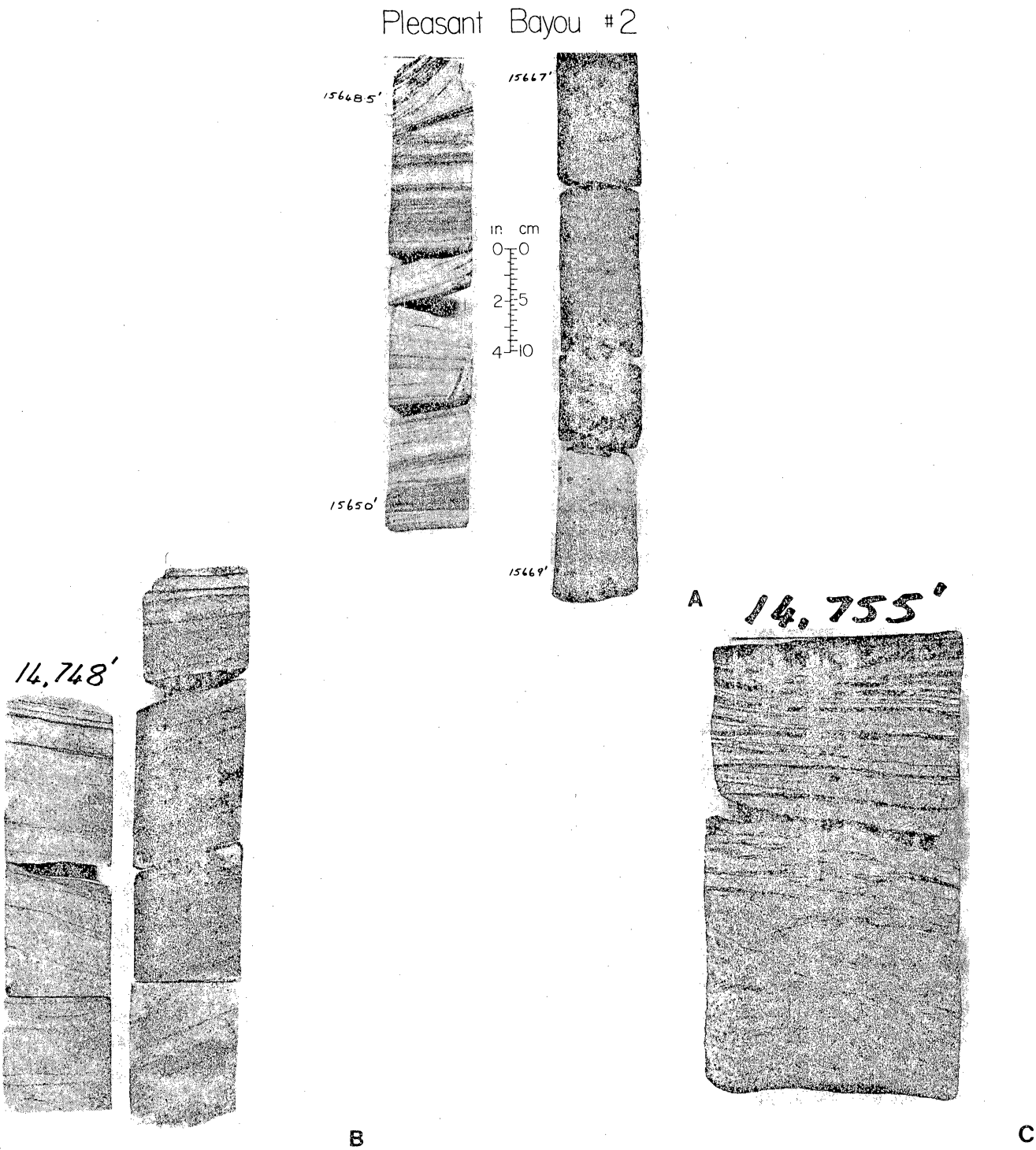

Figure 36. A. Right slab. Large-scale cross-lamination in permeable (729 md), porous (19 percent) sandstone, interpreted as a bed-load distributary-channel deposit (F correlation interval, fig. 35). Intermediate- to small-scale cross beds (left slab) also deposited within bed-load channels in this interval have negligible permeabilities (less than 1 md) and significantly lower porosities (10 to 12 percent) than sandstones with large-scale cross-lamination. B. Intermediate- to small-scale crossbedded sandstone of the production interval (fig. 33B). Porosity (16.5 percent) and permeability (100 md) are less than that of large-scale crossbedded sandstone. C. Ripple-laminated sandstone overlain by horizontally bedded sandstone with thin mud drapes. Ripple-laminated sandstone has the lowest permeability and comparatively low porosity in the production interval (see fig. 33B).

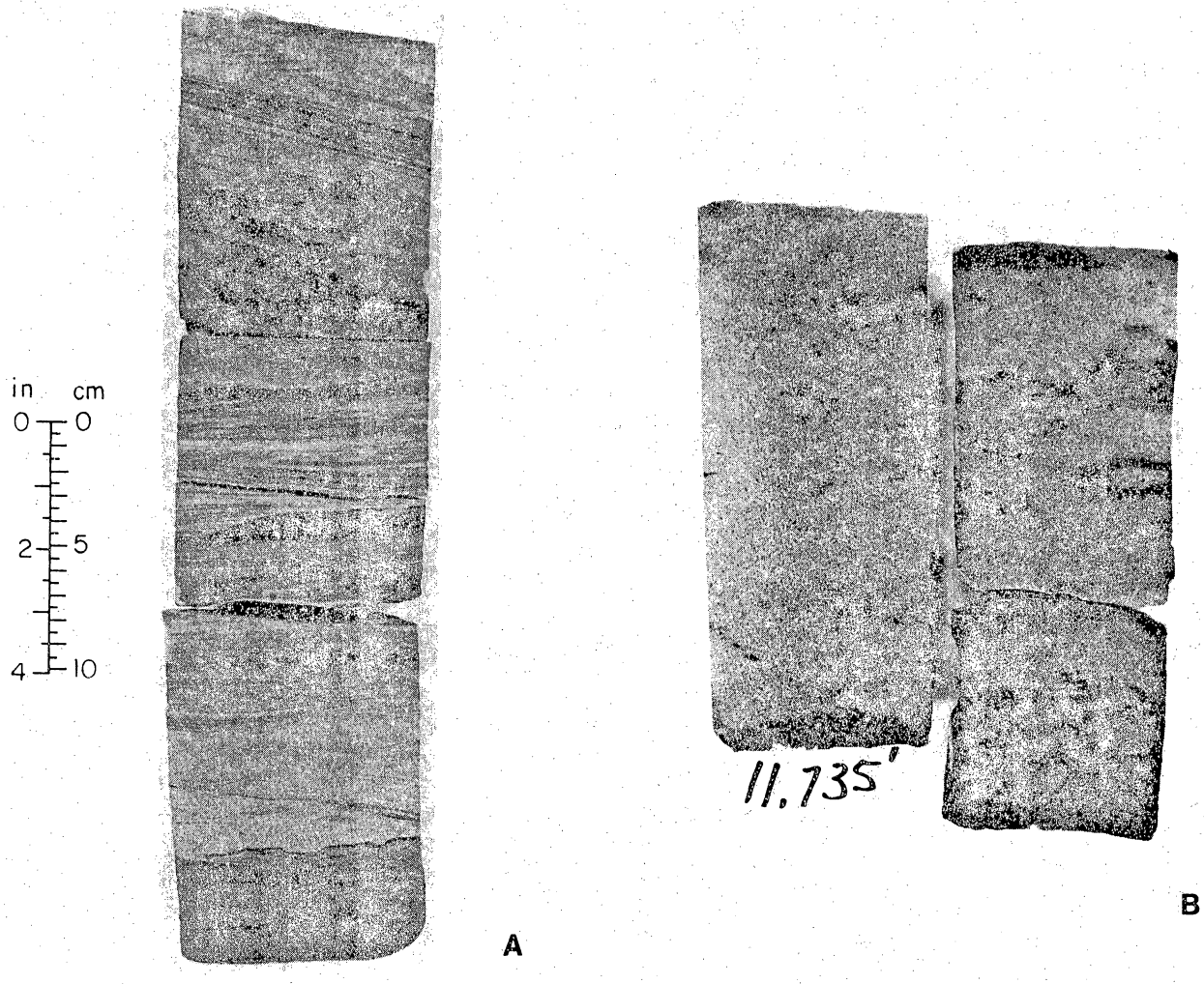

Figure 37. A. Interlaminated very fine grained sandstone and siltstone interpreted as shallow-marine storm-related sequences. Undeformed units have higher porosities (2 to 3 percent) than adjacent contorted deposits (see fig. 34). B. Highly bioturbated sandstone (trace fossil Ophiomorpha) in which porosities and permeabilities have been substantially reduced owing to destruction of primary sedimentary structures and introduction of fine-grained detritus. In these lower shoreface deposits porosities were reduced from 23 percent in unbioturbated sandstones to 7.5 percent, and permeability was reduced from 60 md to 1 md (fig. 32).

along bedding planes. Furthermore, porosity and permeability reductions are partly attributed to mixing of finer grained detritus into the sand by the organisms. An example of the effects of bioturbation on reservoir quality is illustrated in figure 32 (11,743 to 11,732 ft). Three zones of intensely bioturbated, very fine grained sand are interbedded with weakly to moderately bioturbated sands, in which sedimentary structures are still recognizable. In the bioturbated zones, primary sedimentary structures are obliterated by burrowing of organisms, their activities now recorded by the trace fossil Ophiomorpha (fig. 37B). Permeability in the weakly bioturbated zones (11,741 and 11,735 ft) is significantly higher than in the adjacent intensely bioturbated sands. Permeabilities decrease from an average of 50 md to less than 30 md (two of the zones have permeabilities of less than 1 md).

The response of porosity to bioturbation is varied. In the bioturbated interval 11,741 to 1,737 ft (fig. 32), porosity in one of the samples was similar to that of adjacent weakly bioturbated sandstones, while the other was 5 percent lower. Where bioturbation is accompanied by a change in grain size, porosities decrease markedly (23 to 7.5 percent; 11,735 to 11,732 ft). Introduction by the organisms of finer grained detritus from the overlying deposits into the sandstones is the probable cause of this decrease.

The influence of textural variations on porosity and permeability in the Pleasant Bayou cores is masked to a large extent by the overriding effects of diagenesis. However, the importance of textural controls on reservoir quality is indicated in figure 33B (14,760 to 14,766 ft). Here, changes in sorting from poor to moderate, and in grain shape from subangular to subrounded is accompanied by an increase in permeability (125 md to an average of 850 md) within sandstones of a constant grain size and similar scale of structure. The reverse also holds true as a decrease in sorting and rounding results in a decrease in permeability and porosity (fig. 33B, 14,750 to 14,754 ft).

Induration

Induration refers to the hardness and cohesiveness of sandstones and can be an indicator of porosity and permeability. Well-indurated sandstones in the Frio Formation (fig. 33A, B; and fig. 35) have negligible permeabilities. On the other end of the spectrum, indurated but friable sandstones are characterized by comparatively high permeabilities (fig. 35).

Porosity and Permeability as a Function of Depositional Environment

Environments of deposition of the sandstones intersected by the Pleasant Bayou cores were interpreted on the basis of sandstone geometries (Bebout and others, 1978, 1980) and vertical arrangement of grain size and primary sedimentary structures. The nature and intensity of bioturbation and micropaleontological evidence (Appendix A) were also taken into account. The broad depositional setting of the geopressured Frio in the Chocolate Bayou/Danbury Dome area is inferred to be a high-constructive deltaic system with individual depositional sequences exhibiting lobate net-sand patterns. A variety of subenvironments within this deltaic system are represented in the cores. Because of the dynamic nature of the deltaic-marine interface, there is often a rapid alteration of subenvironments within the deltaic-shallow marine system. For example, marine reworking of delta-plain sediments following lobe abandonment and switching of fluvial activity elsewhere on the delta plain results in nearshore marine deposits of variable thickness interbedded within a predominantly subaerial sequence (fig. 35, 15,660 ft). Vertical alternation of subenvironments in this instance (marine sandstone interbedded in fluvial sandstone) would not influence reservoir behavior as markedly as superposition of more distal marine facies (lower shoreface siltstones or offshore mudstones) or floodplain mudstones (fig. 35, 15,625 ft) in the sequence. Therefore prediction of reservoir behavior should

always consider the dynamic nature of the systems responsible for deposition and accumulation of the reservoir host rocks.

Porosity and permeability trends within these subenvironments are directly related to grain size, sedimentary structures, and bioturbation. Thus, the lower shoreface, which is composed of bioturbated, very fine grained, horizontally laminated sandstone, has lower porosities and permeabilities than do the sparsely bioturbated, crossbedded, very fine to fine-grained sandstones of the upper shoreface (figs. 32 and 34). Similarly, the medium-grained crossbedded sandstones of distributary-mouth bars (fig. 33A, B) and sand-filled distributary channels have relatively higher porosities and permeabilities than do associated subenvironments (fig. 35).

In summary, a knowledge of grain-size trends, sedimentary structures, and bioturbation associated with specific depositional environments is critical in predicting reservoir quality in adjacent areas for which core data are unavailable. In general, crossbedded, moderately sorted and rounded, relatively coarser grained sandstones (upper shoreface, fluvial channel, distributary-mouth bar subenvironments) have higher permeabilities than do the associated ripple-laminated and horizontally laminated, bioturbated, poorly sorted, finer grained sandstones of the lower shoreface, distal delta-front, and levee subenvironments.

Facies Control on Reservoir Continuity

Sandstone reservoirs are rarely the uniform, laterally persistent sheet sands they are often assumed to be. Sandstone depositional geometries differ markedly as a result of deposition under widely divergent conditions; for example, thick, laterally persistent sheet sands deposited as distributary-mouth bars in the delta-front setting of a constructive lobate delta (for example, the Andrau or C sand, figs. 38 and 39) constitute more attractive targets than thin,

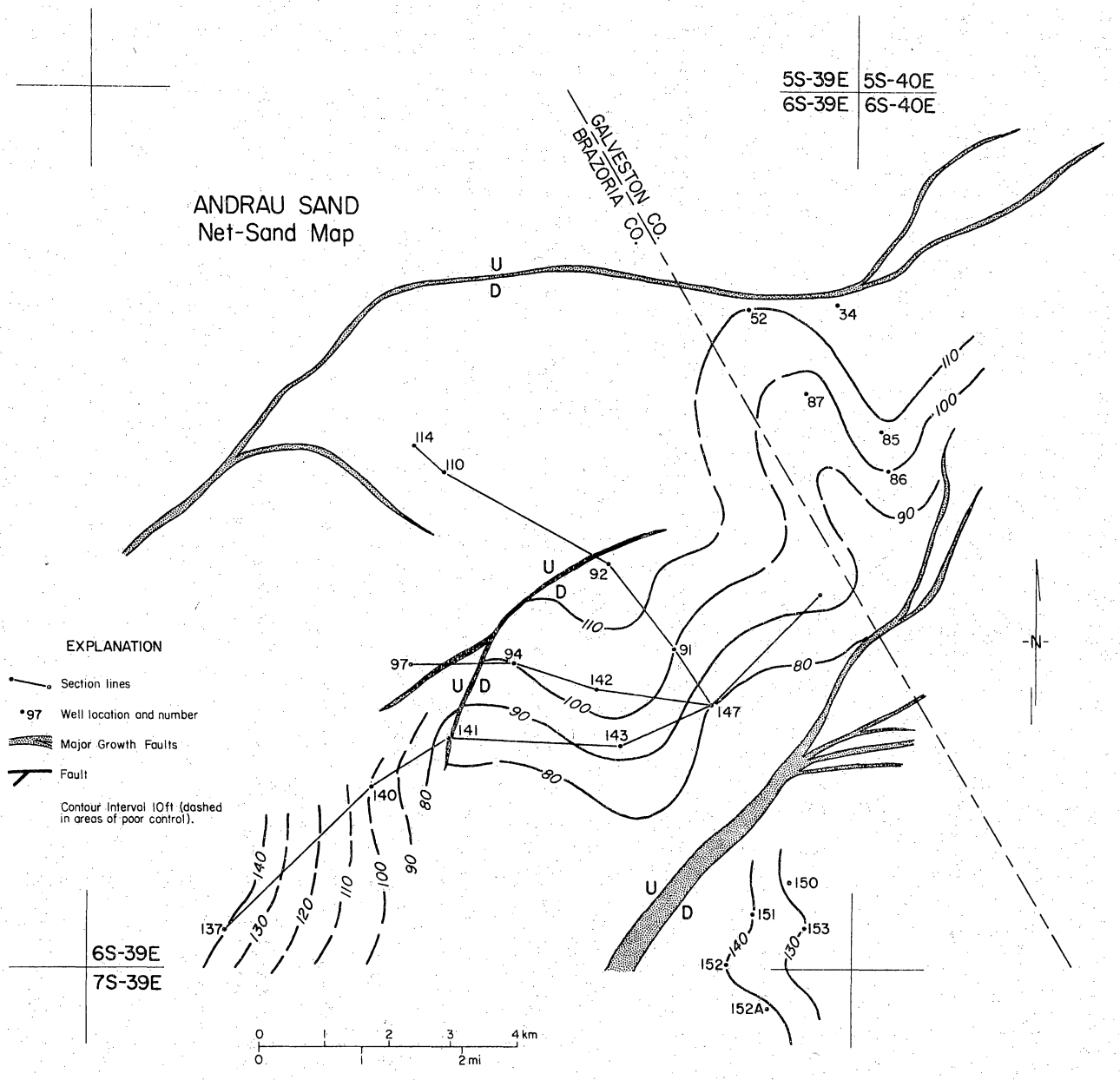

Figure 38. Net-sand map of the sub-T5 Andrau Sand (the potential geopressured geothermal production interval) and location of the fence diagram presented in figure 39. The isolith map suggests a high-constructive lobate deltaic origin for the Andrau Sand.

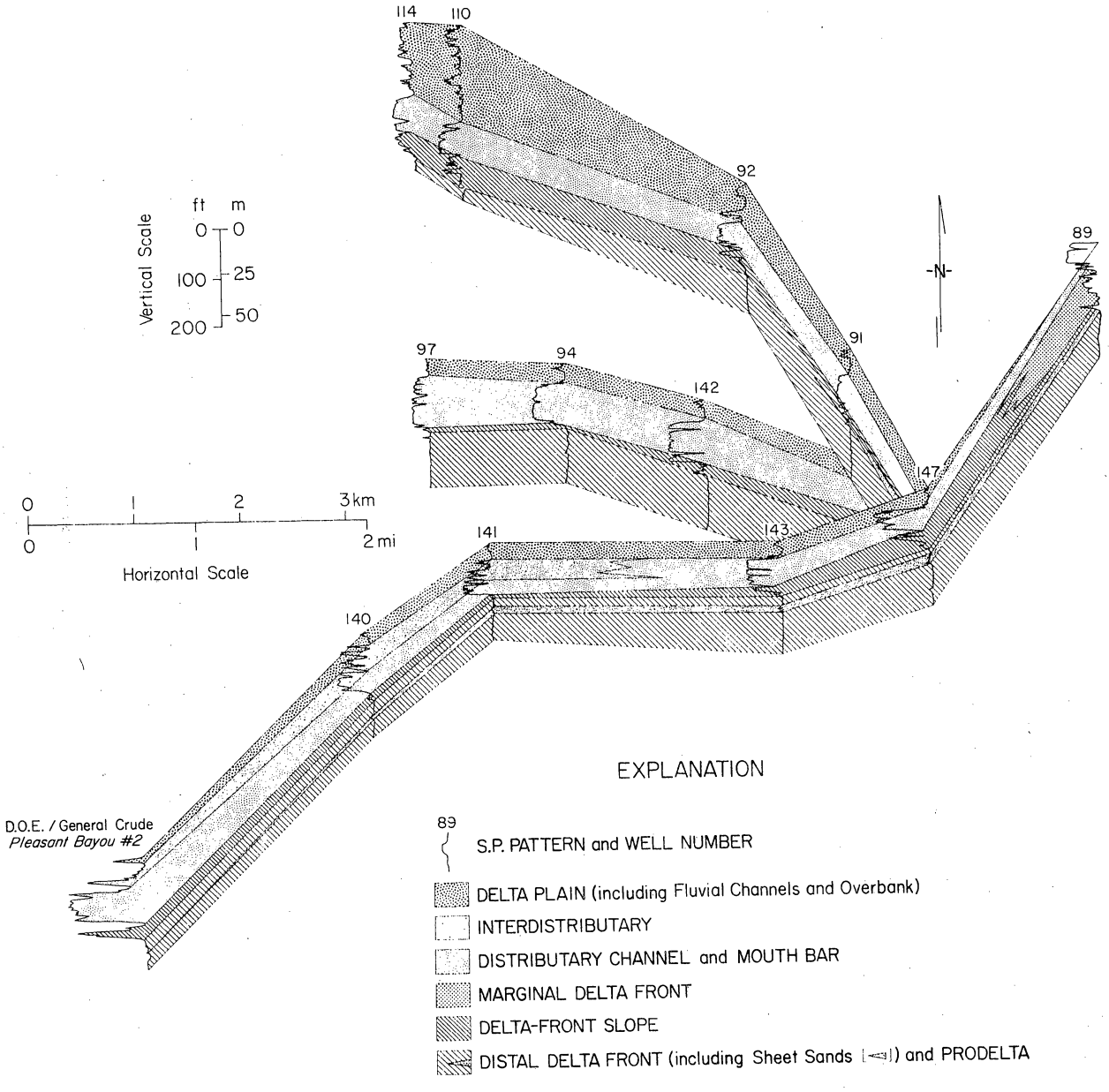

Figure 39. Fence diagram illustrating the continuity of depositional units of the production interval. Delta-front sheet sands and distributary-mouth bar and channel deposits are laterally persistent and comprise a more attractive exploration target than the thin impersistent sands of the delta plain and delta margin.

impersistent, fluvial sandstones of the delta plain. Similarly, thin, "shaly" sandstones of the reworked delta margin have a lower production potential than do continuous sand stringers (possibly deposited under storm-related conditions) of the distal delta front. Figure 39 illustrates the lateral extent of the delta front and channel and mouth bar deposits and their favorability as exploration targets compared to thin impersistent sands of the delta plain or delta margin.

In addition to the influence of depositional geometry on reservoir continuity, vertical and lateral superposition of subenvironments creates heterogeneity in prospective reservoirs. Thinly interbedded interdistributary mudstones and sandstones that prograded over laterally extensive distributary-channel and mouth-bar sandstones (fig. 39) inhibit vertical permeabilities in the potential reservoir and make positioning of well locations and perforated intervals critical. Similarly, laterally continuous mudstones interbedded within fluvial sandstones of a stratigraphically higher delta system that, based on net sand patterns, was of the high-constructive lobate variety (fig. 40) increase the heterogeneity (and reduce the continuity) of a potential production interval (fig. 41). Distributary mouth-bar sands in this lobate delta thicken and become more laterally persistent in a basinward direction but are not as extensive as in the previous example (fig. 39). This is possibly a result of positioning the cross sections in the proximal reaches of the delta and not in the region of maximum marine reworking of the fluvial sediments. Marine reworking of the delta front winnows the finer fraction, creating clean, laterally persistent sheet sands in which inhomogeneities are minor. On a smaller scale, distributary mouth-bar sands have been shown to be composed of the coarsest grain size and contain large primary sedimentary structures (fig. 33) and, as such, compose the most favorable reservoir in the constructive deltaic setting.

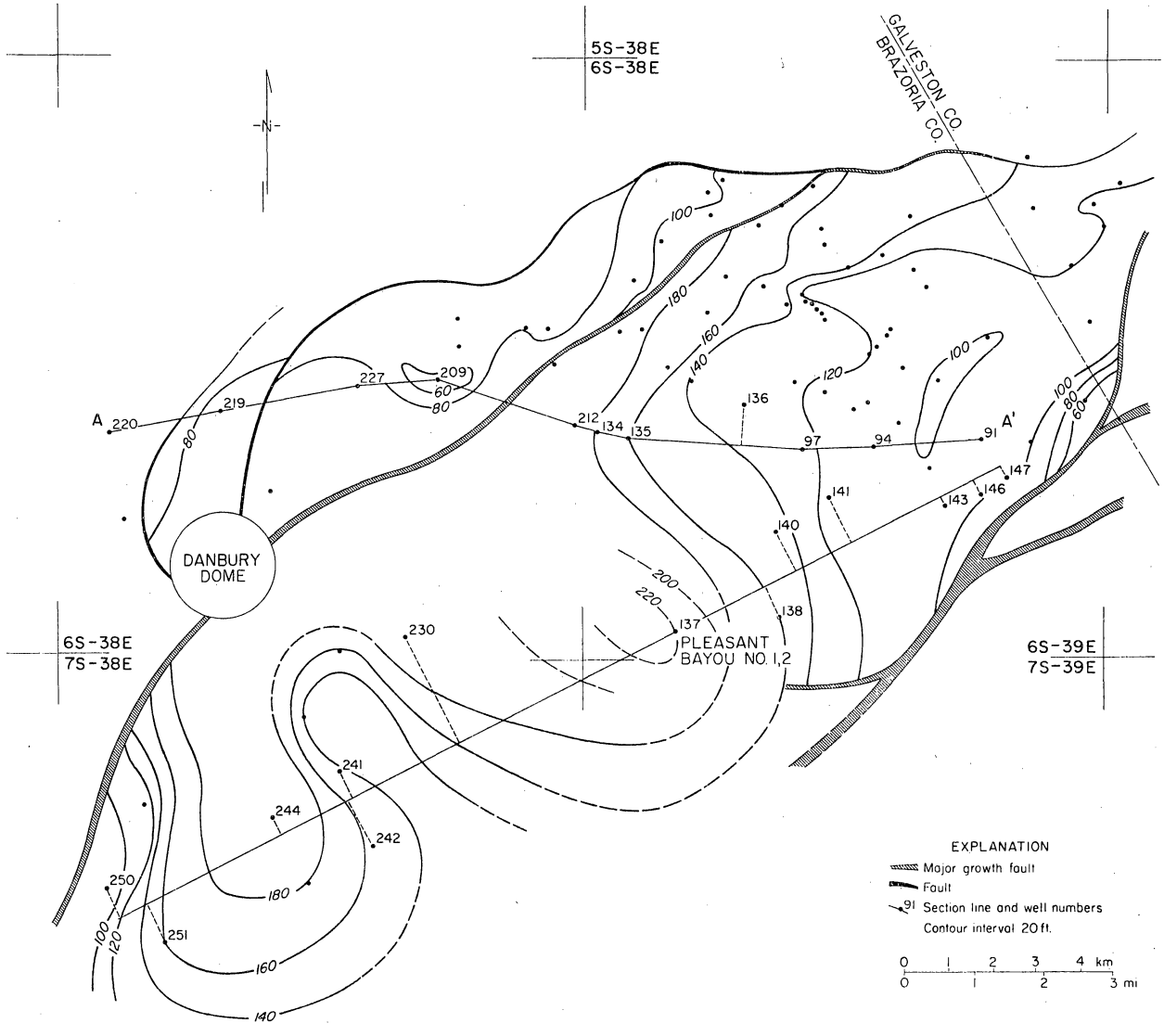

Figure 40. Lobate net-sand pattern of the T3 correlation interval and location of cross sections illustrated in figure 41.

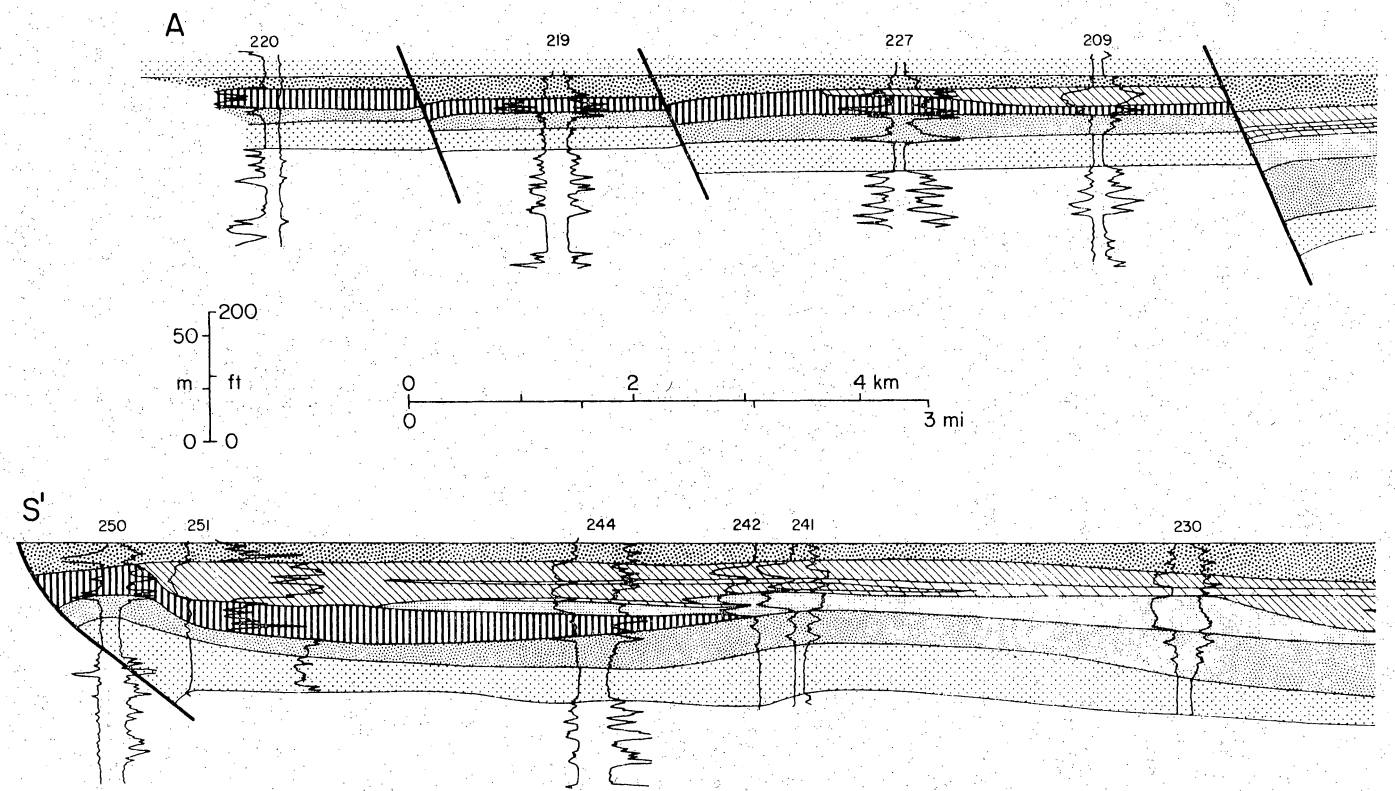

Figure 41. Cross sections through the T3 depositional interval. Note thickening of the assemblage across growth faults, the relative persistence of the

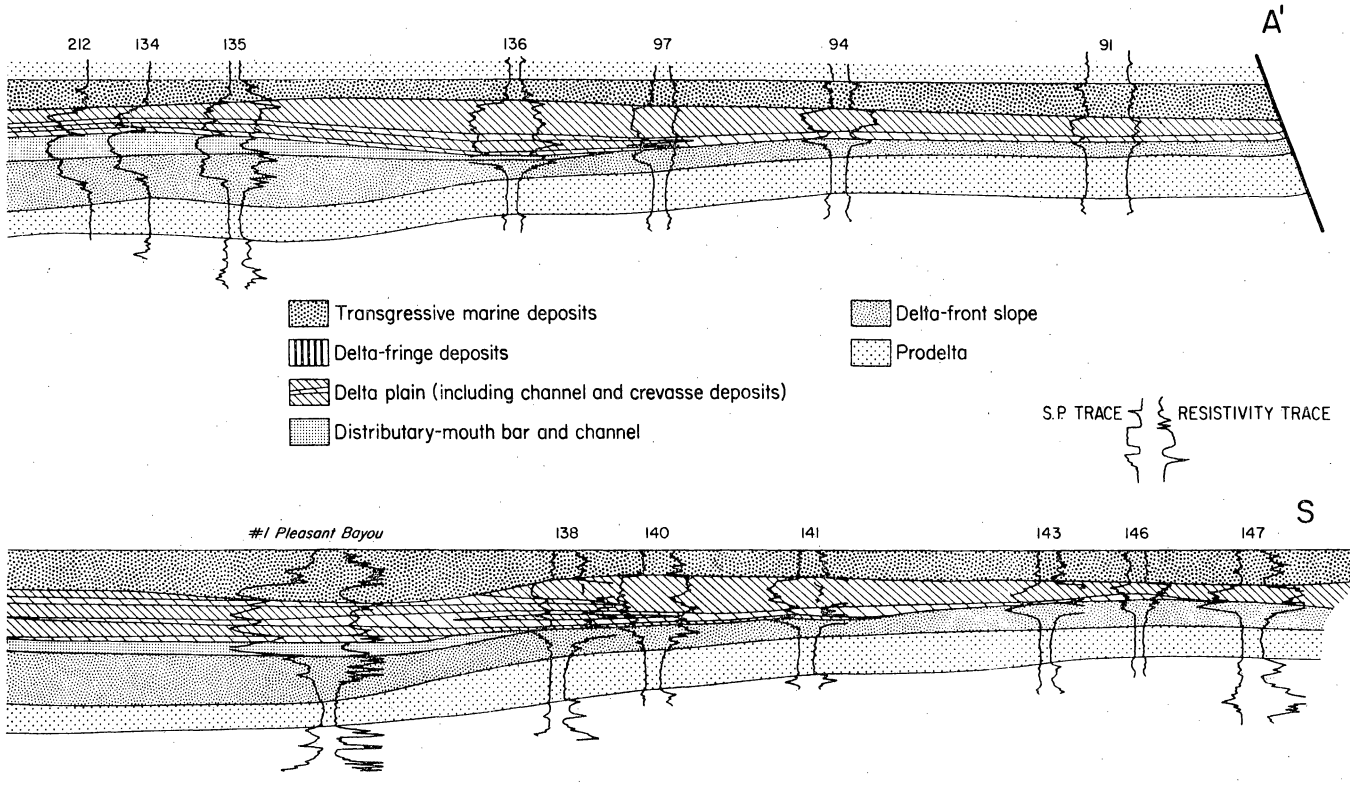

distributary-mouth bar and channel facies, and the presence of mudstone drapes that inhibit vertical fluid flow in the delta-plain deposits.

Vertical Patterns

Porosity and permeability values reported for modern sands (Pryor, 1973; Fulton, 1975), outcrops (Hutchinson and others, 1961; Polasek and Hutchinson, 1967), and whole-core analyses (figs. 24, and 32 to 35) provide a wealth of data for interpreting vertical changes in pore properties. Earlier workers relied on nonuniform variants and statistical (Monte Carlo) techniques to describe and represent permeability in reservoir models because variations were thought to be random (Warren and others, 1961). For example, Polasek and Hutchinson (1967) measured outcrop permeabilities for seven vertical outcrop sections in the Cretaceous Almond sandstone and concluded that permeability differences were randomly distributed. However, examination of their data reveals definite permeability trends dipping across the outcrop at 1 degree (apparent structural dip?) with cycles of higher and lower permeability about 15 to 20 ft thick. Reevaluation of pore properties in this report using depositional models gives more order and meaning to variability that previously was considered random.

Porosity and permeability are not directly related; however, the vertical trends of porosity and permeability within sandstones are remarkably consistent and form repetitive patterns. Of the six basic patterns documented (fig. 42) five are systematic (upward increase, upward decrease [fig. 33], central increase, central decrease [fig. 35], and uniformly low [fig. 34]), whereas the sixth is irregular or a composite (fig. 32) of the other types.

In their simplest form, patterns one and two reflect upward-coarsening and upward-fining sequences; pattern three usually represents original pore trends or tight streaks associated with the upper and lower sandstone boundaries; pattern five represents late-stage cementation, occlusion of primary porosity, and drastic reduction of permeability; and pattern six is usually associated with thick amalgamated sandstones, each with variable internal properties and separated from one another by shale. Higher porosities and permeabilities near the

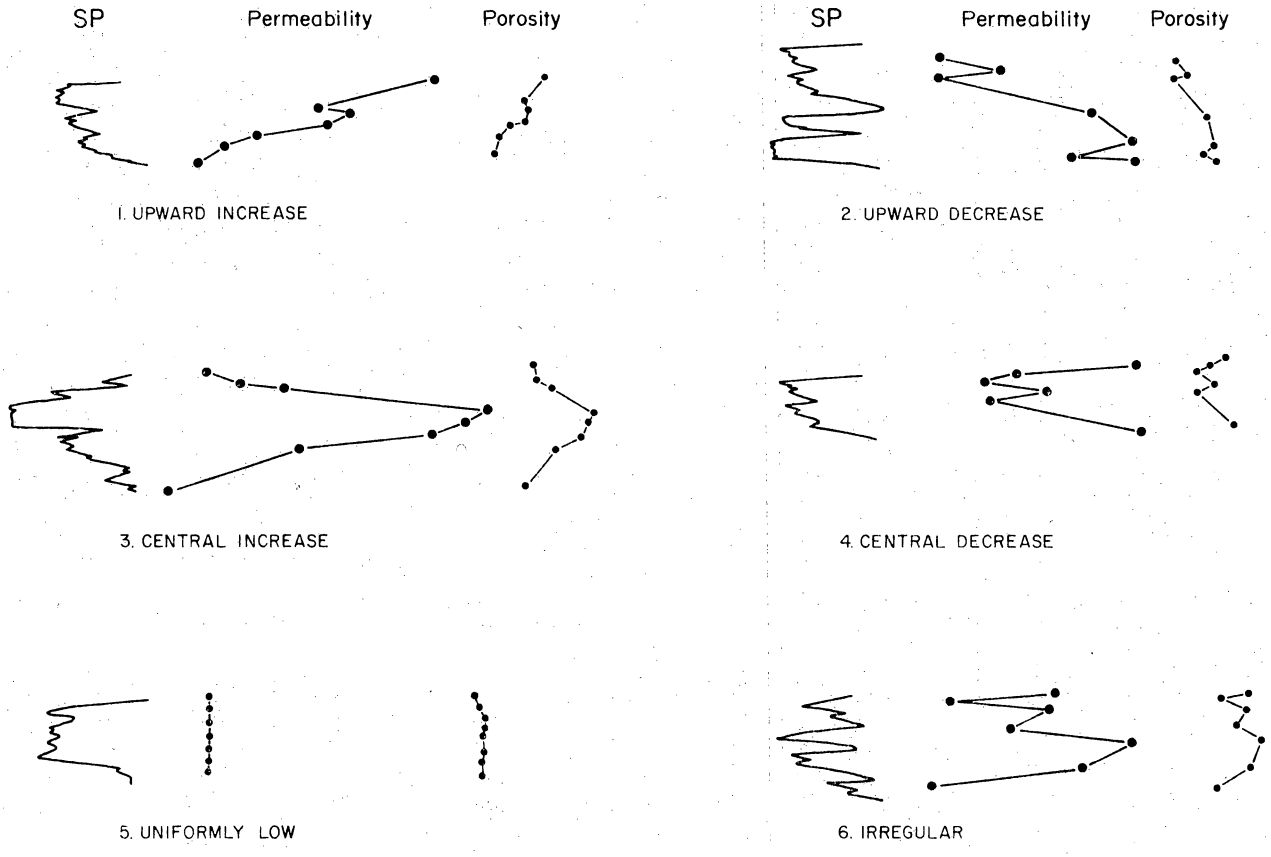

Figure 42. Generalized patterns for vertical changes in pore properties within a sand body.

sandstone margin, shown by pattern four, are difficult to explain. Perhaps they reflect alteration and leaching by ground water, or they may represent an inverse relation to original textural properties whereby clean well-sorted sands were tightly cemented, while moderately sorted sands were less affected by cementation. In any case, pattern four is the least common.

Pore Properties and Stratification

Judging from limited published data (Mast and Potter, 1963; Pryor, 1973) and available core analyses, porosity and permeability are indirectly related to internal stratification because sedimentary structures are partly controlled by grain size. In modern sands, a relative ranking of permeabilities from highest to lowest corresponds to (1) foresets and large-scale troughs, (2) horizontal and low-angle inclined parallel stratification, and (3) small-scale troughs and ripple cross-stratification. Similar conclusions can be derived from the data of Hewitt and Morgan (1965), Polasek and Hutchinson (1967), and Dodge and others (1971). These relationships, however, should be used in the context of properties of surrounding sediments, for as Pryor (1973) noted, "a bedding unit of higher permeability completely surrounded by units of lower permeability will not demonstrate its ultimate through-flow capability but will have an effective permeability influenced and largely determined by the lower permeabilities of the bounding units."

Mast and Potter (1963), among others, found that permeability is highest parallel to stratification and grain-fabric orientation. Therefore, high vertical permeabilities may indicate fracturing across bedding surfaces.

Frequency and Arrangement of Flow Barriers

According to Polasek and Hutchinson (1967), fluid movement is largely determined by the distribution of sand and shaly sand rather than by permeability

variations within a sand. Therefore, gross arrangement of sediment types predicted from sedimentary models may aid in evaluating reservoir performance.

The distribution of pore space and flow barriers can be related to the environment of deposition interpreted from the SP and short-normal resistivity curves (Sneider and others, 1977). Establishment of these relationships allows better prediction of flow barriers, their effect on reservoir production, and the probable locations of isolated segments within a sand body that remain undrained during primary production.

Porosity and permeability variations in fluvial sandstones are slightly more predictable in fine-grained, mixed-load and suspended-load channels than in coarse-grained, bed-load channels because channel deposits of mixed-load and suspended-load streams typically fine upward. The high percent of silt and clay transported by these streams gives rise to a broad range of grain sizes that are mixed and sorted at various stages of stream discharge. The resulting assemblages of sedimentation units are commonly graded or at least capped by numerous clay drapes that are preserved as discontinuous shale partings. The frequency of shale layers and the proportion of silt and clay gradually increase upward, resulting in upward decreases in porosity and permeability and vertical continuity.

In contrast, streams transporting coarse-grained sediment do not exhibit systematic vertical changes in size, hence, the relative positions of major permeability changes are uncertain. Judging from Pryor's (1973) data, abrupt decreases in porosity and permeability occur at the tops and bottoms of coarse-grained channel deposits. The lower permeabilities near the channel base are caused by intercalated mud layers formed during rapid fall in flood stage. These slack-water deposits within the thalweg are commonly eroded or completely removed during subsequent stages of flashy discharge, but some are preserved as thin shale lenses or wedges.

Coarse-grained river deposits are commonly poorly sorted and contain large-scale sedimentary structures. These conditions lead to highly tortuous flow paths because dip directions in the master bedding and sedimentary structures are variable and often opposite.

Percent sand, sand thickness, and bulk permeability (product of reservoir thickness and permeability) decrease toward the margins of fluvial and distributary channels, but bulk permeability varies greatly within the sand body (Houser and Neasham, 1976), owing to truncations and other bedding disruptions, and to changes in grain fabric.

The commonly recognized upward-coarsening sequence attendant with delta progradation provides a rational basis for predicting gross internal properties of delta-front and delta-margin sands. For purposes of this discussion, a practical distinction can be made between complete and incomplete progradational sequences. The former are characterized by superposition of distributary-channel sands over sands of delta-front or distributary-mouth origin. In contrast, delta-front sands are usually overlain by shelf or delta-plain muds if progradation is incomplete because of distributary abandonment. The significance of this difference is that the number and thickness of shale interbeds decrease upward in the complete progradational sequence, whereas delta-front sands of incomplete cycles may be overlain as well as underlain by interbedded sands and shales.

Sorting improves, and sand percent and sand-bed thickness increase upward in delta-front and delta-fringe deposits. Both delta-front and delta-fringe sands are highly continuous, but delta-fringe sands have poor vertical permeability because of numerous laterally extensive clay beds. Sands become more poorly sorted, sand beds thin, and grain sizes decrease away from distributary channels. The physical changes cause reduction in the bulk permeability of delta-fringe deposits (Houser and Neasham, 1976).

Vertical trends of porosity and permeability in barriers and strandplains are somewhat analogous to those found in delta fronts and distributary-mouth bars because of upward-coarsening textures, but beyond that similarity they are quite different in at least two respects. First, the strong wave action and sediment sorting along barrier and strandplain shorelines produce cleaner and better sorted sands with practically no mud deposited on the upper shoreface and beach. Moreover, the lateral continuity of thick barrier and strandplain sand bodies far exceeds that of most delta fronts and distributary-mouth bars (tables 1 and 2). Consequently, in their unaltered state, barriers and strandplains possess the greatest lateral and vertical continuity of the common sandstone types.

Outer shelf and slope sands are best developed in submarine channel and fan complexes. The distribution of low-permeability zones in these deep-water sandstones is similar to the spatial patterns in deltaic deposits. The thickest and cleanest sands are associated with submarine channel deposits that are laterally restricted and vertically separated by shaly intervals. Thin-bedded sands associated with the submarine fan deposits are remarkably uniform in thickness and laterally continuous over broad areas. However, vertical continuity in these sandstones is extremely low because interbedded shales are comparable to or greater than the sand layers in thickness. Turbidites are also characterized by some contorted and bioturbated zones with extremely low permeabilities. Except for the thick channel sands, turbidites generally make poor reservoirs for production of liquids.

IMPLICATIONS FOR GEOPRESSURED ENERGY DEVELOPMENT

On the basis of energy production requirements, sand bodies can be ranked according to sand volume, lateral continuity, and internal heterogeneity. Ideal

reservoirs consist of large laterally extensive sand bodies with minimal interference to flow from internal permeability barriers. Some natural reservoirs approach this high standard, but most are less than ideal because of external and internal discontinuities. In theory, barrier and strandplain sandstones oriented parallel to regional structural fabric approximate the ideal reservoir. These deposits also have high permeabilities in the upper part of the sand body, an added advantage with regard to production of gravity-segregated fluids such as oil and gas.

Fluvial sandstones oriented normal to regional structural fabric rank second according to the favorable criteria. These meanderbelt systems may contain substantial quantities of sand interlaced and interconnected throughout the valley-fill network. A close third are distributary channel sands and associated delta-front and distributary-mouth bar sands oriented normal to depositional strike. The channel and bar-finger sands are commonly thicker and narrower than alluvial channels although they both exhibit similar pore properties. Favorable reservoir potential markedly decreases toward the delta fringe and distal delta front.

Submarine channels and fans oriented normal to regional structural fabric provide the least volume and lateral continuity of the common sandstone types. A disadvantage of these and other channel sandstones is that highest permeabilities are often associated with the coarsest grain sizes and largest sedimentary structures found near the channel base. Although channel sands make excellent reservoirs when completely filled with hydrocarbons, they are less suitable when only partially filled because reservoir continuity and permeabilities decrease toward the top of the sand body. However, basal channel sands are suitable for solution gas production if structure and gravity segregation of the fluids are unimportant.

The relative ranking of these sand bodies is greatly simplified, and undoubtedly there are numerous exceptions. However, the ranking can serve as a guide to drainage efficiency on the basis of shaliness. Conceptually, upper shoreface and beach sands should provide greater lateral continuity, fewer restrictions to flow, and, consequently, greater drainage efficiency than distal delta-front sands. Inhomogeneities within the sand body account in part for the poor agreement between reservoir volumes estimated from geological maps and calculated from production data.

ACKNOWLEDGMENTS

This work was made possible through funding by the U.S. Department of Energy, Division of Geothermal Energy, under contract no. DE-AC08-79ET27111. We acknowledge the support provided by personnel at the Bureau of Economic Geology who assisted in preparing this report. The manuscript was typed by Margaret T. Chastain and Dorothy C. Johnson, under the direction of Lucille Harrell. Illustrations were prepared under the direction of Dan Scranton.

REFERENCES

Bebout, D. G., Loucks, R. G., and Gregory, A. R., 1978, Frio sandstone reservoirs in the deep subsurface along the Texas Gulf Coast: The University of Texas at Austin, Bureau of Economic Geology, Report of Investigations No. 91, 92 p.

Bebout, D. G., Weise, B. R., Gregory, A. R., and Edwards, M. B., 1979, Wilcox sandstone reservoirs in the deep subsurface along the Texas Gulf Coast: The University of Texas at Austin, Bureau of Economic Geology, Report to the U.S. Department of Energy, contract no. DE-AS05-76ET28461, 219 p.

Bebout, D. G., Loucks, R. G., and Gregory, A. R., 1980, Geological aspects of Pleasant Bayou geopressured geothermal test well, Austin Bayou prospect, Brazoria County, Texas, in Dorfman, M. H., and Fisher, W. L., eds., Proceedings, Fourth geopressured geothermal energy conference: The University of Texas at Austin, Center for Energy Studies, p. 11-45.

Berg, R. R., and Davies, D. K., 1968, Origin of Lower Cretaceous Muddy Sandstone at Bell Creek field, Montana: American Association of Petroleum Geologists Bulletin, v. 52, p. 1888-1898.

Berg, R. R., and Findley, R. L., 1973, Deep-water interpretation of upper Wilcox sandstones from core study, Katy field, Texas: Gulf Coast Association of Geological Societies Transactions, v. 23, p. 259-265.

Berg, R. R., Marshall, W. D., and Shoemaker, P. W., 1979, Structural and depositional history, McAllen Ranch field, Hidalgo County, Texas: Gulf Coast Association of Geological Societies Transactions, v. 29, p. 24-83.

Berg, R. R., and Tedford, F. J., 1977, Characteristics of Wilcox gas reservoirs, Northeast Thompsonville Field, Jim Hogg and Webb Counties, Texas: Gulf Coast Association of Geological Societies Transactions, v. 27, p. 6-19.

Berg, R. R., and Powers, B. K., 1980, Morphology of turbidite-channel reservoirs, lower Hackberry (Oligocene), southeast Texas: Gulf Coast Association of Geological Societies Transactions, v. 30, p. 41-48.

Bernard, H. A., Major, C. F., Jr., Parrot, B. S., and LeBlanc, R. J., 1970, Recent sediments of southeast Texas--a field guide to the Brazos alluvial and deltaic plains and Galveston barrier island complex: The University of Texas at Austin, Bureau of Economic Geology, Guidebook 11, 83 p.

Boardman, C. R., 1980, Implications of geopressured aquifer volumes obtained from pressure and production records of selected Gulf Coast geopressured gas fields: C. K. GeoEnergy, Las Vegas, Report to the U.S. Department of Energy, contract no. DOE-ET-10024-2.

Bouma, A. H., 1962, Sedimentology of some flysch deposits--a graphic approach to facies interpretations: Amsterdam, Elsevier, 168 p.

Bouma, A. H., 1968, Distribution of minor structures in Gulf of Mexico sediments: Gulf Coast Association of Geological Societies Transactions, v. 18, p. 26-33.

Boyd, D. R., and Dyer, B. R., 1966, Frio barrier bar system of South Texas: American Association of Petroleum Geologists Bulletin, v. 50, p. 170-178.

Brown, L. F., Jr., Brewton, J. L., Evans, T. J., McGowen, J. H., White, W. A., Groat, C. G., and Fisher, W. L., 1980, Environmental geologic atlas of the Texas Coastal Zone, Brownsville-Harlingen area: The University of Texas at Austin, Bureau of Economic Geology, 140 p.

Casey, S. R., and Cantrell, R. B., 1941, Davis sand lens, Hardin field, Liberty County, Texas, in Stratigraphic type oil fields: American Association of Petroleum Geologists, Special Publication, p. 564-599.

Chierici, G. L., Clucci, G. M., Sclocchi, G., and Terzi, L., 1978, Water drive from interbedded shale compaction in superpressured gas reservoirs--model study: Journal of Petroleum Technology, v. 30, p. 937-944.

Chuber, S., 1972, Milbur (Wilcox) field, Milam and Burleson Counties, Texas: American Association of Petroleum Geologists Memoir 16, p. 399-405.

Coleman, J. M., and Garrison, L. E., 1977, Geological aspects of marine slope stability, northwestern Gulf of Mexico: Marine Geotechnology, v. 2, p. 9-44.

Conatser, W. E., 1971, Grand Isle: a barrier island in the Gulf of Mexico: Geological Society of America Bulletin, v. 82, p. 3049-3068.

Craft, B. C., and Hawkins, M. F., 1959, Applied petroleum reservoir engineering, Englewood Cliffs, New Jersey, Prentice-Hall, 437 p.

Curtis, D. M., 1970, Miocene deltaic sedimentation, Louisiana Gulf Coast, in Deltaic sedimentation, modern and ancient: Society of Economic Paleontologists and Mineralogists Special Publication 15, p. 293-308.

DePaul, G. J., 1980, Environment of deposition of upper Wilcox sandstones, Katy gas field, Waller County, Texas: Gulf Coast Association of Geological Societies Transactions, v. 30, p. 61-70.

Dickinson, K. A., Berryhill, H. L., Jr., and Holmes, C. W., 1972, Criteria for recognizing ancient barrier coastlines, in Rigby and Hamblin, eds.: Society of Economic Paleontologists and Mineralogists Special Publication 16, p. 192-214.

Dodge, C. F., Holler, D. P., and Meyer, R. L., 1971, Reservoir heterogeneities of some Cretaceous sandstones: American Association of Petroleum Geologists Bulletin, v. 55, p. 1814-1828.

Dodge, M. M., and Posey, J. S., 1981, Structural cross sections, Tertiary formations, Texas Gulf Coast: The University of Texas at Austin, Bureau of Economic Geology cross sections.

Doyle, J. D., 1979, Depositional patterns of Miocene facies, Middle Texas Coastal Plain: The University of Texas at Austin, Bureau of Economic Geology Report of Investigations No. 99, 25 p.

Duggan, J. O., 1972, The Anderson "L"--an abnormally pressured gas reservoir in South Texas: Journal of Petroleum Technology, v. 24, p. 132-138.

Edwards, M. B., 1980, The Live Oak delta complex: an unstable shelf/edge delta in the deep Wilcox trend of South Texas: Gulf Coast Association of Geological Societies Transactions, v. 30, p. 71-79.

Edwards, M. B., 1981, Upper Wilcox Rosita delta system of South Texas: growth-faulted shelf-edge deltas: American Association of Petroleum Geologists Bulletin, v. 65, no. 2, p. 54-73.

Fisher, W. L., and McGowen, J. H., 1967, Depositional systems in Wilcox Group of Texas and their relationship to occurrence of oil and gas: Gulf Coast Association of Geological Societies Transactions, v. 17, p. 105-125.

Fisher, W. L., Brown, L. F., Jr., Scott, A. J., and McGowen, J. H., 1969, Delta systems in the exploration for oil and gas: The University of Texas at Austin, Bureau of Economic Geology, 185 p.

Fisher, W. L., and Brown, L. F., Jr., 1972, Clastic depositional systems--a genetic approach to facies analysis: The University of Texas at Austin, Bureau of Economic Geology, 211 p.

Fisk, H. N., 1955, Sand facies of recent Mississippi delta deposits: 4th World Petroleum Congress Proceedings, Section 1-C, p. 377-398.

Fisk, H. N., 1959, Padre Island and the Laguna Madre Flats, coastal South Texas, in Russell, R. H., chm.: 2nd Coastal Geology Conference, Louisiana State University, April 6-9, p. 103-151.

Fisk, H. N., 1961, Bar-finger sands of Mississippi delta, in Peterson, J. A., and Osmond, J. C., eds., Geometry of sandstone bodies: American Association of Petroleum Geologists, p. 29-52.

Frazier, D. E., 1967, Recent deltaic deposits of the Mississippi River; their development and chronology: Gulf Coast Association of Geological Societies Transactions, v. 17, p. 287-315.

Frazier, D. E., 1974, Depositional-episodes: their relationship to the Quaternary stratigraphic framework in the northwestern portion of the Gulf Basin: The University of Texas at Austin, Bureau of Economic Geology Geological Circular 74-1, 28 p.

Frazier, D. E., and Osanik, A., 1961, Point-bar deposits, Old River Locksite, Louisiana: Gulf Coast Association of Geological Societies Transactions, v. 11, p. 121-137.

Freeman, J. C., 1949, Strandline accumulation of petroleum, Jim Hogg County, Texas: American Association of Petroleum Geologists Bulletin, v. 33, p. 1260-1270.

Fulton, K. J., 1975, Subsurface stratigraphy, depositional environments, and aspects of reservoir continuity--Rio Grande delta, Texas: University of Cincinnati, Ph.D. dissertation, 330 p.

Galloway, W. E., 1968, Depositional systems of the Lower Wilcox Group--North Central Gulf Coast Basin: Gulf Coast Association of Geological Societies Transactions, v. 18, p. 275-289.

Galloway, W. E., Hobday, D. K., and Magara, K., in press, Frio Formation of the Texas Gulf Coast Basin--depositional systems, structural framework, and hydrocarbon origin, migration, distribution, and exploration potential: The University of Texas at Austin, Bureau of Economic Geology Report of Investigations.

Garg, S. K., 1980, Shale recharge and production behavior of geopressured reservoirs: Geothermal Research Council Transactions, v. 4, p. 325-328.

Gotautas, V. A., Gordon, G. E., Johnson, J., and Lee, C., 1972, Southwest Lake Arthur Field, Cameron Parish, Louisiana, in King, R. E., ed., Stratigraphic oil and gas fields--classification, exploration methods, and case histories: American Association of Petroleum Geologists, Memoir 16, p. 389-398.

Gould, H. R., 1970, The Mississippi delta complex, in Morgan, J. P., ed., Deltaic sedimentation, modern and ancient: Society of Economic Paleontologists and Mineralogists Special Publication 15, p. 3-30.

Gregory, J. L., 1966, A lower Oligocene delta in the subsurface of southeastern Texas: Gulf Coast Association of Geological Societies Transactions, v. 16, p. 227-241.

Halbouty, M. T., and Barber, T. D., 1961, Port Acres and Port Arthur fields, Jefferson County, Texas: Gulf Coast Association of Geological Societies Transactions, v. 11, p. 225-234.

Hartman, J. A., 1972, G2 channel sandstone, Main Pass, Block 35 field, offshore Louisiana: American Association of Petroleum Geologists Bulletin, v. 56, p. 554-558.

Hewitt, C. H., and Morgan, J. T., 1965, The Fry in situ combustion test--reservoir characteristics: Journal of Petroleum Technology, v. 17, p. 337-342.

Houser, J. F., and Neasham, J. W., 1976, Bed continuity and permeability variations of recent deltaic sediments (abs.): American Association of Petroleum Geologists Bulletin, v. 60, p. 681.

Hutchinson, C. A., Jr., Dodge, C. F., and Polasek, T. L., 1961, Identification, classification and prediction of reservoir nonuniformities affecting production operations: Journal of Petroleum Technology, p. 223-229.

Law, J., 1944, A statistical approach to the interstitial heterogeneity of sand reservoirs: Journal of Petroleum Technology, T. P. 1732, p. 1-20.

LeBlanc, R. J., Jr., 1977, Distribution and continuity of sandstone reservoirs: Journal of Petroleum Technology, parts 1 and 2, p. 774-804.

Loucks, R. G., 1979, Sandstone distribution and potential for geopressured geothermal energy production in the Vicksburg Formation along the Texas Gulf Coast: The University of Texas at Austin, Bureau of Economic Geology Geological Circular 79-4, 27 p.

Loucks, R. G., Richmann, D. L., and Milliken, K. L., 1981, Factors controlling reservoir quality in Tertiary sandstones and their significance to geopressured

geothermal production: The University of Texas at Austin, Bureau of Economic Geology Report of Investigations No. 111, 41 p.

Martyn, P. F., and Sample, C. H., 1941, Oligocene stratigraphy of East White Point Field, San Patricio and Nueces Counties, Texas: American Association of Petroleum Geologists Bulletin, v. 25, p. 1967-2009.

Mast, R. F., and Potter, P. E., 1963, Sedimentary structures, sand-shape fabrics, and permeability: Journal of Geology, part 2, v. 71, p. 548-565.

Milliken, K. L., Land, L. S., and Loucks, R. G., 1981, History of burial diagenesis determined from isotopic geochemistry, Frio Formation, Brazoria County, Texas: American Association of Petroleum Geologists Bulletin, v. 65, p. 1397-1413.

Morton, R. A., and Donaldson, A. C., 1978, The Guadalupe River and delta of Texas - a modern analogue for some ancient fluvial-deltaic systems, in Miall, A. D., ed., Fluvial sedimentology: Canadian Society of Petroleum Geologists, Memoir 5, p. 773-787.

Morton, R. A., and McGowen, J. H., 1980, Modern depositional environments of the Texas Coast: The University of Texas at Austin, Bureau of Economic Geology, Guidebook 20, 167 p.

Morton, R. A., Winker, C. D., and Garcia, D. D., 1980, Seismic studies in Austin-Pleasant Bayou and Cuero Prospects--a summary of research activities: The University of Texas at Austin, Bureau of Economic Geology, Report to the U.S. Department of Energy, contract no. DE-AS05-76ET28461, 57 p.

Nanz, R. H., Jr., 1954, Genesis of Oligocene sandstone reservoir, Seeligson field, Jim Wells and Kleberg Counties, Texas: American Association of Petroleum Geologists Bulletin, v. 38, p. 96-117.

Oomkens, E., 1970, Depositional sequences and sand distribution in the postglacial Rhone delta complex, in Morgan, J. P., ed., Deltaic sedimentation, modern and ancient: Society of Economic Paleontologists and Mineralogists Special Publication 15, p. 198-212.

Overby, W. K., Jr., and Henniger, B. R., 1971, History, development, and geology of oil fields in Hocking and Perry Counties, Ohio: American Association of Petroleum Geologists Bulletin, v. 55, p. 183-203.

Paine, W. R., 1971, Petrology and sedimentation of the Hackberry sequence of southwest Louisiana: Gulf Coast Association of Geological Societies Transactions, v. 21, p. 37-55.

Polasek, T. L., and Hutchinson, C. A., Jr., 1967, Characterization of non-uniformities within a sandstone reservoir from a fluid mechanics standpoint: Proceedings, 7th World Petroleum Congress, v. 2, p. 397-407.

Pryor, W. A., 1973, Permeability-porosity patterns and variations in some Holocene sand bodies: American Association of Petroleum Geologists Bulletin, v. 57, p. 162-189.

Scruton, P. C., 1960, Delta building and the deltaic sequence, in Recent sediments northwestern Gulf of Mexico: American Association of Petroleum Geologists, p. 82-102.

Simons, D. B., Richardson, E. V., and Nordin, C. F., 1965, Sedimentary structures generated by flow in alluvial channels: Society of Economic Paleontologists and Mineralogists Special Publication 12, p. 34-52.

Smith, D. A., 1980, Sealing and non-sealing faults in Louisiana Gulf Coast salt basin: American Association of Petroleum Geologists Bulletin, v. 64, p. 145-172.

Sneider, R. M., Richardson, F. H., Paynter, D. D., Eddy, R. E., and Wyant, I. A., 1977, Predicting reservoir rock geometry and continuity in Pennsylvanian reservoirs, Elk City Field, Oklahoma: Journal of Petroleum Technology, p. 851-866.

Solis Iriarte, R. F., 1980, Late Tertiary and Quaternary depositional systems in the subsurface of Central Coastal Texas: The University of Texas at Austin, Ph.D. dissertation, 155 p.

Southard, J. B., 1971, Representation of bed configurations in depth-velocity-size diagrams: Journal of Sedimentary Petrology, v. 41, p. 903-915.

Stuart, C. A., 1970, Geopressures: supplement to the Proceedings, Second Symposium on Abnormal Subsurface Pressure: Louisiana State University, Baton Rouge, 121 p.

Visher, G. S., Saitta, B. S., and Phares, R. S., 1971, Pennsylvanian delta patterns and petroleum occurrences in eastern Oklahoma: American Association of Petroleum Geologists Bulletin, v. 55, p. 1206-1230.

Walker, R. G., 1979, Facies models: Geological Association of Canada, Reprint Series No. 1, 211 p.

Wallace, W. E., 1969, Water production from abnormally pressured gas reservoirs in south Louisiana: Journal of Petroleum Technology, v. 21, p. 969-982.

Warren, J. E., Sciba, F. F., and Price, S. H., 1961, An evaluation of the significance of permeability measurements: Journal of Petroleum Technology, p. 739-744.

Weise, B. R., Jirik, L. A., Hamlin, H. S., Hallam, S. L., Edwards, M. B., Schatzinger, R. A., Tyler, N., and Morton, R. A., 1981, Geologic studies of geopressured and hydropressured zones in Texas: supplementary tasks: The University of Texas at Austin, Bureau of Economic Geology, Report prepared for Gas Research Institute under contract no. 5011-321-0125.

Williams, C. E., Travis, L. R., and Hoover, E. M., 1974, Depositional environments interpreted from stratigraphic, seismic and paleo-environmental analysis, upper Wilcox, Katy field, Texas: Gulf Coast Association of Geological Societies Transactions, v. 24, p. 129-137.

Winker, C. D., 1979, Late Pleistocene fluvial-deltaic deposition, Texas Coastal Plain and shelf: The University of Texas at Austin, Master's thesis, 187 p.

Winker, C. D., Morton, R. A., Ewing, T. E., and Garcia, D. D., 1981, Depositional setting and structural style in three geopressured geothermal areas, Texas Gulf Coast: The University of Texas at Austin, Bureau of Economic Geology,

Report prepared for the U.S. Department of Energy, Division of Geothermal Energy, Contract No. DE-AC08-79ET27111.

Woltz, D., 1980, Block 25 Field, Chandeleur Sound, St. Bernard Parish, Louisiana: Gulf Coast Association of Geological Societies Transactions, v. 30, p. 243-249.

Wood, A. W., 1962, Northeast Thompsonville Field, in Contributions to geology of South Texas: South Texas Geological Society, San Antonio, Texas, p. 241-245.

Young, L. F., Jr., 1966, Northeast Thompsonville Field, South Texas, key to future exploration for downdip Wilcox production: American Association of Petroleum Geologists Bulletin, v. 50, p. 505-517.

APPENDIX

Microfossil Recovery and Paleoenvironmental Interpretation for DOE/General Crude No. 1 and No. 2 Pleasant Bayou Cores Brazoria County, Texas

Micropaleontological analysis and interpretation of 31 core samples were undertaken by Clarence Albers of Amoco Production Company, Houston, Texas. Samples selected for analysis were taken from mudstones and silty mudstones of the Pleasant Bayou wells. Fossils present were identified, and the paleoecology of the depositional system interpreted. Fossil numbers recorded are vague because initial rock volumes processed were not measured, as relative numbers are adequate for paleoecological interpretation. The paleoecological interpretations based on fossil evidence agree very well with interpretations of depositional systems based on depositional geometry and core characteristics.

Microfossil Recovery

#1 Pleasant Bayou

10229
Textularia cf. *dibollensis* - numerous
Nonion aff. *struma* - single
Buliminella cf. *elegantissima*
Cytheridea sp.
Cytheretta jeffersonensis - single

10232
Textularia cf. *dibollensis* - several
Textularia cf. *mornhinvegi* - single
Textularia spp. - few
Discorbis nomada - several
Trochammina sp. - rare
Nonionella sp. - several, very small
Buliminella cf. *elegantissima* - common
Bolivina cf. *striatula* - few
Virgulina cf. *pontoni* - rare
Globigerina sp. - single
Cytheretta jeffersonensis - few
Pyritized diatoms

10233.5
Discorbis nomada - rare
Nonionella sp. - rare
Virgulina pontoni - single
Haplocytheridea israelskyi - fragment
Haplocytheridea sp. - fragments

10236.5
Discorbis nomada - common
Textularia mornhinvegi - fairly common
Textularia sp.
Buliminella cf. *elegantissima* - common
Cibicides hazzardi - two
Virgulina pontoni - fragment
Bolivina cf. *striatula* - several
Nonionella sp.
Elphidium incertum - two
Angulogerina sp. - single
Trochammina sp. - common
Ammobaculites cf. *salsus* - two
Haplocytheridea israelskyi - single
Cytheretta jeffersonensis - single & fragments

10239
Textularia mornhinvegi - few
Textularia sp.
Discorbis nomada - several
Bolivina cf. *striatula* - rare
Trochammina sp. - several
Cibicides hazzardi - single
Haplocytheridea israelskyi - fragment

10242
Textularia mornhinvegi - several
Textularia sp. - several
Discorbis nomada - rare
Trochammina sp. - few
Ammobaculites cf. *salsus* - rare
Cytheretta jeffersonensis - single
Cytheridea ? sp. - fragment

10246
Discorbis nomada - two
Cibicides hazzardi - single
Bolivina cf. *striatula* - rare
Textularia mornhinvegi - few
Textularia sp. - single
Trochammina sp. - rare
Ammobaculites cf. *salsus* - rare
Haplocytheridea israelskyi - single

10249
Cibicides hazzardi - rare
Nonion pizarrense - single
Cyclammina sp. - compressed
Eponides cf. *ellisorae* - fragments
Trochammina sp. - rare
Robulus sp. - very poor

} very poorly preserved

10260 *Eponides ellisorae* - three
Textularia cf. *dibollensis*
Textularia sp.
Ammobaculites cf. *salsus* - several
Cytheridea ? sp. - fragment

10262 *Ammobaculites* cf. *salsus* - few
Cyclammina sp. - small, several
Discorbis ? sp.
Amphistegina ? sp.
Eponides ? sp.
Amphistegina ? sp.
} very poorly preserved, worn

11752 No fossils noted

11761 No fossils noted

14065 No fossils noted

14069 *Trochammina* sp. - compressed, fairly common
Ammobaculites cf. *salsus* - several
Pyritized diatoms - rare

14072.5 *Trochammina* ? sp. - rare, poor
Pyritized diatoms - rare

14075 *Discorbis nomada* - several
Discorbis sp.
Nonionella sp. - single, pyritized
Ammobaculites cf. *salsus* - few
Trochammina sp. - fairly common, very small
Pyritized diatoms

14079 *Textularia seligi* - single
Textularia sp.
Ammobaculites cf. *salsus* - fairly common
Trochammina sp. - common
Pyritized diatoms - common

14080.5 *Textularia seligi* - three
Ammobaculites cf. *salsus* - several
Trochammina sp. - fairly common, very small

14086.9 No fossils noted

14103 *Ammobaculites* (?) sp. - very rare

14105 No fossils noted

15559.2 *Ammobaculites* cf. *salsus* - common

15561.2 *Ammobaculites* cf. *salsus* - fairly common

15562 *Ammobaculites* cf. *salsus* - several

15592 No fossils noted

#2 Pleasant Bayou

No marine fossils noted in the six samples provided in the interval 15624-15674.

Paleoenvironmental Interpretation

#1 Pleasant Bayou	
10229-10262	Inner neritic
11752-11761	Unfossiliferous - non-marine?
14065-14072.5	Transitional - bay, lagoon
14075-14080.5	Inner neritic
14086.9-14105	Unfossiliferous or transitional
15559.2 - 155562	Transitional - bay, lagoon
15592	Unfossiliferous

#2 Pleasant Bayou	
15624-15674	Unfossiliferous - high lignite content indicates marsh or swamp deposit.